This is to certify that the

dissertation entitled

Performance, Stability, and Localization
of Systems of Vibration Absorbers

presented by

Abdallah Saleh Alsuwaiyan

has been accepted towards fulfillment
of the requirements for

Ph.D. degree in Mechanical Engineering

Major professor

Date July 20, 1999

DATE DUE	DATE DUE	DATE DUE
JAN 0 2 2 2005		

PERFORMANCE, STABILITY, AND LOCALIZATION OF SYSTEMS OF VIBRATION ABSORBERS

By

Abdallah Saleh Alsuwaiyan

A DISSERTATION

Submitted to
Michigan State University
in partial fulfillment of the requirements
for the degree of

DOCTOR OF PHILOSOPHY

Department of Mechanical Engineering

1999

ABSTRACT

PERFORMANCE, STABILITY, AND LOCALIZATION OF SYSTEMS OF VIBRATION ABSORBERS

By

Abdallah Saleh Alsuwaiyan

This work addresses the dynamics of systems of identical and nearly-identical tuned vibration absorbers. Of particular interest are the details of the dynamic response and the manner in which these relate to the performance of the absorber system. The results are analytical in nature, and based on both linear and nonlinear dynamic models of absorber systems. In all cases the results obtained are verified using extensive simulations.

The main focus of the thesis is on the reduction of torsional vibrations via the use of centrifugal pendulum vibration absorbers (CPVAs). However, many of the results extend directly to the case of translational absorbers, and this is pointed out and exploited in some special cases. CPVAs are small masses that move along designer-specific paths relative to the rotor whose vibration is to be suppressed. Until recently, designs of CPVA systems were based on the response of a single absorber mass or the dynamically equivalent case of multiple absorber masses moving in unison. Recent studies of multiple absorbers that ride on a specific absorber path, namely, the so-called tautochronic path, showed that the unison response does not always prevail, due to dynamic instabilities that arise from nonlinear effects. In the present work, the more general case where systems of multiple absorbers ride on general paths is considered. The existence and stability of unison motions and the general effects

of path type and path mistuning are investigated by utilizing a physically relevant scaling of the system parameters that allows for the application of the asymptotic method of averaging. The existence and stability of the unison response and some types of non-unison responses are considered in detail. It is found that the stability of the unison motion depends on both the path type and the level of mistuning. For the commonly used circular paths, and paths close to them, two types of instabilities were found. One is the well-known classical jump, which maintains the unison nature of the response, and the other is a bifurcation that gives rise to one or more types of non-unison responses. Steady-state responses other than unison were found to exist for over-tuned circular paths and paths close to them. In cycloidal paths, no instabilities occur for realistic ranges of mistuning, and therefore these shortcomings are completely avoided.

Another theme of this thesis is the investigation of localization phenomena in systems of vibration absorbers. Localization corresponds to a response in which the system's vibration energy is concentrated in a single absorber (or a small subset of absorbers), resulting in much higher amplitudes of vibration than expected for that (those) absorber(s). This behavior is investigated for both free and forced vibrations. In the linearized models, it occurs for the free vibration modes as well as the harmonically forced, steady-state responses for both translational and torsional vibration absorber systems. Steady-state localization, as a particular form of non-unison motion, is also found to occur for the nonlinear forced vibration of systems of CPVAs riding on over-tuned circular paths and paths close to them.

Based on the findings of this thesis, one can conclude that slightly positively mistuned cycloidal paths are the best choice for practical implementation of systems of nearly-identical CPVAs, and, similarly, that a slight hardening nonlinearity is desirable for systems of nearly-identical translational absorbers. This avoids the instabilities while not sacrificing system performance.

To my great father Saleh M. Alsuwaiyan

ACKNOWLEDGMENTS

All prayers and glories are due to the all mighty ALLAH whose help is the key to any accomplishment.

My appreciations and thanks are due to my advisor, Prof. S. W. Shaw who was very helpful and cooperative. He enriched me with valuable information and guidance throughout my work. He is like an ocean full of knowledge. I learned a lot from him.

My thanks are also due to my Ph.D committee members, Prof. J. Schuur, Prof. A. Haddow, and Prof. B. Feeny. In addition to being a member in my Ph.D committee, every one of them taught me a graduate course which I found to be very useful and helpful.

Here, I find it a good opportunity to extend my thanks to a great Professor from whom I also learned a lot. He is Prof. H. Khalil of the Electrical Engineering department.

My sincere thanks are also due to my sponsoring agency, the general organization for technical education and vocational training (GOTEVT) of Saudi Arabia, for giving me this opportunity to learn and achieve my Ph.D degree. I also deeply appreciate partial support from the U.S. National Science Foundation.

I will never forget to thank my parents and my wife's parents whose continuous prayers and directions were like the light that showed me the way.

Last but not least, I keep my deep thanks for my wife for her support throughout my studies here in the US. I ask ALLAH to reward her the best in this life and in the hereafter.

TABLE OF CONTENTS

LIST OF FIGURES

LIST OF TABLES

CHAPTER 1

Introduction

Tuned vibration absorbers are one of the most successful and widely used methods for reducing excessive vibration levels in mechanical systems. The linear theory of simple vibration absorber systems is very well established. However, there remains much to learn about the dynamics of systems composed of multiple absorbers, especially when nonlinear behavior is taken into account. In this thesis we focus on the linear and nonlinear dynamic response of systems of nearly identical absorbers of both translational and torsional types.

Many methods can be employed to reduce vibration levels, including the addition of inertia, such as lumped masses or flywheels [1], or the implementation of tuned vibration dampers [2, 3, 4]. These methods, however, each have some shortcomings. Increased inertia has several undesirable side effects, while tuned dampers dissipate energy and are typically valid only for a range near a single resonance frequency (or a small set of them). In cases where the excitation frequency is known and essentially fixed, lightly damped, tuned absorber systems are very effective. Such system are the focus of this investigation.

The thesis considers the general problem of a primary inertia that is subjected to a fluctuating load and to which are attached several identical, or nearly identical, tuned vibration absorbers that are used to reduce the vibration amplitude of the primary mass. Such arrangements of absorbers are quite common and are used to balance inertias and forces in the system. It is typically expected that these absorbers move in a synchronous, or unison, manner, thereby rendering the system dynamically equivalent to that with a single absorber mass. The overall objective of this thesis is to explore the effects of weak nonlinearities and small imperfections among the absorbers. Of particular interest are dynamic instabilities and bifurcations, non-unison responses, and localized responses in which one absorber moves with a much larger amplitude than the others. Since the mathematical structure of the dynamic equations are very similar, both translational and torsional vibration absorbers are considered. However, the main emphasis is on torsional absorbers, since it is more common to use light damping in these systems.

Much of the work in this thesis deals specifically with centrifugal pendulum vibration absorbers (CPVAs), a particular type of torsional absorber. CPVAs are a very effective method for reducing torsional vibrations in rotating machinery. They consist of small masses mounted on the rotor whose vibration is being addressed. During operation, these masses move along specific paths relative to the rotor, and these paths are designed to dynamically counteract the applied torque that causes torsional vibration. CPVAs have been successfully used in IC engines and helicopter rotors. These absorbers take advantage of the centrifugal field of rotation in order to self-tune to a given order of excitation over a range of rotation rates. The selection of the path of the absorber masses allows one to set a desired linear tuning, as well as to design for a beneficial large-amplitude, nonlinear behavior. In this system other nonlinearities arise due to large-amplitude coupling effects. These are accounted for in the analysis, but are shown to be of higher order.

The remainder of this chapter consists of a brief history and some background on vibration absorbers, followed by an overview of the content of the main body of the thesis.

1.1 History and Background

1.1.1 History

A good review of the developments of tuned vibration absorbers for vibration and noise suppression is given by Sun *et al.* [5], from which the following summary was distilled. Since its invention almost a century ago, many designs for the tuned vibration absorber have been developed and successfully used. The simplest and the most favorable is a spring-mass oscillator. Some other designs included an ER-fluid rotary dynamic absorber, a dynamic absorber of ring type with a distributed support spring, a beam-type absorber, and a magnetic dynamic absorber that uses eddy currents to provide damping. Tuned absorbers with multi degrees of freedom, which allow for vibration reduction at several excitation frequencies, have also been studied.

As mentioned before, CPVAs have been efficiently used to reduce torsional vibrations in rotating and reciprocating machinery. The original ideas for CPVAs go back to the early 1900's, although it was not until WWII that they came into wide use. A thorough history on the theory and implementation of CPVAs can be found in the works by C. T. Lee [6], V. Garg [7], and C. P. Chao [8]. What follows is a brief history summary that will provide a better understanding of the objectives of this work.

CPVAs were used in IC (internal combustion) engines as early as 1929 [9]. They have been effectively employed to reduce torsional vibrations in light aircraft engines [3], diesel cam-shafts, and automotive racing engines and there are continuous efforts to investigate and improve their performance. It should be noted however, that until around 1980, all designs used circular paths for the absorber masses. In recent years, other paths that offer improved performance have been introduced. Cycloidal path absorbers are used in helicopter rotors [10], and epicycloidal path absorbers have been proposed for use in automotive engines [11, 12, 13]. There are many possible physical arrangements for CPVA systems. The treatise by Wilson [3] offers a thorough background and overview of CPVA systems, as well as detailed analyses of their application to flexible rotating shafts using linear vibration theory.

One of the earliest considerations of nonlinear effects is found in the paper of Den Hartog [14], where the shortcomings of circular paths are described. The paper also outlines a remedy for this problem, by intentionally mistuning the path so that it comes into more favorable tuning as the amplitude grows. Newland [15] expanded on this idea by providing a detailed analysis of the failure of circular paths and offering a guideline for the level of mistuning. After that, much of the work focused on linear vibration applications, although the patent of Madden [10], in which cycloidal paths are put forward, was an important step forward into the nonlinear regime. Subsequently, the work of Denman and co-workers [11, 12] pushed the subject even further by exploring more paths as well as implementation in an experimental automotive four-cylinder engine.

In a study that considered a wider range of possibilities for the absorber paths, Lee and Shaw [16] investigated the performance of a single CPVA mass for the case of perfectly tuned absorber paths with a quite general nonlinear character. They confirmed the well known shortcomings of circular paths and demonstrated the improvements offered by cycloidal and epicycloidal paths. (The epicycloidal path is special, since it yields essentially linear absorber dynamics over a large amplitude range.) Those results were generalized to also include the effects of intentional linear mistuning by Shaw *et al.* [17]. It was shown that circular path absorbers with some positive mistuning work quite well and behave very linearly over a wide amplitude range (these are widely used in practice), but that perfectly tuned cycloids offer even better performance.

In a treatment of a purely nonlinear absorber system, Lee *et al.* [18] considered a pair of absorbers riding on what they called sub-harmonic epicycloidal paths, which are tuned to an order equal to one-half that of the applied torque excitation. In this case the desired response is a sub-harmonic motion in which the absorbers move exactly out of phase with respect to one another. This arrangement offers ideal performance in terms of vibration reduction, but requires more space for implementation. Chao and Shaw [19] investigated the effects of intentional mistuning on these sub-harmonic absorber systems and showed that their dynamic stability can be made quite robust by a slight over-tuning at the linear or nonlinear order.

In the area of identical, multi-absorber systems, Chao *et al.* [20] studied the stability of the unison motion for systems of multiple CPVAs riding on perfectly tuned epicycloidal paths, and considered the post-bifurcation dynamics of these systems [21]. They showed that the unison response could become unstable, resulting in a type of nonlinear localized response in which one absorber moves with a much larger amplitude than the others. It was shown that this response actually slightly improved the vibration reduction characteristics of the system, but that it significantly reduced the torque operating range of the system. Chao and Shaw [22] also considered the stability and performance of multiple pairs of sub-harmonic absorbers, including the effects of imperfections and mistuning. They showed that multiple pairs of absorbers can be made to behave like a single pair, again by imposing a very slight over-tuning at the linear order.

Another topic that arises in the study of systems of absorbers is the phenomenon of mode localization. This follows since the absorber system possesses several nearly-identical subsystems that are weakly coupled through the primary inertia, which is typically much larger than the total absorber inertia. Such a system is ripe for localization, since it is known that if the degrees of freedom of a nominally periodic structure are weakly coupled, and there exist some small imperfections in the structure, then the free vibration modes typically localize in terms of spatial energy distribution. This results in confined regions of the structure where vibration amplitudes are much larger than predicted using the perfectly tuned model. This type of localization was first considered in the field of solid state physics by Anderson [23], who showed that in a randomly disordered linear chain of particles, the quantum-mechanical wave function of the chain can exhibit spatially confined modes of motion. One of the earliest studies of the phenomenon of localization in the field of structural dynamics was made by Hodges [24]. Subsequently, Pierre and Dowell [25] investigated the localization phenomenon for a chain of coupled oscillators, and Pierre *et al.* [26] theoretically and experimentally investigated localization of the free modes of vibration of disordered multi-span beams constrained at irregular intervals. Wei and Pierre [27, 28] studied both free and forced vibration localization in nearly periodic mistuned assemblies with cyclic symmetry. Also, it has recently been found that localization can occur in nonlinear systems, even when the subsystems are perfectly tuned. In this case, the mistuning is caused by the amplitude dependence of the subsystems' frequencies. Samples of work on localization phenomenon in both linear and nonlinear systems can be found in [29, 30, 31].

The present work fills in some important gaps in the results known for multi-absorber systems, and offers another application of mode localization. In particular, the case of multiple identical absorbers with general paths, including a range of linear mistunings and nonlinearities, is considered. In addition, mode localization is investigated for systems of absorbers in which small imperfections exist among the absorbers.

1.1.2 Background

For background purposes, the well-known results from linear vibration theory for both translational and torsional single-mass vibration absorbers are given in this section.

Figures 1.1, and 1.2 show the single-mass translational and torsional vibration absorbers, respectively. In the translational vibration absorber, the absorber parameters, which are the spring stiffness, k_a, and the absorber mass, m_a are chosen such that the absorber's natural frequency, $\sqrt{\frac{k_a}{m_a}}$, is equal to that of the excitation, ω_{dr}. This, as shown on the frequency response curve of Figure 1.3, theoretically results in complete elimination of the steady-state vibration of the primary mass, M at the driving frequency. Damping alters this ideal picture, but small damping only slightly alters the results. (Optimal damping parameters can be selected to reduce the vibration amplitude across the frequency range; this is the common tuned damper [32].) In torsional vibration absorbers, the parameters R and r shown in Figure 1.2 are chosen such that the square root of their ratio, i.e., $\sqrt{\frac{R}{r}}$, is equal to the order of the applied torque n, where the applied torque is approximated to be harmonic of order n. i.e.,

$$T = T_o \sin(n\Omega t)$$

where Ω is the mean rotation rate of the primary inertia. For example, in four-stroke IC (internal combustion) engines, n is equal to half the number of cylinders. When this is done, the path is said to be **tuned** to order n, since the linearized natural frequency of the pendulum in the constant rotation case is equal to n times the rotation rate. The frequency response curve here is similar to that shown in figure 1.3 with the difference that here the pendulum vibration absorber will eliminate the rotor's torsional vibration for any rotor speed, Ω. (Here the system is tuned to a given order, rather than a given frequency.) Also, the lower resonance peak corresponds to a rigid body mode and is therefore at zero frequency.

It should noted here that these results are obtained using the linear theory for a single absorber mass, or the dynamically equivalent case of multiple, identical absorber masses moving in unison.

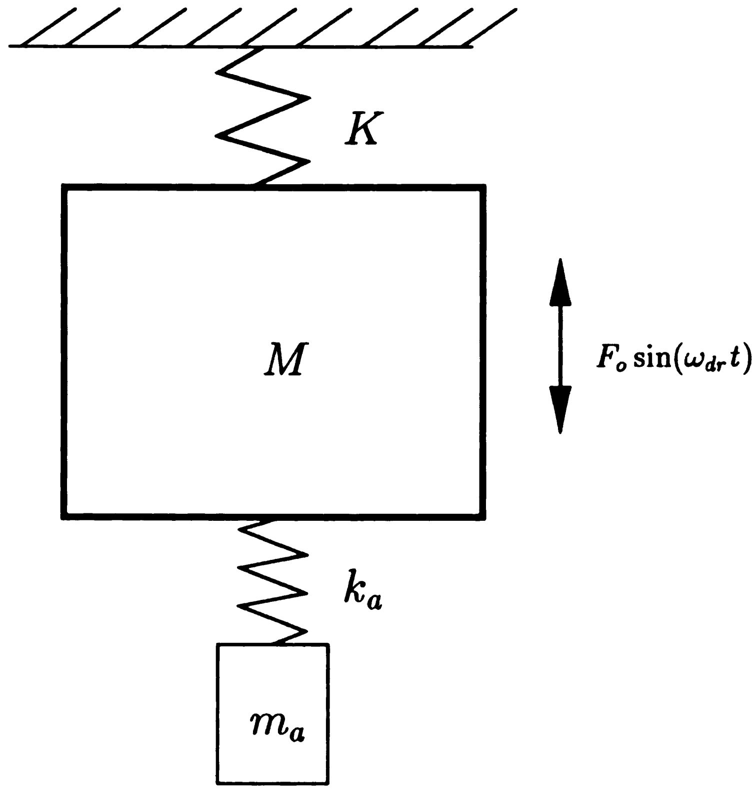

Figure 1.1. Translational vibration absorber.

1.2 Objective and Dissertation Organization

The present research has been aimed toward providing a better understanding of the important problem of determining the conditions under which systems of nearly identical vibration absorbers behave like their single-mass counterparts, and the consequences of situations in which this assumption does not hold. This is done by analyzing and studying the following topics, which form the chapters of the thesis:

- **Forced, unison response of general path CPVAs.**

  The unison response and its stability for multiple absorbers is investigated. General CPVA paths with linear mistuning are considered, and guidelines for designs are provided. This study is presented in Chapter 2.

- **Non-unison steady state responses in CPVA systems.**

  The existence and stability of a certain class of non-unison steady state responses in CPVA systems is investigated. This study is presented in Chapter 3.

- **Localization in vibration absorbers.**

  - Localization in the linear free vibration modes of absorber systems. Systems of nearly identical translational and torsional vibration absorbers are investigated for the possibility of the existence of free vibration mode localization. This problem is different from what is available in the literature in the sense that the coupling between the absorbers is not direct, but rather arises in an indirect manner through the primary inertia. This study is presented in Chapter 4.
  - Linear and non-linear forced, localized response of general path CPVA systems. Here, the existence and stability of forced, localized responses in systems of CPVAs is investigated. The results of this study are presented in Chapter 5.

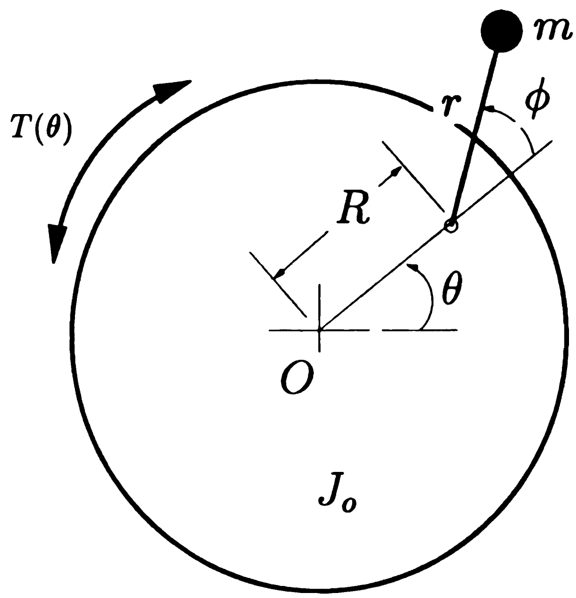

Figure 1.2. Torsional vibration absorber.

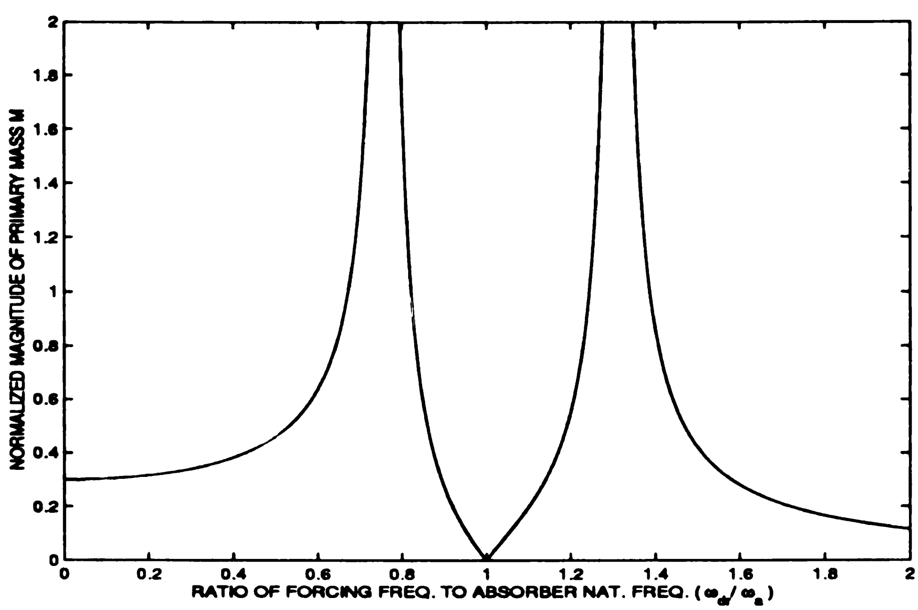

Figure 1.3. Frequency response of the mass M of Figure 1.1

CHAPTER 2

Performance and Dynamic Stability of General-Path CPVAs

In this chapter, the performance and dynamic stability of systems comprised of multiple, identical centrifugal pendulum vibration absorbers that have general paths are considered. The study is carried out by considering a scaling of the system parameters, based on physically realistic ranges of dimensionless parameters, which allows for application of the method of averaging. It is found that the performance of theses systems is limited by two distinct types of instabilities. In one type, the system of absorbers lose their synchronous character, while the other is a classical nonlinear jump behavior that affects all absorbers identically, and leads to highly undesirable system behavior. These results are used to evaluate the common types of absorber paths, namely circles, and cycloids including intentional levels of mistuning. The results are also used to make some recommendations about the selection of paths to achieve design goals in terms of absorber performance and operating range. The analytical predictions are confirmed by numerical simulations.

2.1 Mathematical Model

2.1.1 Equations of Motion

A system of N CPVAs mounted on a rotor of inertia J, as shown schematically in Figure 2.1, is considered. These absorbers, each with a mass of m_i, ride on paths specified by the arc length variables S_i's. These arc length variables are symmetric about their vertices. Their origins are taken to be at their vertices. The distance from any point on the i^{th} absorber path to the center of rotation of the rotor, O, is specified by the variable R_i. At the vertex of the i^{th} absorber path, this distance is R_{io}, *i.e.*, $R_i(S_i = 0) = R_{io}$. For each path, this distance is an even function of the the arc length variable S_i, *i.e.*, $R_i(S_i) = R_i(-S_i)$. This is due to the symmetry of each path. The rotor is subjected to an external torque that has a mean, T_o, and a fluctuating, $T(\theta)$, components.

The kinetic energy of the system consists of the kinetic energy of the rotor and that of the absorbers. The rotor's kinetic energy is

$$T_r = \frac{1}{2}J\dot{\theta}^2,$$

where $\dot{\theta}$ is the rotation rate of the rotor. The kinetic energy of the i^{th} absorber is

$$T_{ai} = \frac{1}{2}m_i\vec{v}_i.\vec{v}_i,$$

where $\vec{v}_i$ is the velocity of the i^{th} absorber. This velocity is given by

$$\vec{v}_i = R_i\dot{\theta}\ \vec{e}_\theta + \dot{S}_i\ \vec{e}_{S_i},$$

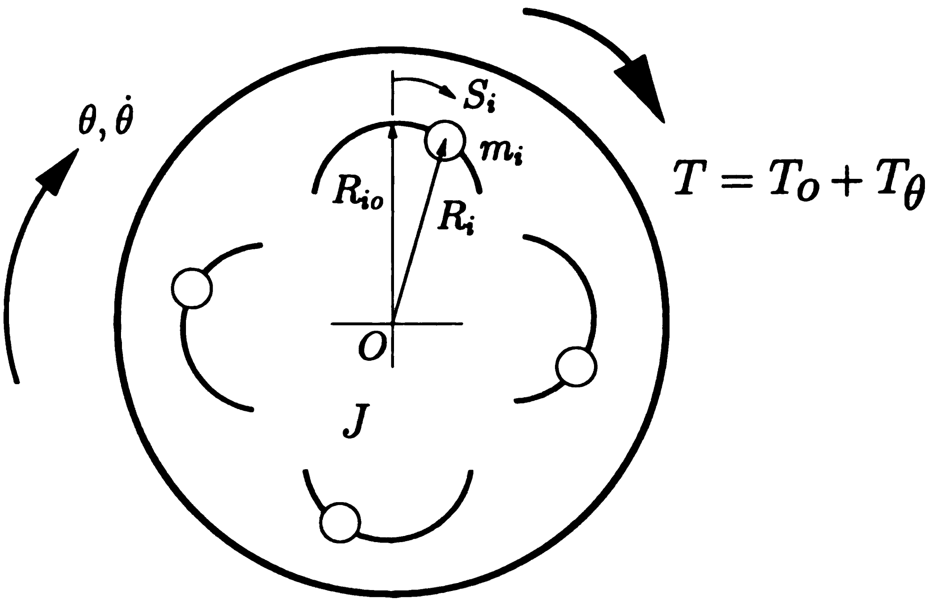

Figure 2.1. Schematic diagram of multiple CPVAs arrangement.

where $\vec{e}_\theta$ and $\vec{e}_{S_i}$ are unit vectors in the θ and S_i direction respectively. Looking at Figure 2.2, it can be seen that the dot product $\vec{e}_\theta.\vec{e}_{S_i}$ is equal to $R_i\frac{d\phi_i}{dS_i}$. It is also clear from Figure 2.2 that the following relationship holds:

$$\begin{aligned}(dS_i)^2 &= (dR_i)^2 + (R_i d\phi_i)^2, \text{ or} \\ \vec{e}_\theta.\vec{e}_{S_i} &= \sqrt{1 - \left(\frac{dR_i}{dS_i}\right)^2}.\end{aligned}$$

The total kinetic energy will then be

$$T = \frac{1}{2}\left\{J\dot{\theta}^2 + \sum_{i=1}^{N} m_i\left(X_i\dot{\theta}^2 + \dot{S}_i^2 + 2\dot{\theta}\dot{S}_i\tilde{G}_i\right)\right\},$$

where

$$\left.\begin{aligned}X_i(S_i) &= R_i^2(S_i), \\ \tilde{G}_i(S_i) &= \sqrt{X_i(S_i) - \tfrac{1}{4}(\tfrac{dX_i}{dS_i}(S_i))^2}.\end{aligned}\right\} \quad (2.1)$$

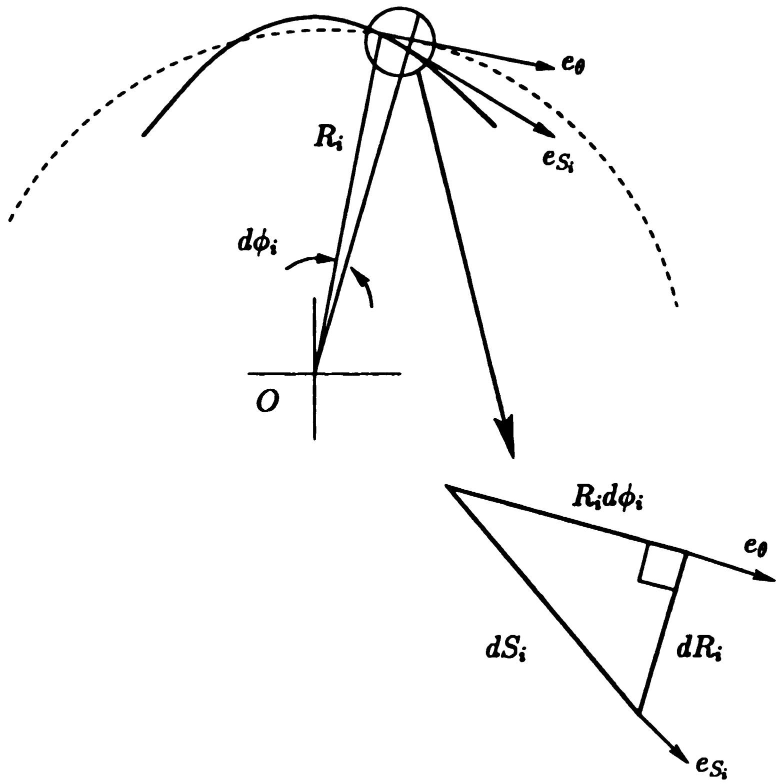

Figure 2.2. CPVAs

To reach to the dynamic equations that govern the system motion, Lagrange's method is applied with the reasonable assumption that potential energy is small and could be ignored. This is due to the fact that potential energy arises only from gravitational effect, which is small compared to centrifugal effects for any reasonable rotation speed of the rotor. Lagrange's method is applied as follows:

$$\frac{d}{dt}\left(\frac{\partial T}{\partial \dot{q}_l}\right) - \frac{\partial T}{\partial q_l} = Q_l, \;\; l = 1, ..., N+1,$$

where $q_1 = \theta$, and $q_j = S_i,\;\; j = 2, 3, ..., N+1$, and $i = 1, 2, ..., N$ are the generalized coordinates. Q_l's are the generalized forces. The generalized forces are:

$$
\begin{aligned}
Q_1 &= -c_o\dot{\theta} + \sum_{i=1}^{N} c_{ai}\dot{S}_i R_i \sqrt{1 - \left(\frac{dR_i}{dS_i}\right)^2} + T_o + T(\theta) \\
&= -c_o\dot{\theta} + \sum_{i=1}^{N} c_{ai}\dot{S}_i \tilde{G}_i + T_o + T(\theta), \\
Q_j &= -c_{aj}\dot{S}_j, \qquad j = 2, 3, ..., N+1,
\end{aligned}
$$

where c_{ai}, and c_o are the damping coefficients for the i^{th} absorber and the rotor bearing respectively. The equations of motion will then be

$$
m_i[\ddot{S}_i + \tilde{G}_i(S_i)\ddot{\theta} - \tfrac{1}{2}\tfrac{dX_i}{dS_i}(S_i)\dot{\theta}^2] = -c_{ai}\dot{S}_i, \tag{2.2}
$$

$$
\begin{aligned}
&J\ddot{\theta} + \textstyle\sum_{i=1}^{N} m_i[\tfrac{dX_i}{dS_i}(S_i)\dot{S}_i\dot{\theta} + X_i(S_i)\ddot{\theta} + \tilde{G}_i(S_i)\ddot{S}_i \\
&\quad + \tfrac{d\tilde{G}_i}{dS_i}(S_i)\dot{S}_i^2] = \textstyle\sum_{i=1}^{N} c_{ai}\tilde{G}_i(S_i)\dot{S}_i - c_o\dot{\theta} + T_o + T(\theta).
\end{aligned} \tag{2.3}
$$

The i^{th} absorber is indirectly coupled to other absorbers through the dynamics of the rotor, as is clear from equation (2.2), which describes its dynamics. Equation (2.3) represents the torque balance on the rotor.

These equations represent an autonomous dynamical system, because the varying component of the applied torque, $T(\theta)$, is expressed as a function of the rotor angle θ. For purposes of subsequent analysis, it is convenient to convert the equations in such a manner that the rotor angle serves as the independent variable, replacing time. To this end, a new non dimensional variable v is defined as the ratio of the rotor angular velocity to the nominal rotor angular velocity , *i.e.*,

$$
v \equiv \frac{\dot{\theta}}{\Omega}. \tag{2.4}
$$

This dynamic variable will be used to represent rotor speed and acceleration. Using the chain rule, one can obtain the following relationships between derivatives with respect to time and derivatives with respect to θ:

$$\left.\begin{aligned}
\ddot{\theta} = \tfrac{d^2\theta}{dt^2} &= \Omega^2 v \tfrac{dv}{d\theta} = \Omega^2 v v', \\
\dot{(.)} = \tfrac{d(.)}{dt} &= \Omega v \tfrac{d(.)}{d\theta} = \Omega v (.)', \\
\ddot{(.)} = \tfrac{d^2(.)}{dt^2} &= \Omega^2 v \tfrac{dv}{d\theta}\tfrac{d(.)}{d\theta} + \Omega^2 v^2 \tfrac{d^2(.)}{d\theta^2}, \\
&= \Omega^2 v v'(.)' + \Omega^2 v^2 (.)''.
\end{aligned}\right\} \tag{2.5}$$

After equations (2.2,2.3) are nondimensionalized, and the independent variable is changed from t to θ, the equations of motion become

$$v s_i'' + [s_i' + \tilde{g}_i(s_i)]v' - \frac{1}{2}\frac{dx_i}{ds_i}(s_i)v = -\mu_{ai} s_i', \tag{2.6}$$

$$\begin{aligned}
&\textstyle\sum_{i=1}^N b_i[\frac{dx_i}{ds_i} s_i' v^2 + x_i(s_i) v v' + \tilde{g}_i(s_i) s_i' v v' \\
&\quad + \tilde{g}_i(s_i) s_i'' v^2 + \frac{d\tilde{g}_i}{ds_i}(s_i) s_i^2 v^2] + v v' \\
&\quad = \textstyle\sum_{i=1}^N b_i \mu_{ai} \tilde{g}_i(s_i) s_i' v - \mu_o v + \Gamma_o + \Gamma(\theta),
\end{aligned} \tag{2.7}$$

where

$$\begin{aligned}
s_i &= S_i/R_{io},\ \ \tilde{g}_i(s_i) = \tilde{G}_i(S_i)/R_{io},\ \ b_i = I_i/J, \\
I_i &= m_i R_{io}^2,\ \ \mu_{ai} = c_{ai}/m_i\Omega,\ \ \mu_o = c_o/J\Omega, \\
\Gamma_o &= T_o/J\Omega^2,\ \ \Gamma(\theta) = T(\theta)/J\Omega^2,
\end{aligned}$$

and

$$\begin{aligned}
x_i(s_i) &= X_i/R_{io}^2, \\
\tilde{g}_i(s_i) &= \sqrt{x_i(s_i) - \tfrac{1}{4}(\tfrac{dx_i}{ds_i}(s_i))^2}.
\end{aligned} \tag{2.8}$$

Note that the system now is non-autonomous, but its order has been reduced, since only first derivatives in v appear. Assuming that all absorbers have equal masses and equal damping, and all paths have the same value of R_i at each vertex, *i.e.*,

$m_i = m,\ c_{ai} = c_a,\ R_{io} = R_o\ \forall i \in [1, N]$, equation (2.7) becomes

$$\begin{aligned}\tfrac{b_o}{N}\textstyle\sum_{i=1}^{N}[\tfrac{dx_i}{ds_i}s_i'v^2 + x_i(s_i)vv' + \tilde{g}_i(s_i)s_i'vv' \\ +\tilde{g}_i(s_i)s_i''v^2 + \tfrac{d\tilde{g}_i}{ds_i}(s_i)s_i^2v^2] + vv' \\ = \tfrac{b_o}{N}\textstyle\sum_{i=1}^{N}\mu_a\tilde{g}_i(s_i)s_i'v - \mu_o v + \Gamma_o + \Gamma(\theta),\end{aligned} \tag{2.9}$$

where

$$b_o = \frac{I_o}{J},\ I_o = m_o R_o^2,\ \mu_a = \frac{Nc_a}{m_o\Omega},\ \text{and}\ m_o = Nm.$$

The fluctuating torque generally contains several harmonics. In most situations only one or two harmonics have significant amplitude, and therefore we approximate the fluctuating torque by its dominant harmonic, taken to be of order n, as follows: $\Gamma(\theta) = \Gamma_\theta \sin(n\theta)$. For example, in four-stroke IC engines, n is equal to half the number of cylinders.

Note on the Damping:

The damping on the main rotor does not have a role on the system other than setting its nominal speed by balancing the mean component of the applied torque. However, the absorber damping has a great effect on the system performance. Due to the fact that this damping is complicated and depends on the way the absorbers are implemented, its modeling is quite difficult. In this work, similar to the linear case, the absorber damping is modeled as an equivalent viscous damping that does not depend on the mass of the absorber. With this, the quantity $\frac{\mu_a}{N} = \frac{c_a}{m_o\Omega}$ is a fixed physical quantity and does not depend on the number of absorbers as long as their total mass is fixed. This indicates that the non-dimensional damping coefficient, μ_a, is proportional to the number of absorbers.

2.1.2 General Path Representation

As described in Denman [11], it is convenient to represent the general path for the i^{th} absorber by the local radius of curvature at any point on the path, given by

$$\rho_i^2 = \rho_{io}^2 - \lambda^2 S_i^2,$$

where ρ_{io} is the path's radius of curvature at the vertex, which dictates the small amplitude nature of the path. λ dictates the large amplitude character of the path, and can take any value from zero to one. Some special cases of interest are: $\lambda = 0$ describes a circular path, $\lambda = \lambda_e = \sqrt{\frac{\tilde{n}_i^2}{(\tilde{n}_i^2+1)}}$ describes an epicycloidal path with its base circle of radius $(R_{io} - \rho_{io})$ centered at the rotor center (the so-called tautochronic path of order $\tilde{n}_i$ [11]), and $\lambda = 1$ describes a cycloidal path. Note that the value of λ dictates the nature of the amplitude-dependent frequency of the absorber when it oscillates freely along its path. In fact, when the rotor speed is constant, the epicycloid case separates softening nonlinearities, like the circular path, from hardening nonlinearities, like the cycloidal path.

The order of the path is given by the square root of the ratio between the distance from the rotor center to the center of the path vertex circle and the path vertex radius of curvature, that is

$$\tilde{n}_i = \sqrt{\frac{R_{io} - \rho_{io}}{\rho_{io}}}. \tag{2.10}$$

This fixes the linearized natural frequency of the i^{th} absorber, when the rotor spins at a constant rate Ω, to be $\tilde{n}_i\Omega$. This frequency is used for tuning the absorber at small amplitudes, but it affects the large amplitude dynamics as well.

In the equations of motion an expression for $x_i(s)$ for the general absorber path is needed (see equations (2.6,2.9)). The following expression can be reached by expanding in s_i,

$$x_i(s_i) = 1 - \tilde{n}_i s_i^2 + \gamma_i s_i^4 + O(s_i^6), \tag{2.11}$$

where

$$\gamma_i = (\frac{1}{12})(\tilde{n}_i^2 + 1)^2(\tilde{n}_i^2 - \lambda^2(1 + \tilde{n}_i^2)).$$

Note that this expanded form is used in the analysis, but the full form of $x_i(s_i)$ is used in the numerical simulations.

2.1.3 Scaling

Since the ratio of the total absorbers' inertia, I_o, to the rotor inertia, J, is small, we define a small parameter ϵ as

$$\epsilon^p = b_o.$$

This parameter will form the basis used for the scaling. Note that in the unperturbed case, $\epsilon = 0$, the rotor dynamically decouples from the absorbers.

Based on the purely linear theory of CPVAs, the order of the path should be tuned to the frequency of the disturbance torque. However, certain nonlinear effects are nicely handled by incorporating a small level of intentional linear mistuning on the path. To account for the mistuning, the path order in this analysis is taken to be

$$\tilde{n}_i = n(1 + \epsilon^q \sigma_i),$$

where σ_i represents a measure of the mistuning of the i^{th} absorber path. Such mistuning is always intentionally built into existing circular path absorbers in order to counteract some undesirable nonlinear effects [15].

The preferred absorber configuration has small damping, since it remains at the set tuning at all rotational speeds. Also, the fluctuating torque amplitude is small compared to the kinetic energy of the rotor, rendering the non-dimensional torque amplitude small. Therefore, the parameters μ_a, μ_o, Γ_o, and Γ_θ can also be taken to be small and are scaled by ϵ as follows:

$$\mu_a = \epsilon^l \tilde{\mu}_a, \;\; \mu_o = \epsilon^l \tilde{\mu}_o, \;\; \Gamma_o = \epsilon^l \tilde{\Gamma}_o, \;\; \Gamma_\theta = \epsilon^r \tilde{\Gamma}_\theta.$$

In addition, the absorber oscillations are assumed to scale with the fluctuating torque level in some manner, and so we take

$$s_i = \epsilon^\nu z_i. \tag{2.12}$$

We now turn to the matter of balancing the desired terms in the equations of motion so that the applied torque, the damping, and the nonlinearities come into play at the same order. We begin with a couple of preliminary expansions.

Note that when $\epsilon = 0$, *i.e.*, $b_o = 0$, equation (2.9) states that the rotor spins at a constant angular speed, Ω. For $0 < \epsilon << 1$, the rotor will have small fluctuations about the constant angular speed, Ω. Therefore, it is convenient to expand the rotor speed as follows:

$$v(\theta) = 1 + \epsilon^w v_w(\theta) + HOT, \tag{2.13}$$

where HOT means higher order terms.

The path function can be expanded in terms of ϵ as well. Evaluating $\tilde{g}_i$ using equation (2.8), along with equation (2.11), and expanding it and γ_i in powers of ϵ^q, the following expressions can be reached

$$\begin{aligned} \tilde{g}_i(s_i) &= 1 - \frac{(n^2 + n^4)s_i^2}{2} + HOT \\ \gamma_i &= \gamma_o + O(\epsilon^q) \end{aligned} \tag{2.14}$$

where

$$\gamma_o = (\frac{1}{12})(n^2+1)^2(n^2-\lambda^2(1+n^2)). \qquad (2.15)$$

Note that $\gamma_o < 0$ (softening) corresponds to $\lambda > \lambda_e$ while $\gamma_o > 0$ (hardening) corresponds to $\lambda < \lambda_e$.

The final preliminary step is to note that in order for the constant torque terms to balance, $\Gamma_o = \mu_o$ must hold. This states that the constant applied torque is offset by the bearing damping torque arising from the mean rotation rate. Note that if a constant load torque is introduced into the equations of motion, it is simply counterbalanced here by Γ_o, such that the mean spin rate is maintained.

Substituting the above scaled parameters, the constant torque balance, the expressions for $\tilde{g}_i(s_i), \gamma_i$, and $v(\theta)$ into equation (2.9), expanding, matching terms according to $r = (p+\nu)$, and keeping the $(r+\nu)$ order terms, one finds that the non-dimensional rotor acceleration is given by

$$vv'(\theta) = \epsilon^r\{\frac{1}{N}\sum_{j=1}^{N} n^2 z_j + \tilde{\Gamma}_\theta \sin(n\theta)\} + \frac{\epsilon^{r+\nu}}{N}\sum_{j=1}^{N} 2n^2 z_j z_j' + HOT. \qquad (2.16)$$

Using this result in equation (2.6), a suitable choice of the scaling orders is found to be

$$q = 1,\ \nu = \tfrac{1}{2},\ l = 1,\ r = \tfrac{3}{2},\ p = 1,\ w = \tfrac{3}{2}.$$

This leads to the desired form of the absorber equations, to which we now turn.

2.1.4 The Averaged Equations

With the above scaling results, the rotor dynamics can be eliminated (using the ϵ^r terms in equation (2.16)), resulting in the following uncoupled equations that describe the absorbers dynamics,

$$
\begin{aligned}
z_i'' + n^2 z_i = \epsilon[2\gamma_o z_i^3 - 2n^2\sigma_i z_i - \tilde{\mu}_a z_i' \\
- \tfrac{1}{N}\textstyle\sum_{j=1}^{N} n^2 z_j - \tilde{\Gamma}_\theta \sin(n\theta)] + HOT.
\end{aligned}
\tag{2.17}
$$

It should be noted here that at the order considered, the only nonlinear effect that appears is the one due to the path, i.e $\gamma_o z_i^3$. Missing at this order are all of the nonlinear terms that arise from the kinematic coupling of the rotation and the absorber motion. The nonlinear path term is zero for epicycloidal paths because $\gamma_o = 0$ (see equation (2.15) along with the definition of λ). In this case, the model reduces to the linearized model, with which it is impossible to capture any nonlinear effects. Therefore, in order to analyze the case of epicycloidal paths, one has to employ a scaling wherein nonlinearities other than the path nonlinearity are retained. Chao *et al.* [20] have done this, and analyzed the case of perfectly tuned epicycloidal paths in some detail. In the present study, epicycloidal paths are not considered.

Note that the absorbers' dynamics are now uncoupled from the rotor dynamics to leading order, and equations (2.17) represent a set of weakly non-linear, weakly coupled oscillators. These have the very special feature that they all have the same unperturbed natural frequency, and are all resonantly excited by the fluctuating applied torque. Furthermore, the absorbers are all coupled to one another in an identical fashion, and when the mistuning is zero ($\sigma_i = 0 \ \forall i$), this forms a system with a special symmetry (see [8]).

The averaging method will be used to determine approximate steady-state solutions of these equations. To obtain the standard periodic form, the usual transformation to polar coordinates is used,

$$
\left.
\begin{aligned}
z_i &= a_i \sin(n\theta + \phi_i), \\
z_i' &= n a_i \cos(n\theta + \phi_i).
\end{aligned}
\right\}
\tag{2.18}
$$

The standard periodic form for the equations is then found to be,

$$\begin{aligned} a_i' &= \tfrac{\epsilon}{n} f_i \cos(n\theta + \phi_i) + HOT, \\ \phi_i' &= -\tfrac{\epsilon}{na_i} f_i \sin(n\theta + \phi_i) + HOT, \end{aligned} \tag{2.19}$$

where

$$\begin{aligned} &f_i = 2\gamma_o a_i^3 \sin^3(n\theta + \phi_i) - 2n^2\sigma_i a_i \sin(n\theta + \phi_i) \\ &-\tilde{\mu}_a n a_i \cos(n\theta + \phi_i) - \tfrac{1}{N}\textstyle\sum_{j=1}^{N} n^2 a_j \sin(n\theta + \phi_j) \\ &-\tilde{\Gamma}_\theta \sin(n\theta). \end{aligned} \tag{2.20}$$

The functions f_i are periodic in the independent variable θ, with a period of $(\frac{2\pi}{n})$. Averaging these equations over one period, one reaches the following averaged equations

$$\left.\begin{aligned} &\bar{a}_i' = \epsilon[-\tfrac{\tilde{\mu}_a}{2}\bar{a}_i + \tfrac{\tilde{\Gamma}_\theta}{2n}\sin(\bar{\phi}_i) \\ &\qquad + \tfrac{n}{2N}\textstyle\sum_{j=1, j\neq i}^{N} \bar{a}_j \sin(\bar{\phi}_i - \bar{\phi}_j)] \\ &\qquad + HOT, \\ &\bar{a}_i\bar{\phi}_i' = \epsilon[-\tfrac{3\gamma_o}{4n}\bar{a}_i^3 + n(\sigma_i + \tfrac{1}{2N})\bar{a}_i \\ &\qquad + \tfrac{\tilde{\Gamma}_\theta}{2n}\cos(\bar{\phi}_i)] \\ &\qquad + \tfrac{n}{2N}\textstyle\sum_{j=1, j\neq i}^{N} \bar{a}_j \cos(\bar{\phi}_i - \bar{\phi}_j)] \\ &\qquad + HOT, \end{aligned}\right\} \tag{2.21}$$

where an overbar indicates the averaged value of the corresponding variable. These equations are the basis of the analysis of the system dynamics.

2.1.5 Existence and Stability of the Unison Response

In this section we consider the case in which all absorbers are identical and move in a perfectly synchronous manner. This is the desired response of the absorbers, so its existence and stability are of interest.

One objective of this study is to determine the effects of intentional linear mistuning, and so we fix an identical level of mistuning for all absorber paths, as follows,

$$\sigma_i = \sigma \qquad \forall i \in [1, N].$$

When a unison response occurs, all the absorbers have the same vibration amplitude and phase, *i.e.*,

$$\bar{a}_i = \bar{a}_j = r_z,$$

$$\bar{\phi}_i = \bar{\phi}_j = \phi_z.$$

When these are substituted into equations (2.21), they become pairwise identical and reduce to the following,

$$\left.\begin{aligned} r_z' &= \epsilon[-\tfrac{\tilde{\mu}_a}{2} r_z + \tfrac{\tilde{\Gamma}_\theta}{2n}\sin(\phi_z) + HOT, \\ r_z\phi_z' &= \epsilon[-\tfrac{3\gamma_o}{4n} r_z^3 + n(\sigma + \tfrac{1}{2}) r_z \\ &\qquad + \tfrac{\tilde{\Gamma}_\theta}{2n}\cos(\phi_z)] + HOT. \end{aligned}\right\} \tag{2.22}$$

The steady-state conditions are given by,

$$\left.\begin{aligned} \tfrac{\tilde{\mu}_a}{2} r_z &= \tfrac{\tilde{\Gamma}_\theta}{2n}\sin(\phi_z), \\ \tfrac{3\gamma_o}{4n} r_z^3 - n(\sigma + \tfrac{1}{2}) r_z &= \tfrac{\tilde{\Gamma}_\theta}{2n}\cos(\phi_z). \end{aligned}\right\} \tag{2.23}$$

Eliminating the phase in the standard manner, and solving for the torque amplitude in terms of the absorber amplitude (for ease of plotting, etc.), one obtains,

$$\tilde{\Gamma}_\theta = 2n\sqrt{[\frac{\tilde{\mu}_a}{2} r_z]^2 + [\frac{3\gamma_o}{4n} r_z^3 - n(\sigma + \frac{1}{2}) r_z]^2}. \tag{2.24}$$

These results relate in a simple manner the absorber response, in terms of amplitude and phase, to the system path parameters, the damping level, and the fluctuating torque amplitude.

In order to analyze the stability of this unison response, the Jacobian of the system given by equations (2.21) must be evaluated at the steady state conditions.

This yields a matrix of the form

$$A = \begin{bmatrix} A1 & A2 & . & . & . & A2 \\ A2 & A1 & A2 & . & . & A2 \\ . & . & . & . & . & . \\ A2 & . & . & . & A1 & A2 \\ A2 & . & . & . & . & A1 \end{bmatrix}_{2NX2N} \tag{2.25}$$

where $A1$ and $A2$ are 2 by 2 matrices with the following entries:

$$\begin{aligned}
A1_{11} &= -\frac{\mu_a}{2}, \\
A1_{12} &= \frac{n}{2N}(N-1)r_z + \frac{\tilde{\Gamma}_\theta}{2n}\cos(\phi_z), \\
A1_{21} &= -\frac{3\gamma_o}{2n}r_z - \frac{\tilde{\Gamma}_\theta}{2nr_z^2}\cos(\phi_z) - \frac{n(N-1)}{2Nr_z}, \\
A1_{22} &= -\frac{\tilde{\Gamma}_\theta}{2n}\sin(\phi_z),
\end{aligned}$$

$$A2_{11} = 0, \;\; A2_{12} = -\frac{n}{2N}r_z, \;\; A2_{21} = \frac{n}{2Nr_z}, \;\; A2_{22} = 0.$$

If all the eigenvalues of the Jacobian matrix have negative real parts, the unison response is exponentially stable. For a system with a Jacobian of a form similar to that of the system considered, it can be shown that each eigenvalue of the 2 by 2 matrix $[A1 - A2]$ is an eigenvalue of the Jacobian matrix A repeated $(N-1)$ times, and the remaining two eigenvalues are the eigenvalues of the matrix $[A1 + (N-1)A2]$ [33]. For the stability evaluation, we will use the fact that the eigenvalues of a 2 by 2 matrix have negative real parts if and only if its determinant is positive and its trace is negative.

The matrix $[A1 - A2]$ is given by

$$A1 - A2 = \begin{bmatrix} -\frac{\mu_a}{2} & \frac{3\gamma_o}{4n}r_z^3 - n\sigma r_z \\ \frac{n\sigma}{r_z} - \frac{9\gamma_o}{4n}r_z & -\frac{\mu_a}{2} \end{bmatrix} \tag{2.26}$$

Its trace is equal to $-\mu_a$ and is always negative. Its determinant is given by

$$Det[A1 - A2] = \frac{27\gamma_o^2}{16n^2}r_z^4 - 3\gamma_o\sigma r_z^2 + (n^2\sigma^2 + \frac{\tilde{\mu}_a^2}{4}). \tag{2.27}$$

The matrix $[A1 + (N-1)A2]$ is given by

$$A1 + (N-1)A2 = \begin{bmatrix} -\frac{\mu_a}{2} & \frac{3\gamma_o}{4n}r_z^3 - n(\sigma + \frac{1}{2})r_z \\ n(\sigma + \frac{1}{2})\frac{1}{r_z} - \frac{9\gamma_o}{4n}r_z & -\frac{\mu_a}{2} \end{bmatrix} \tag{2.28}$$

Its trace is also equal to $-\mu_a$ and its determinant is given by

$$\begin{aligned} Det[A1 + (N-1)A2] = {} & \tfrac{27\gamma_o^2}{16n^2}r_z^4 - \tfrac{3}{2}\gamma_o(1 + 2\sigma)r_z^2 + [n^2\sigma + n^2\sigma^2 \\ & + \tfrac{1}{4}(n^2 + \mu_a^2)]. \end{aligned} \tag{2.29}$$

Since the traces are both negative, no Hopf bifurcations to quasi-periodic motions are possible. The conditions at which stability changes occur are captured by setting $Det[A1 - A2] = 0$ and $Det[A1 + (N-1)A2] = 0$. It is quite simple to solve these conditions for the corresponding critical values of the absorber amplitude, yielding values of r_z at which bifurcations occur. The attendant critical torque levels can then be found from equation (2.24).

It should be noted that solutions coming from equation (2.27) represent critical amplitudes at which the unison motion becomes unstable, but continues to exist, rendering some type of non-synchronous, steady state response. On the other hand, solutions coming from equation (2.29) represent the condition at which the unison response is annihilated in a saddle-node bifurcation, representing a sudden jump in the absorbers' motion to another response branch, which may or may not be of unison type. One can see that $Det[A1 + (N-1)A2] = 0$ corresponds to instabilities that preserve the unison nature of the response by considering the stability of the equivalent single-absorber mass system represented by equation (2.22), and noting that it gives the same instability condition.

When equations (2.27, 2.29) are equated to zero and solved for r_z, the following results are obtained.

For the bifurcation to a non-unison response, *i.e.*, $Det[A1 - A2] = 0$:

$$r_{zbif} = \frac{4n}{\sqrt{54\gamma_o}} \left[3\sigma - \left((3\sigma)^2 - \frac{27}{4n^2}(n^2\sigma^2 + \frac{\tilde{\mu}_a^2}{4}) \right)^{\frac{1}{2}} \right]^{\frac{1}{2}}. \tag{2.30}$$

For the jump condition, *i.e.*, $Det[A1 + (N-1)A2] = 0$

$$r_{zj} \approx \frac{2n}{3} \sqrt{\frac{(\sigma + \frac{1}{2})}{\gamma_o}}, \tag{2.31}$$

where the approximation is noted because we have neglected the damping term in the torque equation, since it is very small compared to other terms. These can be used in equation (2.24) to find the critical torque levels.

The following general observations can be made by considering these two critical conditions:

From the first condition:

- For $\gamma_o > 0$, bifurcation to non-unison can exist only when the level of mistuning is greater than some positive value set by the damping level and n. To be able to see this observation, the damping term was not neglected in this equation as was done in the second equation. (More about this below).

- For $\gamma_o < 0$, bifurcation to non-unison can exist only when the level of mistuning is negative. Fortunately, negative mistunings are not of practical importance as will be shown later. So, this is an advantage for the paths with $\gamma_o < 0$.

From the second condition:

- For $\gamma_o > 0$, a jump exists only when $\sigma > -\frac{1}{2}$.

- For $\gamma_o < 0$, a jump exists only when $\sigma < -\frac{1}{2}$.

It should be recalled here that $\gamma_o > 0$ includes paths where $0 \leq \lambda < \lambda_e$, (see equation (2.15)), that is, paths ranging from circular, up to, but not including, epicycloidal paths. Similarly, $\gamma_o < 0$ includes paths where $\lambda_e < \lambda \leq 1$, that is, paths ranging from, but not including, epicycloidal up to cycloidal.

To see how the absorber damping, as modeled in this work, can alter the value of the critical mistuning level above which bifurcation to non-unison can exist, as was mentioned in the first observation above, the argument of the inner square root in equation (2.30) is equated to zero and solved for that critical mistuning level, σ_{cr}. When this is done, the following equation is obtained:

$$\sigma_{cr} = \frac{\sqrt{3}}{2n}\tilde{\mu}_a.$$

Note that the number of the absorbers, N, is an implicit parameter in this equation. This is because the scaled damping coefficient, $\tilde{\mu}_a$, is proportional to N (see note on the damping above) which means that increasing the number of absorbers increases the damping level. Figure 2.3 represents a plot of this equation for different number of absorbers for the case when the applied torque order, n, is 2. For a better absorbers performance, the damping level should be kept small, as will be shown later. In addition, as it is clear from Figure 2.3, for practical $\tilde{\mu}_a$ values, the the critical mistuning levels below which bifurcations to non-unison can not exist are small. This implies that in the presence of reasonable mistuning levels, it is practically not possible to avoid bifurcations to non-unison.

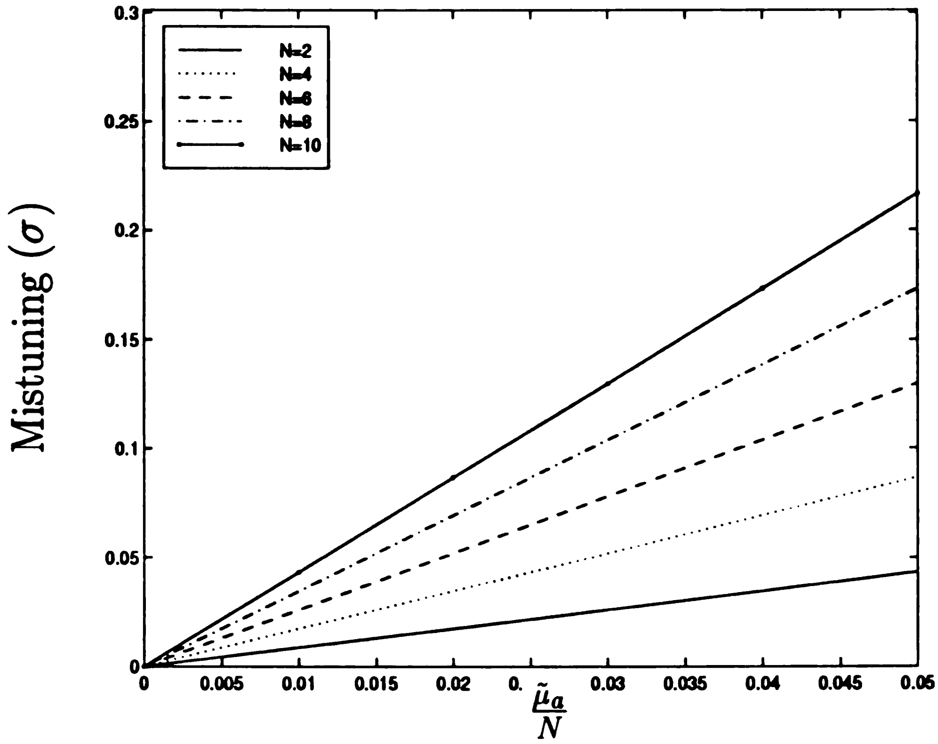

Figure 2.3. Mistuning levels below which non-unison motions do not exist. n=2.

Application to Some Common Absorber Paths

Circular paths:

For circular paths, $\lambda = 0$, which when used in equation (2.15) gives the following expression for the non-linear path coefficient, γ_o:

$$\gamma_o = \frac{1}{12}n^2(1+n^2)^2. \tag{2.32}$$

When this is substituted in equations (2.27,2.29), the following expressions are obtained:

$$Det[A1-A2]_{cir} = \frac{3}{256}n^2(1+n^2)^4 r_z^4 - \frac{1}{4}n^2(1+n^2)^2\sigma r_z^2 + (n^2\sigma^2 + \frac{\tilde{\mu}_a^2}{4}), \tag{2.33}$$

$$Det[A1+(N-1)A2]_{cir} = \frac{3}{256}n^2(1+n^2)^4r_z^4 - \frac{1}{8}n^2(1+n^2)^2(1+2\sigma)r_z^2 + \frac{1}{4}[n^2(1+2\sigma)^2+\tilde{\mu}_a^2], \tag{2.34}$$

corresponding to the bifurcation to non-unison and the jump conditions, respectively.

Cycloidal paths:

Here $\lambda = 1$ and γ_o is given by,

$$\gamma_o = -\frac{1}{12}(1+n^2)^2. \tag{2.35}$$

When this is substituted in equations (2.27,2.29), the following expressions are obtained:

$$Det[A1 - A2]_{cyc} = \frac{3}{256n^2}(1+n^2)^4r_z^4 + \frac{1}{4}(1+n^2)^2\sigma r_z^2 + (n^2\sigma^2 + \frac{\tilde{\mu}_a^2}{4}), \tag{2.36}$$

$$Det[A1+(N-1)A2]_{cyc} = \frac{3}{256n^2}(1+n^2)^4r_z^4 + \frac{1}{8}(1+n^2)^2(1+2\sigma)r_z^2 + \frac{1}{4}[n^2(1+2\sigma)^2+\tilde{\mu}_a^2], \tag{2.37}$$

corresponding to the bifurcation to non-unison and the jump conditions, respectively.

2.2 Numerical Examples and Discussion

Here, we fix the values of all parameters except the path parameters and the fluctuating torque level. CPVA systems with an inertia ratio (ϵ) of $\frac{1}{20}$ are considered. The order of the applied fluctuating torque (n) is taken to be 2. The non-dimensional absorber damping coefficient is taken to be $\frac{\tilde{\mu}_a}{N} = 0.02$, and the dimensionless rotor damping coefficient is taken to be $\mu_o = 0.005$.

Note on Numerical Simulations

Throughout this work, in all numerical simulations, no expansions in terms of ϵ were used to simplify the equations of motion (equations (2.6,2.9)). Also, the following exact representations of the circular, epicycloidal, and cycloidal paths are used [16]:

Circular Paths:

$$x_i(s_i) = 1 - \frac{2\tilde{n}_i^2 \left\{1 - \cos\left[(\tilde{n}_i^2 + 1)s_i\right]\right\}}{(\tilde{n}_i^2 + 1)^2}$$

Epicycloidal Paths:

$$x_i(s_i) = 1 - \tilde{n}_i^2 s_i^2$$

Cycloidal Paths:

$$x_i(s_i) = 1 - (\tilde{n}_i^2 + \frac{3}{4})s_i^2 + \left(\frac{\sin^{-1}\left[(\tilde{n}_i^2 + 1)s_i\right]}{2(\tilde{n}_i^2 + 1)}\right)^2$$

$$+\frac{\sin^{-1}\left[(\tilde{n}_i^2 + 1)s_i\right] \sin\left[2\sin^{-1}\left[(\tilde{n}_i^2 + 1)s_i\right]\right]}{4(\tilde{n}_i^2 + 1)^2}$$

2.2.1 Effect of Path Type

Path Type Effect on the Stability of the Unison Response:

Using the above numerical values in equations (2.30,2.31), along with equation (2.24), the critical torque levels were obtained as functions of the path coefficient (λ) for various levels of mistuning. The results are presented in Figure 2.4. It is worth mentioning here that the plot shows only positively mistuned paths, ranging from circular up to, but not including, epicycloidal paths ($0 \leq \lambda < \lambda_e$). This is because, as seen earlier, for other paths neither bifurcations to non-unison nor jumps are present for positive mistuning levels. Also, as shown below, negative mistuning levels are not of practical importance and should always be avoided.

It is clear from the figure that the dependence of the critical torque levels on the

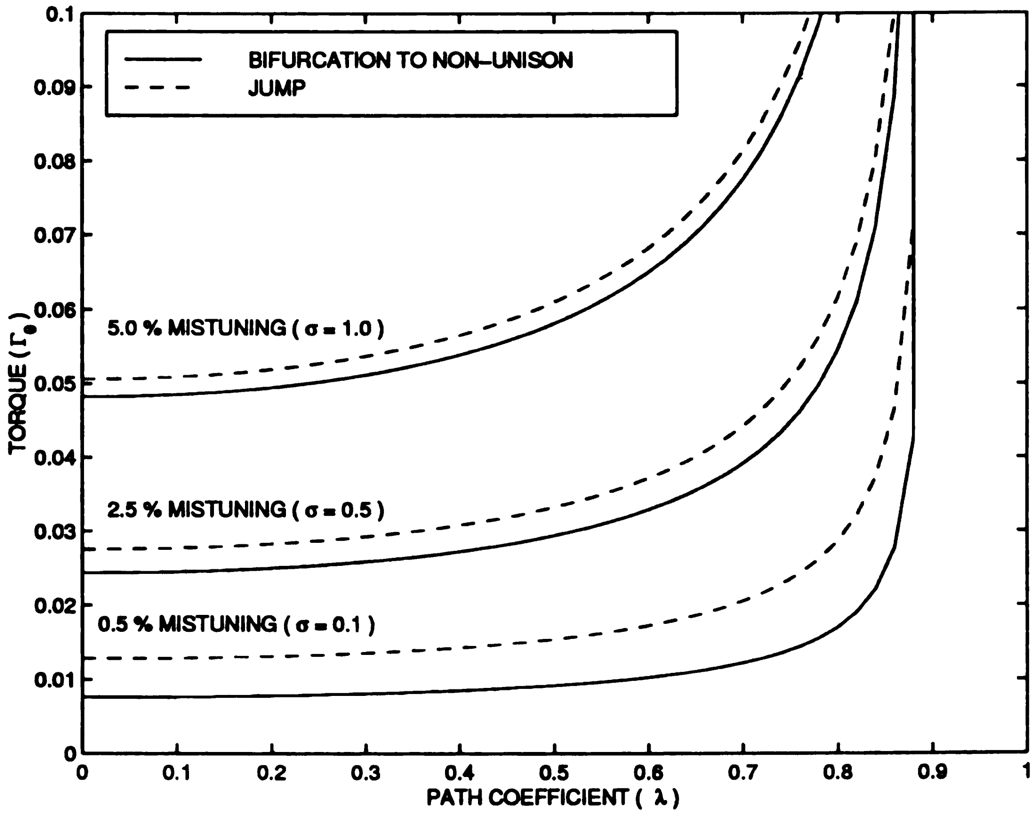

Figure 2.4. Effect of absorber path type on the stability of the unison response.

nonlinear path parameter is not very significant, until one approaches the epicycloid. From the stability point of view, no benefits are gained by changing from the easily-manufactured circular paths to other paths; however, the performance must also be considered before drawing general conclusions, and this is done next. Note that the level of mistuning does have a significant effect on the stability levels, but, again, performance must be taken into account. Also, note that near the epicycloidal path, that is, for $\lambda \approx \lambda_e = 0.89$ the critical torque levels become large. Here the results are not reliable because, as mentioned earlier, the theory does not work for epicycloidal paths, due to the scaling. In both cases — increased mistuning and

$\lambda \approx \lambda_e$ — the response becomes more like that of a linear system, and thus more stable. In the case of increased mistuning, this is due to the fact that we are moving away from a resonance condition. For $\lambda \approx \lambda_e$, the nonlinear part of the path is balanced between softening and hardening; this is the tautochronic condition [11].

Path Type Effect on the Absorbers Performance:

The amplitude of the non-dimensional rotor angular acceleration, $vv'(\theta)$, is used as a measure of the performance of the absorbers. Assuming unison motion, this amplitude is calculated using equation (2.16) for different torque levels and different path types. Two cases are considered here, namely, perfectly tuned paths ($\sigma = 0$), and positively mistuned paths with $\sigma = 0.4$. The results for these two cases are shown in Figures 2.5(a) and (b) respectively. Examining theses figures, it can be seen that the benefits gained by employing a wide range of paths that are not circular are small and does not balance the advantage of the ease in manufacturing circular paths have. However, as one approaches epicycloidal paths, theses benefits become appreciable. The main advantage that will be gained as one approaches the epicycloidal paths is the high operating range as it is clear from the figure. Although, as mentioned earlier, our model reduces to the linear model for the case of epicycloidal paths, the results when the absorbers are in unison is in a very good agreement with numerical simulations. This means that the linear model is an acceptable one for the case of epicycloidal paths as long as the absorbers are in unison. However, it has been shown by Chao *et al.* [20] that at a certain torque level, the absorbers unison response becomes unstable. This, of course, can not be captured by the linear model simply because it is a non-linear effect. This instability is observed through numerical simulation and its effect can be seen in Figure 2.5(a) where the unison motion of the absorbers with epicycloidal paths becomes unstable at approximately $\Gamma_\theta = 0.026$. The theory presented in this work, states that neither

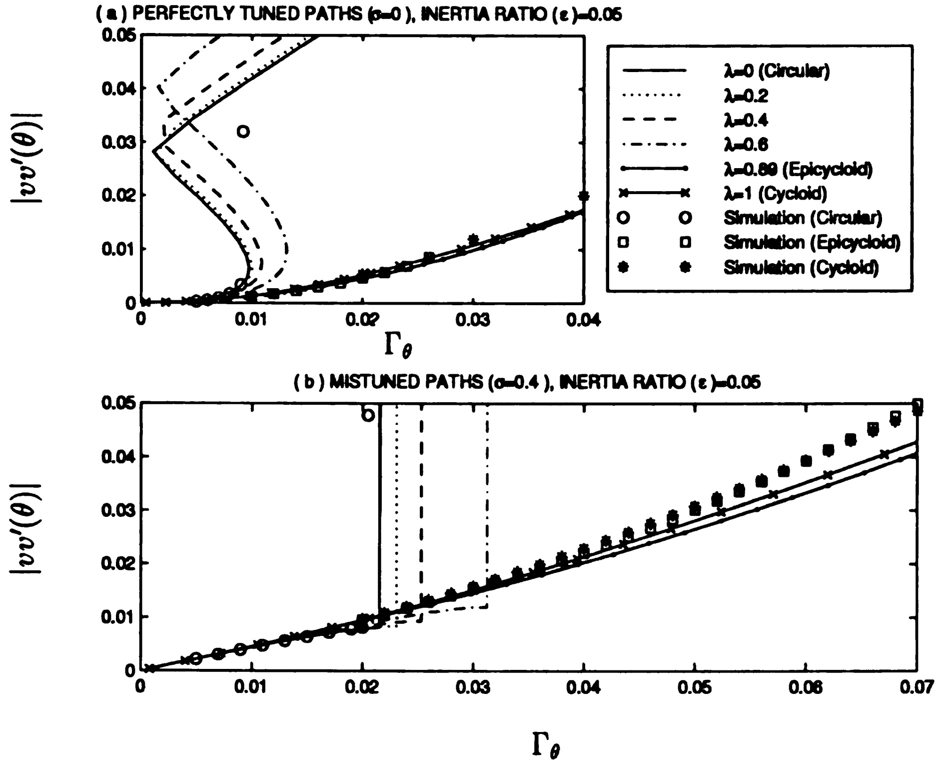

Figure 2.5. Path type effect on the absorbers performance. $\epsilon = 0.05$, $n = 2$. (a) Perfectly tuned, (b) $\sigma = 0.4$.

jumps nor bifurcations to non-unison exist for paths raging from but not including epicycloidal to cycloidal, as mentioned earlier. This is clear in Figure 2.5 as the absorbers with cycloidal path continue to move in unison and does not undergo any jump.

Our goal is to investigate the operating range of absorber systems, as they are limited by the critical torque levels, and to evaluate the effectiveness of the absorbers by computing the angular acceleration of the rotor, which is desired to be small. We focus on circular and cycloidal absorber paths and distill some general conclusions regarding choices of path parameters.

Table 2.1. Effect of the number of absorber on bifurcation to non-unison torque level. Circular paths. (From theory).

N	$\bar{\Gamma}_\theta(\sigma = 0.2)$	$\bar{\Gamma}_\theta(\sigma = 0.4)$	$\bar{\Gamma}_\theta(\sigma = 0.8)$
2	1.048	1.792	3.415
6	1.062	1.798	3.418
10	1.089	1.809	3.424
14	1.131	1.826	3.428

2.2.2 Circular Paths

We begin by demonstrating the accuracy of the analytical results, and then turn to a more systematic investigation. Figure 2.6 depicts the unison absorber response versus torque level, showing both theoretical results from equations (2.33,2.34) and numerical simulation results for $N = 4$ absorbers with 0 and 4% mistuning levels. Note that the method is very accurate on the lower branches, that is, those of greatest interest. Also, the error grows as amplitude increase; this is due to both the scaling and the application of averaging. Figure 2.7(a) shows the critical torque levels above which the unison motion becomes unstable and Figure 2.7(b) shows the critical torque levels above which the jump occurs, both for different mistuning levels, again for $N = 4$. These results demonstrate the validity of the analytical approach employed.

It is clear from equation (2.33) that the only parameter that could be changed to delay the existing bifurcation to non-unison, without introducing some further intentional mistunings to the absorbers' paths, is $\tilde{\mu}_a$, and this can be done by increasing the number of absorbers, N. However, the dependence on this parameter is very small. To see this, three different mistuning levels of the paths in the present numerical example are considered. They are 1%($\sigma = 0.2$), 2% ($\sigma = 0.4$), and 4% ($\sigma = 0.8$). With all other numerical values fixed, increasing the number of absorbers from 2 to 14 in each case increases the critical torque levels at which bifurcation to non-unison

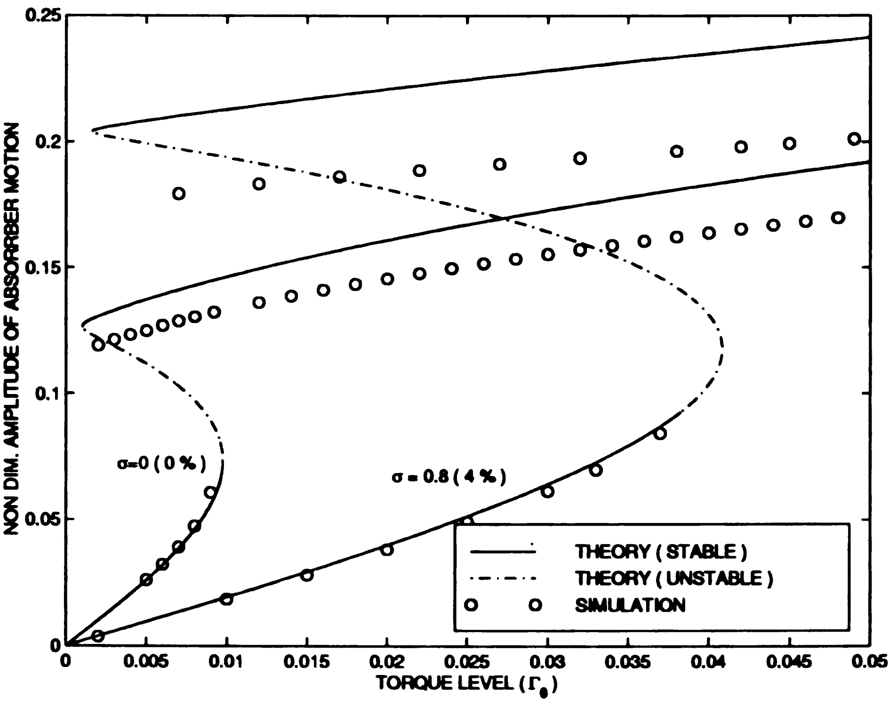

Figure 2.6. Circular path. Upper: 0% mistuning; lower: 4% mistuning

takes place by only 8%, 2%, and 0.4%, respectively (see Table 2.1). The practical method for delaying bifurcation to non-unison, as mentioned earlier and as can be seen from Figure 2.7(a), is to increase the level of mistuning in the paths. In fact, this will significantly delay both of the bifurcation points. The response curves for $N = 4$ with different mistuning levels, depicted in Figure 2.8, also show that the jump point shifts rightward as the level of mistuning is increased. Figure 2.8 also shows that as the level of mistuning is increased, the absorbers' amplitudes become smaller for a given torque level, which implies that the absorbers are cancelling less of the applied torque. This indicates that there is a tradeoff between high operating range and better absorber performance. It should also be noted that as the mistuning level approaches -2.5% ($\sigma = -0.5$), the torque level at which the jump occurs approaches

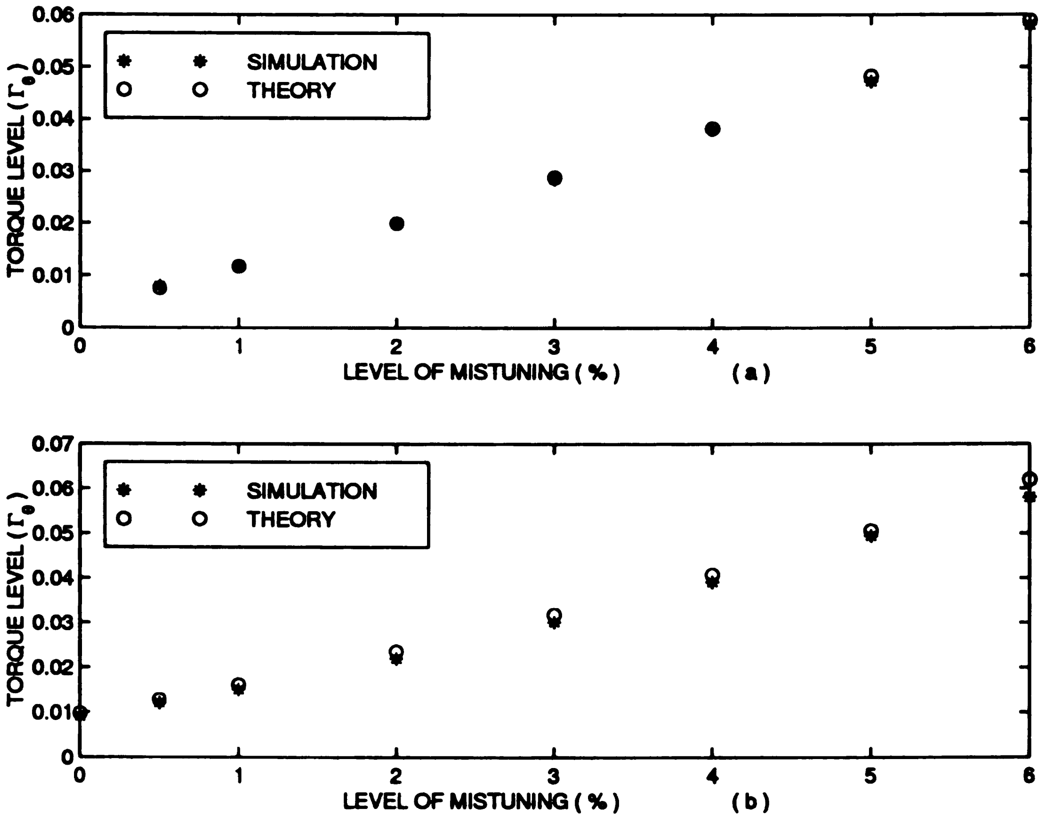

Figure 2.7. Critical torque level versus percentage mistuning for circular path CPVAs (a) Bifurcation from unison, (b) Jump

zero, indicating that the absorbers will jump no matter how small the applied torque is. After the jump, as will be shown later, the absorbers' motions actually add to the applied torque and increase the vibration levels as compared with the rotor without absorbers. Therefore, one should always avoid negative mistuning levels.

The stability of the various steady-state curves in Figure 2.8 are nearly as expected, with one exception. The lower branches are stable up to a torque level just prior to the jump, where the bifurcation to non-unison occurs. The middle branch is, of course, everywhere unstable, and the upper branch is everywhere stable.

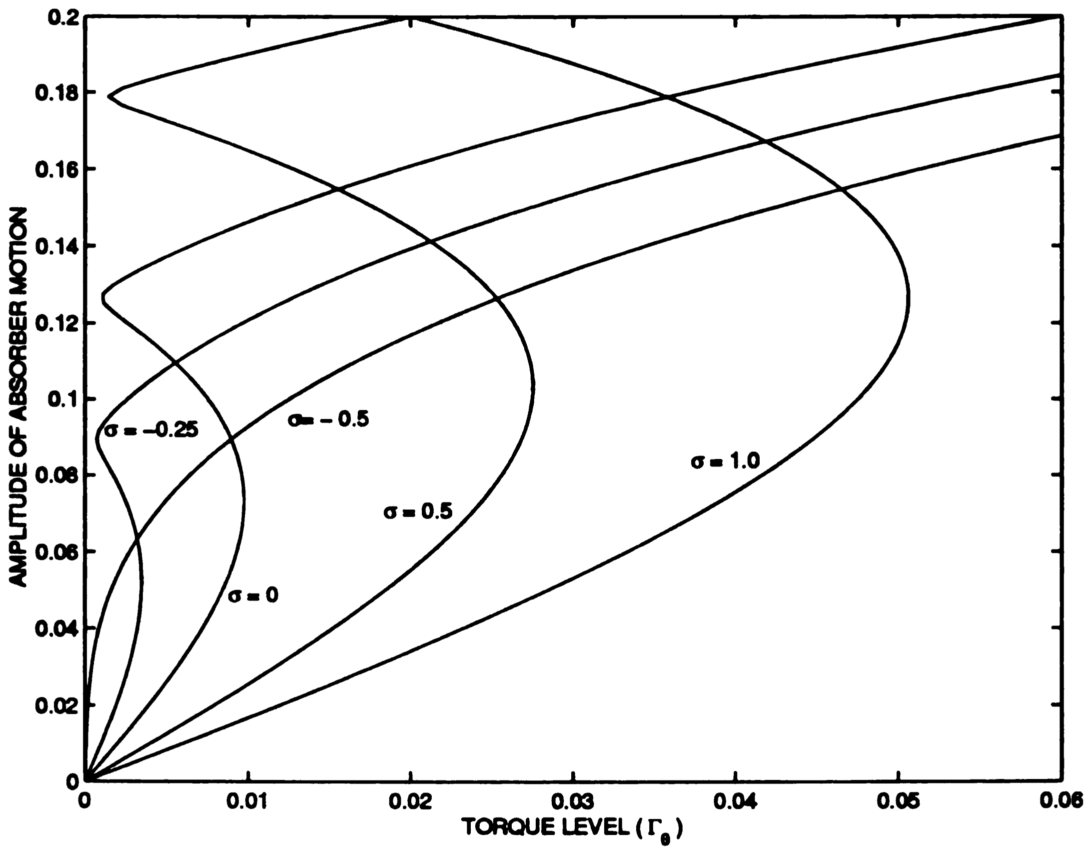

Figure 2.8. Effect of mistuning, circular path CPVAs - analytical. Stability is not indicated here.

Figure 2.9 shows a plot of the the amplitude of the non-dimensional rotor acceleration, $vv'(\theta)$, versus the applied torque level. The previous comment about the tradeoff between performance and range is clear from this figure as well, since the performance degrades as the range is increased. However, in all cases shown, the absorbers reduce the vibration levels when compared to the system with the absorbers locked at their respective vertices (where they play the role of a simple flywheel).

An interesting observation in Figure 2.9 is the presence of a peak acceleration in every theoretical curve just before the jump point whenever a bifurcation to non-unison exists. It has been observed that these peak acceleration points represent the points where bifurcations to non-unison response take place. This can be shown mathematically, as follows. From equation (2.16) and the first of equations (2.18), we have

$$vv'(\theta) = \epsilon^r[n^2 r_z \sin(n\theta + \phi_z) + \tilde{\Gamma}_\theta \sin(n\theta)] + O(\epsilon^{r+\nu})$$

Also, since $\tilde{\mu}_a$ is small, it is seen from equations (2.23) that ϕ_z is close to zero or π. Before the jump, $\phi_z \approx \pi$, as will be shown later. The above equation thus becomes

$$vv'(\theta) \approx \epsilon^r[\tilde{\Gamma}_\theta - n^2 r_z] \sin(n\theta)$$

The acceleration amplitude is given by

$$|vv'(\theta)| \approx \epsilon^r[\tilde{\Gamma}_\theta - n^2 r_z].$$

Differentiating this with respect to $\tilde{\Gamma}_\theta$, and making use of the second of equations (2.23) with $\phi_z = \pi$, the following expression is obtained:

$$\frac{d|vv'(\theta)|}{d\tilde{\Gamma}_\theta} \approx \epsilon^r[1 - \frac{n^2}{2n^2(\sigma + \frac{1}{2}) - \frac{9}{2}\gamma_o r_z^2}].$$

Solving this for the r_z value at which $|vv'(\theta)|$ is a maximum, *i.e.*, where this expression is zero, one finds

$$r_z \approx \frac{2n}{3}\sqrt{\frac{\sigma}{\gamma_o}},$$

which is exactly the same as the expression for r_{zbif} given by equation (2.30) when the term with the damping coefficient $\tilde{\mu}_a$ is ignored. This feature of the response is not well understood.

The general response for circular paths is observed to be a unison response with a smooth increase in absorber amplitude and angular acceleration, up to a point

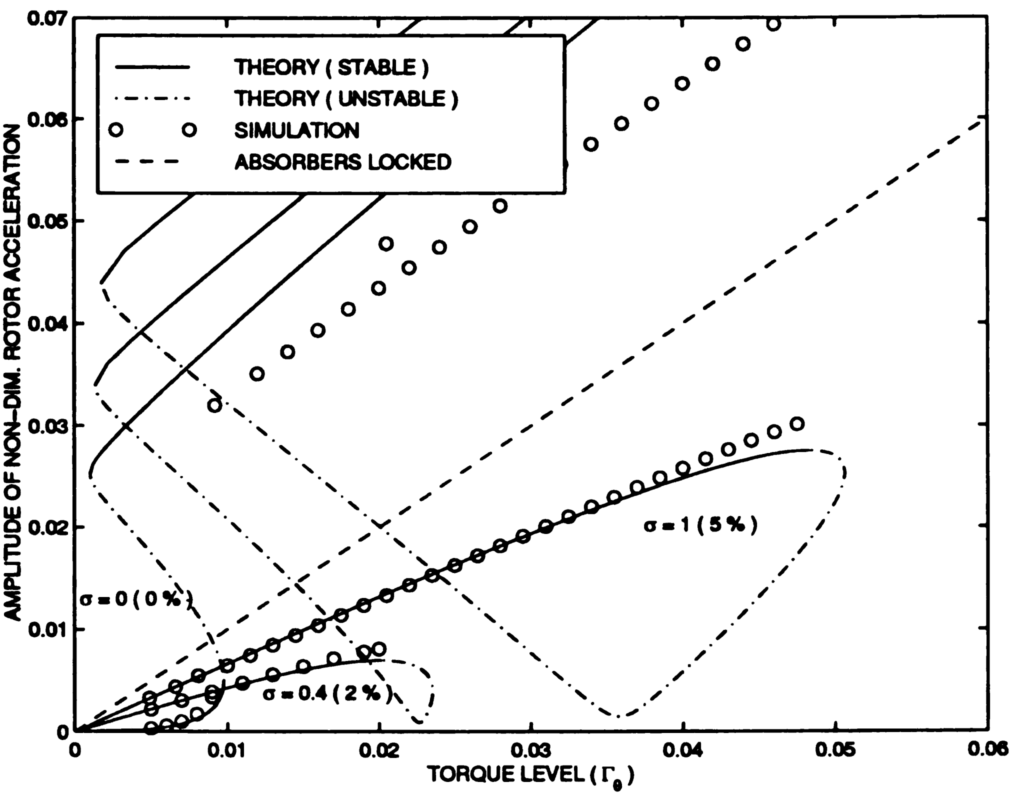

Figure 2.9. Effect of mistuning on rotor acceleration (circular path CPVAs)

at which the acceleration peaks and the system bifurcates to a non-unison motion. Typically, the response beyond this torque level is captured by the undesirable upper branch of the unison response. This is due to the bifurcation being sub-critical, or there being a very small basin of attraction for the post-bifurcation response. In the present case with $N = 4$, the only level of mistuning where it was possible to observe the non-unison response was at 0.5%, as demonstrated in Figure 2.10. Figure 2.10(a) shows the absorbers' unison response at $\Gamma_\theta = 0.0076$ (before bifurcation to non-unison), and Figure 2.10(b) shows the absorbers' non-unison response at $\Gamma_\theta = 0.0080$ (after bifurcation to non-unison), wherein one absorber moves at a lower amplitude

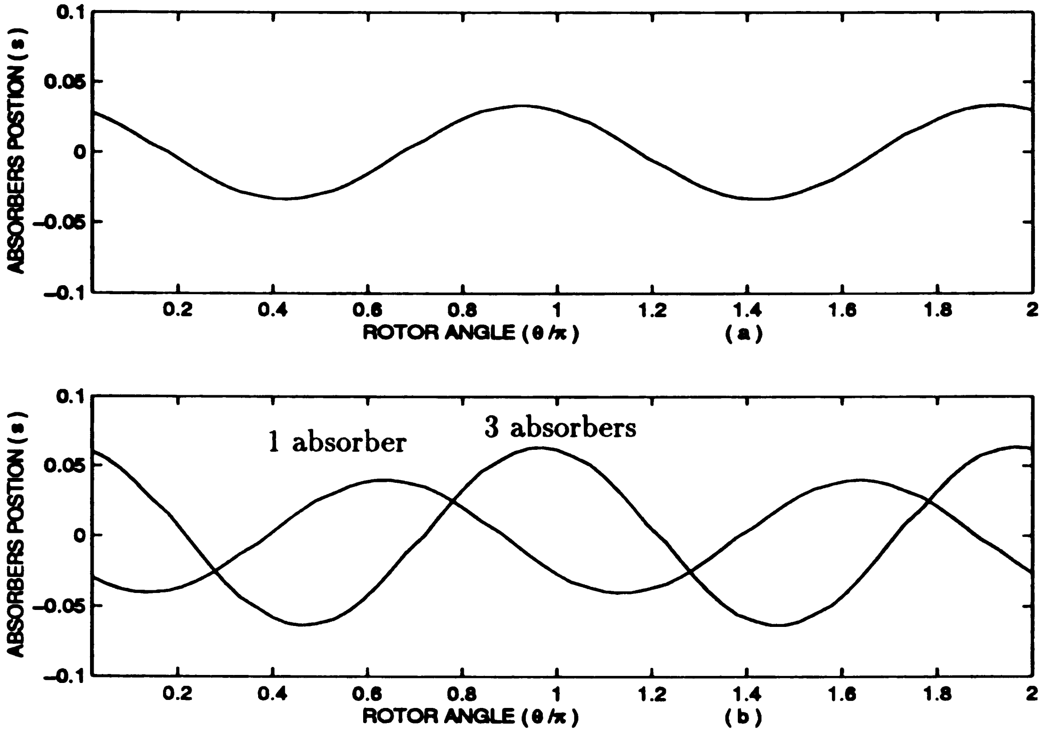

Figure 2.10. N=4 circular path CPVAs with mistuning level of 0.5%, (a) before bifurcation to non-unison ($\Gamma_\theta = 0.0076$), (b) after bifurcation to non-unison ($\Gamma_\theta = 0.0082$) - from numerical simulation.

and lags the other three, which move in relative unison close to the unstable unison response. This is similar to the post-critical response observed for epicycloidal paths [20].

2.2.3 Cycloidal Paths

The cycloidal path offers a slightly hardening nonlinearity ($\gamma_o < 0$, as given by equation (2.35)), and this avoids many of the problems and shortcomings associated with circular paths. For cycloidal absorber paths, neither the bifurcations to non-unison nor jumps are present when $\sigma \geq 0$, as is clear from equations (2.36,2.37). Figure 2.11 shows theoretical and numerical simulation results for $N = 4$ absorbers with 0%, 5%, and 10% mistuning levels, respectively. Similar to circular paths, increasing the mis-

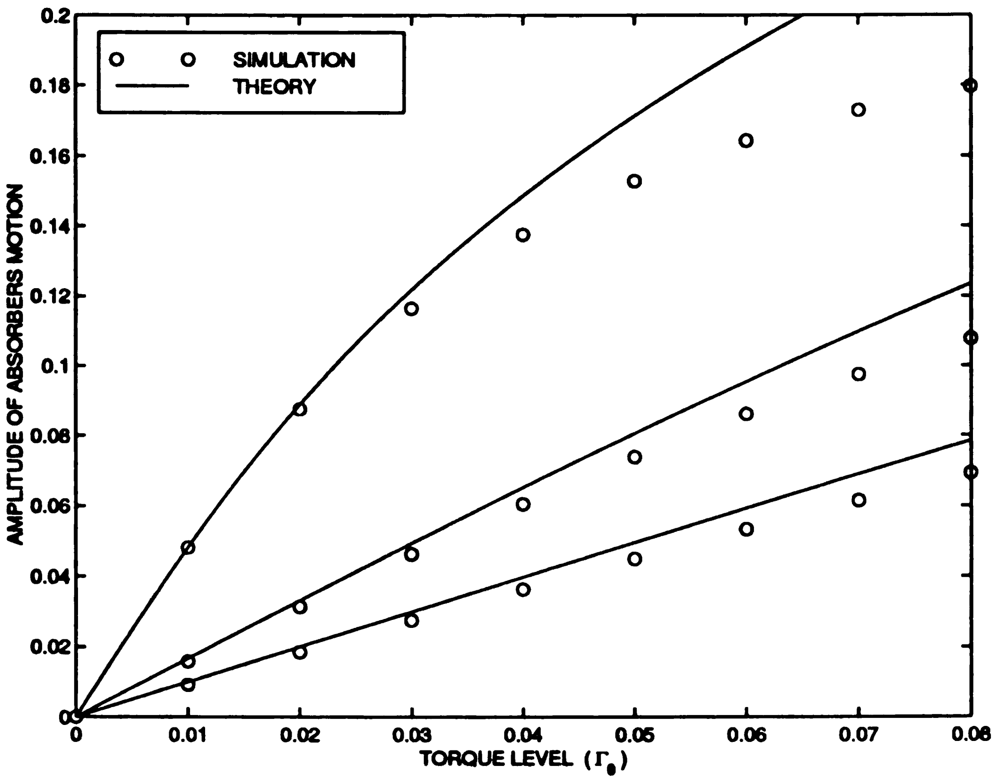

Figure 2.11. Cycloidal paths. Upper 0% mistuning, middle 5% mistuning, lower 10% mistuning

tuning level in cycloidal paths will decrease the amplitude of the absorbers' motion for the same torque level. Figure 2.12 shows theoretical and numerical simulation results for the amplitude of the non-dimensional rotor angular acceleration versus torque level for $N = 4$ absorbers with 0%, 2.5%, 5%, and 10% mistuned cycloidal paths, respectively. These results indicate that the mistuning should be kept as small as possible in order for the absorbers to effectively cancel the fluctuating torque. In this case, in contrast with circular paths, the range is not limited by a jump bifurcation.

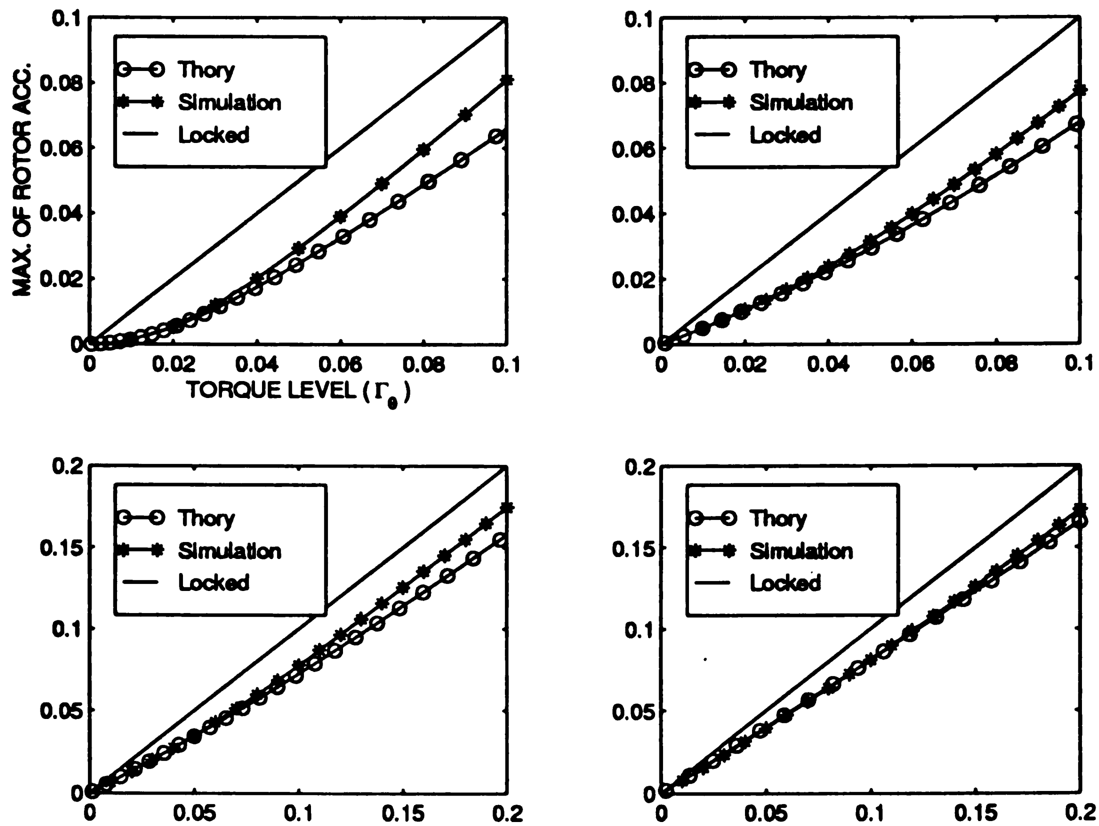

Figure 2.12. Rotor angular acceleration, $vv'(\theta)$ for mistuned cycloidal paths; (a) 0% Mistuning (b) 2.5% Mistuning (c) 5% Mistuning (d) 10% Mistuning

It should be noted here that the agreement between theory and simulation is not as good as it was for circular paths. As mentioned earlier, for $\sigma < -\frac{1}{2}$, the theory predicts jumps. But, this could not be found in the numerical simulations. The reason for this is that cycloidal paths are much closer to epicycloidal paths where, as

Table 2.2. Theoretical ranges of absorbers amplitudes and torque levels at which non unison motions exist for $N = 4$ absorbers with cycloidal paths

Mistuning (σ)	r_{x1}	r_{x2}	$\Gamma_{\theta 1}$	$\Gamma_{\theta 2}$
-0.10	0.30	0.50	0.012	0.022
-0.20	0.42	0.71	0.014	0.032
-0.30	0.51	0.88	0.014	0.039
-0.40	0.58	1.01	0.012	0.045

mentioned earlier, nonlinearities other than the path nonlinearity are also important. In any case, mistunings where $\sigma < -\frac{1}{2}$ are not of practical importance (as described in the following section), and the theory works very well for practical levels of mistuning.

An interesting range of mistuning that deserves further mention is $-\frac{1}{2} < \sigma < 0$. For every mistuning level in this range, the theory predicts an amplitude of motion range where the unison response is unstable. This range can be found using equation (2.36). For cycloids, it was possible to numerically find some stable steady state non-unison responses in these ranges. Table 2.2 shows the theoretical ranges of absorber amplitudes and torque levels at which the unison response is unstable for a system with $N = 4$ absorbers, and for different mistuning levels. Figures 2.13 and 2.14 show the numerically simulated steady-state absorbers' responses for $\sigma = -0.1$, and $\sigma = -0.2$, respectively for sets of torque levels that run through the unstable ranges. These results indicate that a rather complicated set of bifurcations takes place in these ranges, resulting in a variety of possible non-unison steady-state responses.

Other negative mistuning levels are not important because, similar to circular paths, the absorbers will not be working properly as is shown in the following section.

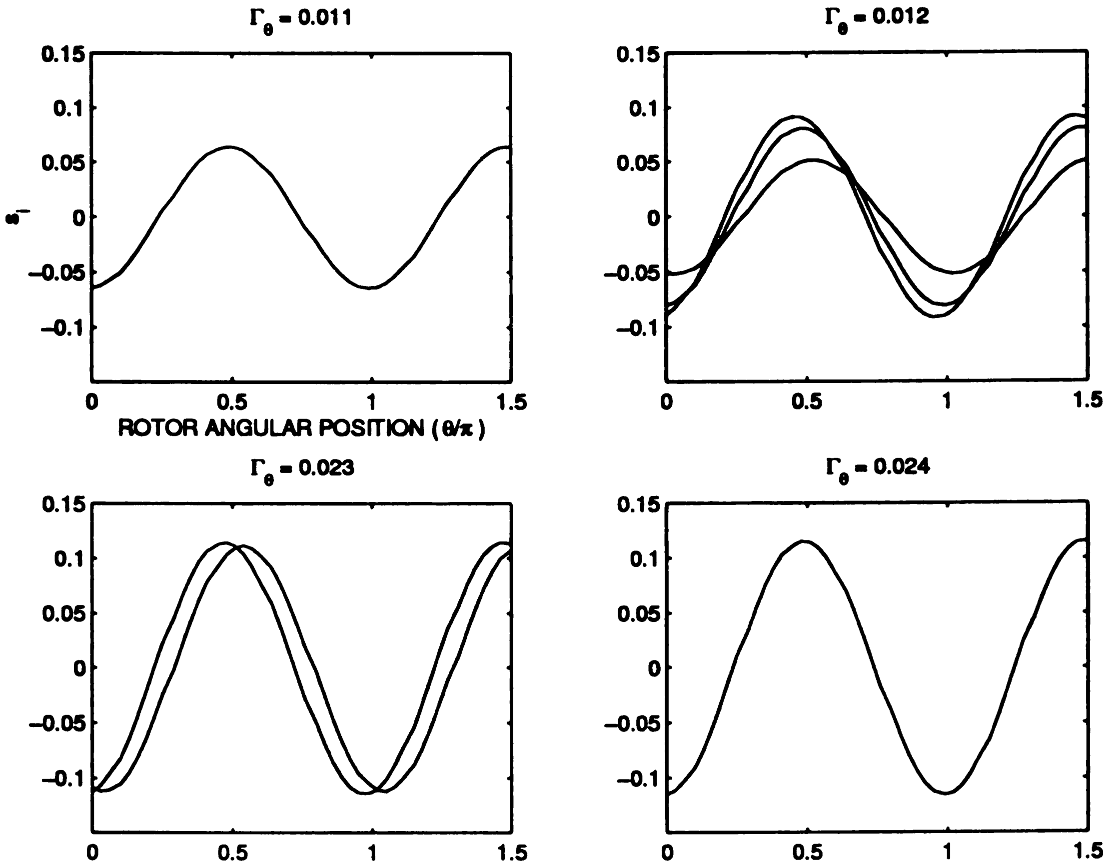

Figure 2.13. Numerically simulated absorbers responses for $\sigma = -0.1$ (N=4 cycloidal path absorbers)

2.2.4 Note on the Absorber System Performance

In order to determine how the performance of the absorbers is affected by the level of mistuning, one can consider equation (2.23), along with the fact that $\tilde{\mu}_a$ is small. It can be clearly seen that the absorbers' steady state phase angle ϕ_z is either close to 0 or close to π. For paths with $\gamma_o > 0$, for example circular paths, if $\sigma > -\frac{1}{2}$ and the absorbers' amplitude of vibration is small enough, which is the case here, then ϕ_z is close to π. Then, from equation (2.16), along with equation (2.18), one concludes

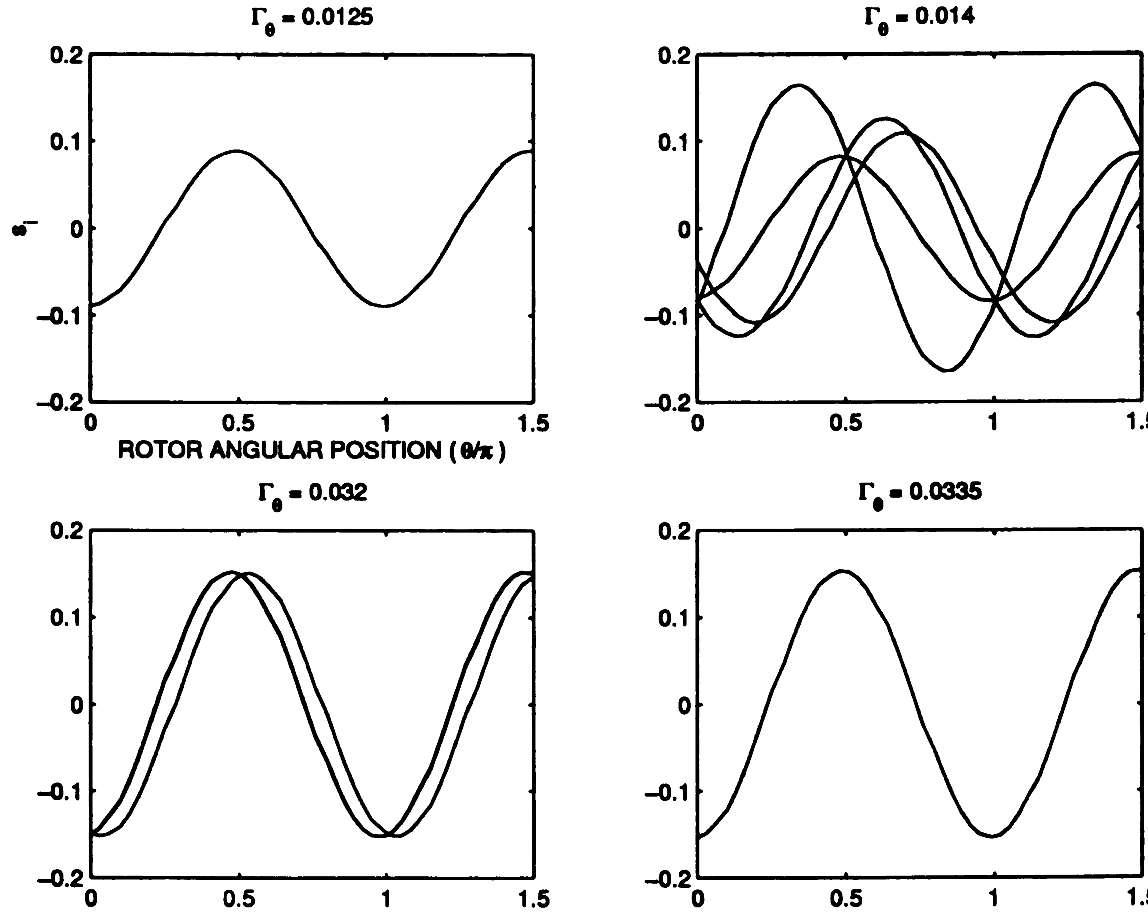

Figure 2.14. Numerically simulated absorbers responses for $\sigma = -0.2$ (N=4 cycloidal path absorbers)

that the absorbers are producing a torque which is opposite to the applied torque. If the the absorbers' amplitude of vibration is increased, say, by increasing the applied torque level, then it will reach a value where $\cos(\phi_z)$ will jump from near (-1) to near (+1). This corresponds to the jump onto the upper part of the response curve, at which point the absorbers add to the fluctuating applied torque to the rotor. For $\sigma \leq -\frac{1}{2}$, $\cos(\phi_z)$ is always near (+1) and the absorbers add torque to the rotor. This is demonstrated by the simulation results for $N = 4$ absorbers, as shown in Figure 2.15.

This figure shows the rotor non-dimensional angular acceleration, $vv'(\theta)$, versus rotor angle for steady state responses on the lower and the upper portions of the response curve for a 5% mistuning, and a torque level of 0.02. It also shows $vv'(\theta)$ for the same torque level but with a mistuning level of -5% (where the absorbers are in phase with the applied torque), and for the absorbers locked at their vertices. Note that the absorbers actually increase the vibration level when on the upper branch of the response curve.

For paths with $\gamma_o < 0$, for example cycloidal paths, if $\sigma > -\frac{1}{2}$, then ϕ_z is close to π and the absorbers are reducing the torsional vibrations as long as they move in unison. Since for $-\frac{1}{2} < \sigma < 0$ there are ranges of applied torques where non-unison motions exist, one can not conclude that the absorbers are working properly in these torque ranges. For $\sigma \geq 0$, the absorbers are reducing torsional vibrations at all torque levels. This is because for $\sigma \geq 0$, neither bifurcations to non-unison nor jumps are present. When $\sigma \leq -\frac{1}{2}$, equation (2.23) indicates that ϕ_z is near 0, which means that the absorbers are always adding torsional vibrations to the rotor. Figure 2.16 shows numerical simulation results for the non-dimensional rotor angular acceleration for $N = 4$ cycloidal path absorbers with 0%, 5%, and -5% mistuning levels, subjected to the same torque level of 0.02. The effect of negative mistuning mentioned above is clearly demonstrated here.

2.3 Summary and Conclusions

The following points summarize the findings of this study:

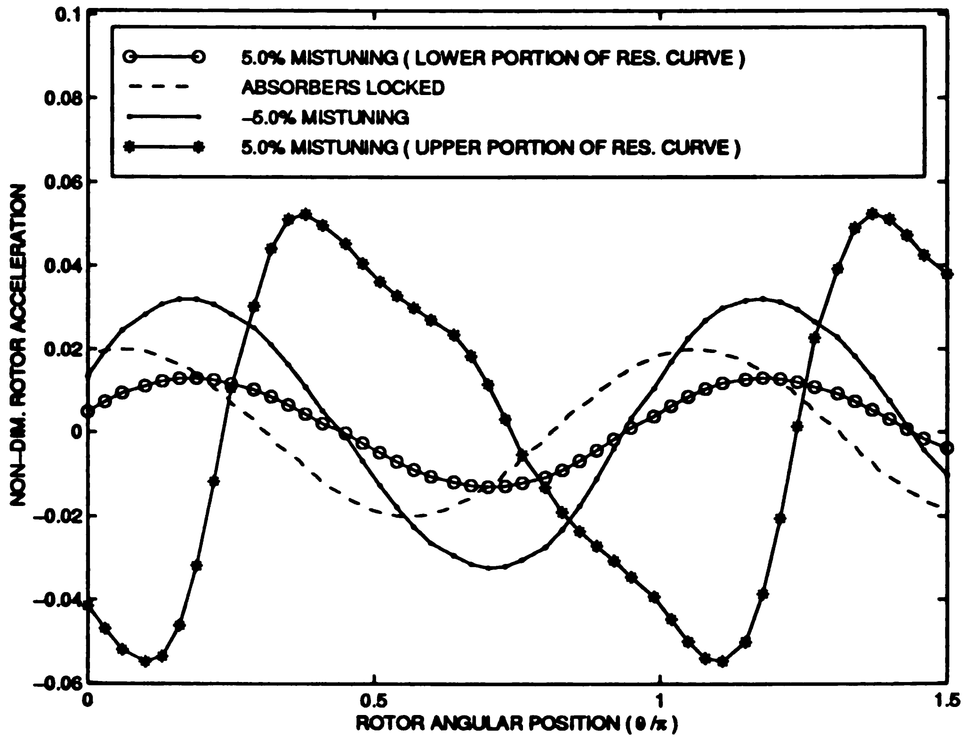

Figure 2.15. Rotor angular acceleration, $vv'(\theta)$, for $\Gamma_\theta = 0.02$ for mistuned circular paths - from numerical simulations

For paths ranging from circular up to, but not including, epicycloidal paths, $0 \leq \lambda < \lambda_e$*:*

- There are positive mistuning levels below which no bifurcations to non-unison are present. These levels are usually very small and are parameter dependent.
- Jumps are always present for paths with $\sigma > -\frac{1}{2}$.
- Paths other than circular do not have significant benefits over the easily-manufactured circular path.
- For paths with $\sigma > -\frac{1}{2}$, the absorbers reduce torsional vibrations for absorber

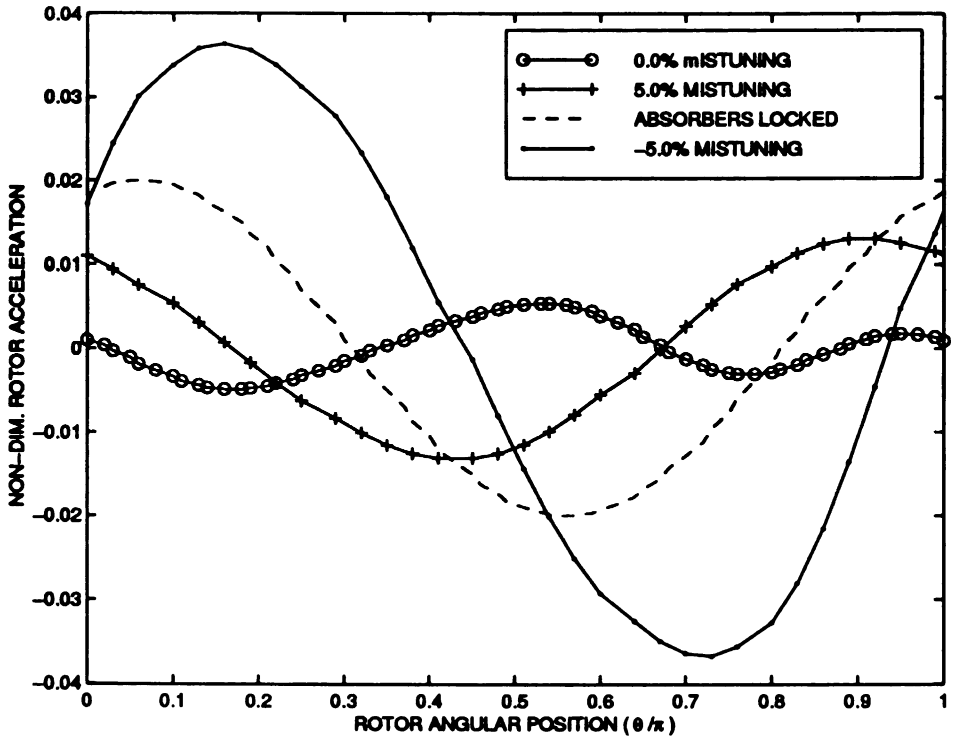

Figure 2.16. Rotor angular acceleration, $vv'(\theta)$, for mistuned cycloidal paths, $\Gamma_\theta = 0.02$ - from numerical simulations, (N=4)

responses that are on the lower portions of the response curves, but they increase torsional vibration for responses on the upper portions of the response curves.

For paths ranging from, but not including, epicycloidal paths up to cycloidal paths, $\lambda_e < \lambda \leq 1$*:*

- Neither bifurcations to non-unison nor jumps are present for perfectly tuned and positively mistuned paths.

- For negatively mistuned paths, there are torque ranges where non-unison motions exist.

- The method presented predicts jumps for paths with $\sigma < -\frac{1}{2}$, but these are not found in the numerical simulations.

For all paths considered:

- As the mistuning levels are positive and increased, the bifurcation to non-unison and the jump points, if they exist, are delayed, and they approach each other, resulting in increased operating ranges.

- When the operating ranges are increased by increasing the mistuning levels, the effectiveness of the absorber system is reduced.

- With $\sigma \leq -\frac{1}{2}$, the absorbers actually increase, rather than reduce, the levels of torsional vibration.

In light of these observations, one can conclude that for any type of absorber path, when the operating torques are kept very small, it is best not to have any mistuning, *i.e.*, perfectly tuned paths are the best choice. However, if one wants to increase the operating range, positive mistuning levels should be selected, keeping in mind that the absorbers' performance will be reduced. Negative mistuning levels should always be avoided.

When the performances of absorber systems with circular and cycloidal paths are compared, it is concluded that absorbers with cycloidal paths are preferred because, in addition to their much larger working ranges, they neither undergo jump bifurcations nor bifurcations to non-unison steady state responses. This implies that only one steady-state response exists at each torque level, and this response is equivalent to that predicted by using a model with a single absorber mass, making design analysis much easier. Also, they are dynamically robust and therefore suitable for practical implementations.

CHAPTER 3

Non-synchronous Steady-State Responses of Tuned Pendulum Vibration Absorbers

In this chapter, an approach is taken that allows one to investigate the dynamics of multi-absorber systems that have quite general paths for the absorber masses, including those used in practice. Of particular interest here are the existence and stability of certain classes of non-unison responses. It is shown via the method of averaging that these steady state responses may exist and be stable for certain types of paths, including the commonly-used mistuned circular path. Furthermore, it is shown that these responses can co-exist with a stable unison response, even for very small torque levels. The analytical results are compared with numerical simulations and good agreement is found.

The chapter is organized as follows. The mathematical model, which is identical to that considered in chapter 2, is first briefly described. Some assumptions are given that allow one to derive a relatively simple set of equations that capture the absorber dynamics. These are presented and the method of averaging is applied to investigate the existence and stability of various types of steady state responses. A numerical example is studied in some detail and compared against the analytical predictions. The chapter then closes with some conclusions.

3.1 Mathematical Formulation

From chapter 2, the equations that describe the dynamics of N torsional vibration absorbers, each of mass m, mounted on a rotor of inertia J are:

$$\begin{aligned} z_i'' + n^2 z_i = \epsilon[2\gamma_o z_i^3 - 2n^2\sigma_i z_i - \tilde{\mu}_a z_i' \\ -\tfrac{1}{N}\textstyle\sum_{j=1}^{N} n^2 z_j - \tilde{\Gamma}_\theta \sin(n\theta)] + HOT \\ i = [1, N], \end{aligned} \tag{3.1}$$

where HOT, as indicated before, refers to higher order terms. Again $(.)'$ represents differentiation with respect to the rotor angular orientation, θ. Ω denotes the average angular speed of the rotor, upon which the torsional vibrations are superimposed. The scaling and the definitions of system variables and parameters are the same as those given in chapter 2. The following description briefly summarizes them. The base scaling parameter used is ϵ, which is the ratio of the absorbers' inertia to that of the rotor, $\epsilon = NmR_o^2/J$, which is small in practice. The scaled absorber displacement variables z_i are given by $z_i = \epsilon^{\frac{1}{2}} s_i$, where s_i represents the non-dimensional arc length variable for the position of the i^{th} absorber, *i.e.*, $s_i = \frac{S_i}{R_o}$, where S_i and R_o are as indicated in Figure 2.1. $\tilde{\mu}_a$ is the scaled absorber damping coefficient, $\mu_a = \epsilon\tilde{\mu}_a = \frac{c_a}{m\Omega}$, where c_a is the physical damping constant for each absorber (assumed to be identical). The applied torque is assumed to be harmonic of order n, *i.e.*, $\Gamma_\theta \sin(n\theta)$, where Γ_θ is the amplitude of the fluctuating component of the applied torque, nondimensionalized by the kinetic energy of the rotor and scaled by ϵ, as follows, $\Gamma_\theta = \frac{T_\theta}{J\Omega^2} = \epsilon^{\frac{3}{2}}\tilde{\Gamma}_\theta$. The parameter σ_i accounts for the effects of mistuning between the applied torque and the tuned frequency of the absorber, and is defined by

$$\tilde{n}_i = n(1 + \epsilon\sigma_i),$$

where $\tilde{n}_i$ represents the dimensionless tuning frequency of the i^{th} absorber path (the actual frequency is given by $\tilde{n}_i\Omega$), and is geometrically given by the square root of the ratio between the distance from the rotor center to the center of the path vertex and the radius of curvature of the absorber path at the vertex. Such mistuning is intentionally built into circular path absorbers, in order to counteract some undesirable nonlinear effects at moderate vibration amplitudes. The parameter γ_o is a parameter that describes the nonlinear nature of the absorber path. Its appearance in the equations comes from moderate amplitude kinematic effects, and it is given by,

$$\gamma_o = (\frac{1}{12})(n^2 + 1)^2(n^2 - \lambda^2(1 + n^2)). \tag{3.2}$$

where λ is a convenient parameter that describes various path types by taking on values from zero to one. Some special cases of interest are: $\lambda = 0$ describes a circular path, $\lambda = \sqrt{\frac{\tilde{n}_i^2}{(\tilde{n}_i^2+1)}}$ describes an epicycloidal path with its base circle centered at the rotor center, and $\lambda = 1$ describes a cycloidal path. It should be noted here that this formulation is not suitable for studying epicycloidal paths where $\gamma_o = 0$. This is because for epicycloidal paths, this model will reduce to the linearized one (see [20] for the case of epicycloidal absorbers).

The non-dimensional rotor angular acceleration is given by

$$vv'(\theta) = \epsilon^{\frac{3}{2}}\{\frac{1}{N}\sum_{j=1}^{N} n^2 z_j + \tilde{\Gamma}_\theta \sin(n\theta) + \tilde{\Gamma}_\theta \sin(n\theta)\} + \frac{\epsilon^2}{N}\sum_{j=1}^{N} 2n^2 z_j z_j' + HOT. \tag{3.3}$$

This is the measure used to assess the effectiveness of the absorber system, since torsional acceleration is a measure of deviation from constant rotation speed. In particular, once the absorbers' motion z_i are know, this allows for a quick estimate of the the level of torsional vibration.

The method of averaging is used to determine approximate steady-state solutions of equations (3.1). To reach to the averaged equations, the following standard transformation to polar coordinates is used,

$$\left.\begin{aligned} z_i &= a_i \sin(n\theta + \phi_i) \\ z_i' &= n a_i \cos(n\theta + \phi_i), \end{aligned}\right\} \tag{3.4}$$

and averaging is applied, yielding

$$\left.\begin{aligned} &\bar{a}_i' = \epsilon[-\tfrac{\mu_a}{2}\bar{a}_i + \tfrac{\Gamma_\theta}{2n}\sin(\bar{\phi}_i) + \tfrac{n}{2N}\textstyle\sum_{j=1,j\neq i}^{N} \bar{a}_j \sin(\bar{\phi}_i - \bar{\phi}_j)] + HOT \\ &\bar{a}_i\bar{\phi}_i' = \epsilon[-\tfrac{3\gamma_a}{4n}\bar{a}_i^3 + n(\sigma_i + \tfrac{1}{2N})\bar{a}_i + \tfrac{\Gamma_\theta}{2n}\cos(\bar{\phi}_i)] + \tfrac{n}{2N}\textstyle\sum_{j=1,j\neq i}^{N} \bar{a}_j \cos(\bar{\phi}_i - \bar{\phi}_j)] + HOT, \end{aligned}\right\} \tag{3.5}$$

where an over-bar indicates the averaged value of the corresponding variable.

3.1.1 Existence of Certain Steady State Solutions

To capture a certain class of non-unison steady state responses, the absorbers are divided into two groups. One group consists of M absorbers moving in relative unison with an amplitude of $\tilde{a}_1$ and a phase angle of $\tilde{\phi}_1$, and the other group consists of the remaining $(N - M)$ absorbers, also moving in relative unison with an amplitude of motion of $\tilde{a}_2$ and a phase angle of $\tilde{\phi}_2$. Note that the unison response is a special case in which $M = 0$. Of course, other, more general, types of responses may occur, but these are left for future study. To find the steady state amplitudes and phase angles $(\tilde{a}_j, \tilde{\phi}_j)$ $j = 1, 2$, these conditions are imposed on equations (3.5) and solved. This task is simplified by employing Cartesian coordinates for the slowly varying system.

To do that, the following invertible Van der Pol transformation is used:

$$\begin{pmatrix} z_i \\ z_i' \end{pmatrix} = \Phi \begin{pmatrix} u_i \\ v_i \end{pmatrix} \tag{3.6}$$

where

$$\Phi = \begin{bmatrix} \cos(n\theta) & \sin(n\theta) \\ -n\sin(n\theta) & n\cos(n\theta) \end{bmatrix}$$

Performing this transformation, averaging the resulting equations over one period, and splitting the absorbers into the two groups described above with the assumption that the absorber paths in the first group have an identical mistuning of $\tilde{\sigma}_1$ and those in the second group have an identical mistuning of $\tilde{\sigma}_2$, the following equations (in Cartesian coordinates) that describe the steady state response of the absorbers are reached:

$$\left.\begin{aligned}
0 &= -\tfrac{\tilde{\mu}_a}{2}\tilde{u}_1 + n(\tilde{\sigma}_1 + \tfrac{M}{2N})\tilde{v}_1 - \tfrac{3\gamma_o}{4n}(\tilde{u}_1^2\tilde{v}_1 + \tilde{v}_1^3) + \tfrac{n}{2N}(N-M)\tilde{v}_2 + \tfrac{\tilde{\Gamma}_\theta}{2n} + HOT \\
0 &= -\tfrac{\tilde{\mu}_a}{2}\tilde{v}_1 - n(\tilde{\sigma}_1 + \tfrac{M}{2N})\tilde{u}_1 + \tfrac{3\gamma_o}{4n}(\tilde{v}_1^2\tilde{u}_1 + \tilde{u}_1^3) - \tfrac{n}{2N}(N-M)\tilde{u}_2 + HOT \\
\\
0 &= -\tfrac{\tilde{\mu}_a}{2}\tilde{u}_2 + n(\tilde{\sigma}_2 + \tfrac{(N-M)}{2N})\tilde{v}_2 - \tfrac{3\gamma_o}{4n}(\tilde{u}_2^2\tilde{v}_2 + \tilde{v}_2^3) + \tfrac{n}{2N}M\tilde{v}_1 + \tfrac{\tilde{\Gamma}_\theta}{2n} + HOT \\
0 &= -\tfrac{\tilde{\mu}_a}{2}\tilde{v}_2 - n(\tilde{\sigma}_2 + \tfrac{(N-M)}{2N})\tilde{u}_2 + \tfrac{3\gamma_o}{4n}(\tilde{v}_2^2\tilde{u}_2 + \tilde{u}_2^3) - \tfrac{n}{2N}M\tilde{u}_1 + HOT
\end{aligned}\right\} \tag{3.7}$$

After solving these equations, the results are then transformed back to amplitude and phase coordinates for physical interpretation of the results. The polar and rectangular coordinates are related in the usual way, as follows:

$$\tilde{a}_j = \sqrt{\tilde{u}_j^2 + \tilde{v}_j^2}, \quad \tilde{\phi}_j = \tan^{-1}(\frac{\tilde{u}_j}{\tilde{v}_j}), \quad j = 1, 2, \tag{3.8}$$

which yield the amplitudes and phases for the two groups of absorbers. To ensure the capture of all possible real solutions, a graphical/numerical method is used. This method proceeds as follows. Eliminating one pair of the $(\tilde{u}, \tilde{v})$, here taken as $(\tilde{u}_2, \tilde{v}_2)$, in the above four equations gives a lengthy pair of equations in terms of the remaining variables, here $(\tilde{u}_1, \tilde{v}_1)$. The zero contours for each of these equations are plotted in the $(\tilde{u}_1, \tilde{v}_1)$ plane, and the points where the zero contours intersect represent the steady-state solutions for $(\tilde{u}_1, \tilde{v}_1)$. The corresponding solutions for $(\tilde{u}_2, \tilde{v}_2)$ can be found by using the equations that were used to eliminate them from the original four equations. Note that solutions that satisfy $(\tilde{u}_1, \tilde{v}_1) = (\tilde{u}_2, \tilde{v}_2)$ are unison solutions, and these will be captured by the analysis for any value of M.

3.1.2 Stability of the Steady State Solutions

The stability of the steady state solutions is obtained by numerically computing the eigenvalues of the Jacobian matrix of the system (3.5), evaluated at $\bar{a}_i = \tilde{a}_1, \bar{\phi}_i = \tilde{\phi}_1$ $\forall i \in [1, M]$, and $\bar{a}_i = \tilde{a}_2, \bar{\phi}_i = \tilde{\phi}_2$ $\forall i \in [M+1, N]$. Due to the symmetry of this problem, the Jacobian matrix J has the following block structure:

$$J = \begin{bmatrix} A & B \\ C & D \end{bmatrix} \tag{3.9}$$

where the matrices A, B, C, and D are as follows:

$$A = \begin{bmatrix} A1 & A2 & . & . & . & A2 \\ A2 & A1 & A2 & . & . & A2 \\ . & . & . & . & . & . \\ A2 & . & . & . & A1 & A2 \\ A2 & . & . & . & . & A1 \end{bmatrix}_{2MX2M} , B = \begin{bmatrix} B1 & . & B1 \\ . & . & . \\ B1 & . & B1 \end{bmatrix}_{2MX2(N-M)}$$

$$\mathrm{C}=\begin{bmatrix} C1 & . & C1 \\ . & . & . \\ C1 & . & C1 \end{bmatrix}_{2(N-M)X2M} \qquad D = \begin{bmatrix} D1 & D2 & . & . & . & D2 \\ D2 & D1 & D2 & . & . & D2 \\ . & . & . & . & . & . \\ D2 & . & . & . & D1 & D2 \\ D2 & . & . & . & . & D1 \end{bmatrix}_{2(N-M)X2(N-M)}$$

The matrices A1, A2, B1, C1, D1, and D2 are 2 by 2 with the following entries:

$$A1_{11} = -\frac{\tilde{\mu}_a}{2},\ A1_{12} = \frac{\tilde{\Gamma}_g}{2n}\cos(\tilde{\phi}_1) + \frac{n}{2N}(M-1)\tilde{a}_1 + \frac{n}{2N}(N-M)\tilde{a}_2\cos(\tilde{\phi}_1 - \tilde{\phi}_2),$$
$$A1_{21} = \frac{-3\gamma_o}{2n}\tilde{a}_1 - \frac{1}{\tilde{a}_1^2}\{\frac{n}{2N}[(M-1)\tilde{a}_1 + (N-M)\tilde{a}_2]\cos(\tilde{\phi}_1 - \tilde{\phi}_2) + \frac{\tilde{\Gamma}_g}{2n}\cos(\tilde{\phi}_1)\},$$
$$A1_{22} = -\frac{1}{\tilde{a}_1}[\frac{\tilde{\Gamma}_g}{2n}\sin(\tilde{\phi}_1) + \frac{n}{2N}\tilde{a}_2(N-M)\sin(\tilde{\phi}_1 - \tilde{\phi}_2)],$$

$$A2_{11} = 0,\ A2_{12} = -\frac{n}{2N}\tilde{a}_1,\ A2_{21} = \frac{1}{\tilde{a}_1}\frac{n}{2N},\ A2_{22} = 0,$$

$$B1_{11} = \frac{n}{2N}\sin(\tilde{\phi}_1 - \tilde{\phi}_2), B1_{12} = -\frac{n}{2N}\tilde{a}_2\cos(\tilde{\phi}_1 - \tilde{\phi}_2),$$
$$B1_{21} = \frac{n}{2N\tilde{a}_1}\cos(\tilde{\phi}_1 - \tilde{\phi}_2), B1_{22} = \frac{n\tilde{a}_2}{2N\tilde{a}_1}\sin(\tilde{\phi}_1 - \tilde{\phi}_2)$$

$$C1_{11} = \frac{n}{2N}\sin(\tilde{\phi}_2 - \tilde{\phi}_1), C1_{12} = -\frac{n}{2N}\tilde{a}_2\cos(\tilde{\phi}_2 - \tilde{\phi}_1),$$
$$C1_{21} = \frac{n}{2N\tilde{a}_2}\cos(\tilde{\phi}_2 - \tilde{\phi}_1), C1_{22} = \frac{n\tilde{a}_1}{2N\tilde{a}_2}\sin(\tilde{\phi}_2 - \tilde{\phi}_1)$$

$$D1_{11} = -\frac{\tilde{\mu}_a}{2}, D1_{12} = \frac{\tilde{\Gamma}_g}{2n}\cos(\tilde{\phi}_2) + \frac{n(N-M-1)}{2N}\tilde{a}_2 + \frac{nM}{2N}\tilde{a}_1\cos(\tilde{\phi}_2 - \tilde{\phi}_1),$$
$$D1_{21} = \frac{-3\gamma_o}{2n}\tilde{a}_2 - \frac{1}{\tilde{a}_2^2}\{\frac{n}{2N}[(N-M-1)\tilde{a}_2 + M\tilde{a}_1]\cos(\phi g2 - \tilde{\phi}_1) + \frac{\tilde{\Gamma}_g}{2n}\cos(\tilde{\phi}_2)\},$$
$$D1_{22} = -\frac{1}{\tilde{a}_2}[\frac{\tilde{\Gamma}_g}{2n}\sin(\tilde{\phi}_2) + \frac{nM}{2N}\tilde{a}_1\sin(\tilde{\phi}_2 - \tilde{\phi}_1)],$$

$$D2_{11} = 0, D2_{12} = -\frac{n}{2N}\tilde{a}_2, D2_{21} = \frac{1}{\tilde{a}_2}\frac{n}{2N}, D2_{22} = 0.$$

3.2 Numerical Example and Discussion

Here, the system used in the last chapter will again be considered here. The numerical values are as follows: $N = 4$ CPVAs with an inertia ratio of $\frac{1}{20}$, *i.e.*, $\epsilon = \frac{1}{20}$, the order of the applied fluctuating torque is 2, *i.e.*, $n = 2$, the non-dimensional absorber damping coefficient is 0.02, *i.e.*, $\frac{\tilde{\mu}_a}{N} = 0.02$, the dimensionless rotor damping coefficient, a quantity needed for numerical simulations, is 0.005, *i.e.*, $\mu_o = 0.005$. Two path types are studied, namely, circular and cycloidal paths. For numerical simulations, the full equations of motion and the exact representations of the paths given in chapter 2 are used.

3.2.1 Circular Path

Here, perfectly tuned ($\sigma = 0$), slightly mistuned ($\sigma = 0.1$), and moderately mistuned ($\sigma = 0.5$) paths are analyzed (negative mistuning is not of practical interest (see chapter 2). Figures 3.1(a) and 3.1(b) show typical graphical solutions for the steady state responses at a certain torque level for the perfectly tuned path for steady-state responses of types $M = 1$ and $M = 2$, respectively. Figures 3.2(a) and 3.2(b) show similar results for the case $\sigma = 0.1$, which has more solutions. Every intersection point of the curves represents a steady state response. Figures 3.3–3.8 show absorber response amplitudes versus torque amplitude, in each case showing the hysteretic jump behavior of the unison response. The points P1u, P2u, and P3u, in Figures 3.1 and 3.2 represent points that correspond to unison responses. P1u is a point on the lower unison response curve, P2u is a point on the middle unison response curve, and P3u is a point on the upper unison response curve (see chapter 2 for more details on the unison response branches). The only steady state solutions that could be found for the perfectly tuned paths are the unison responses, see Figures 3.1(a) and 3.1(b). When positive mistuning is introduced, a solution that is usually employed

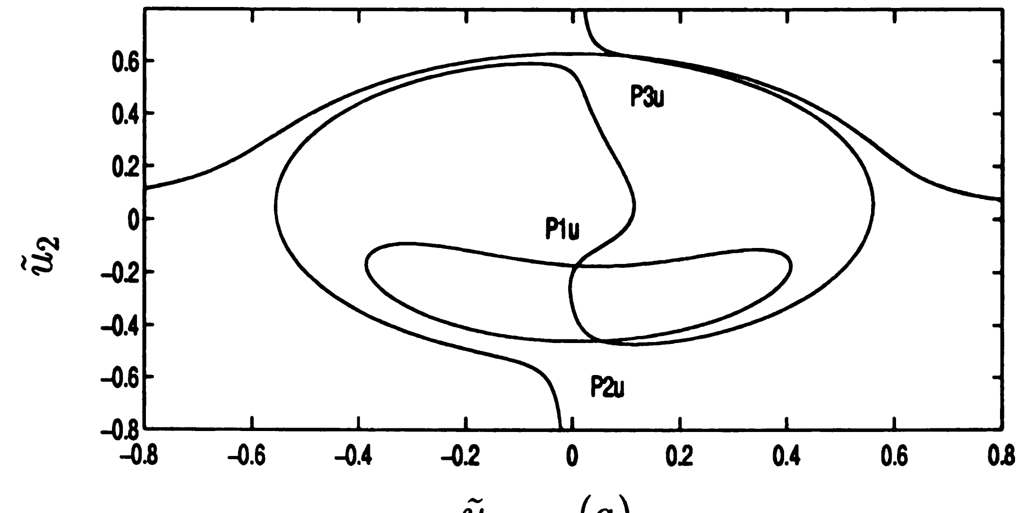

(a)

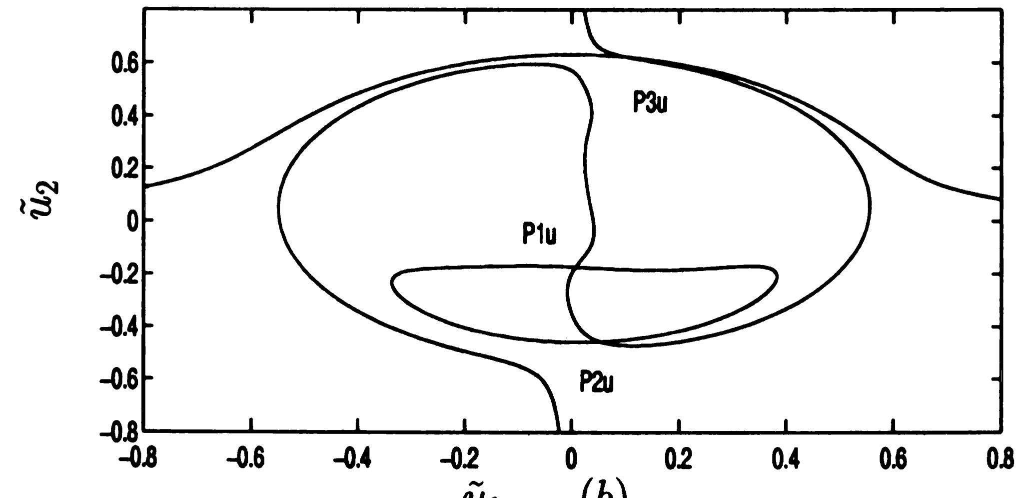

(b)

Figure 3.1. Steady-state solution conditions for a perfectly tuned circular path, (a) M=1, (b) M=2, $\Gamma_\theta = 0.007$.

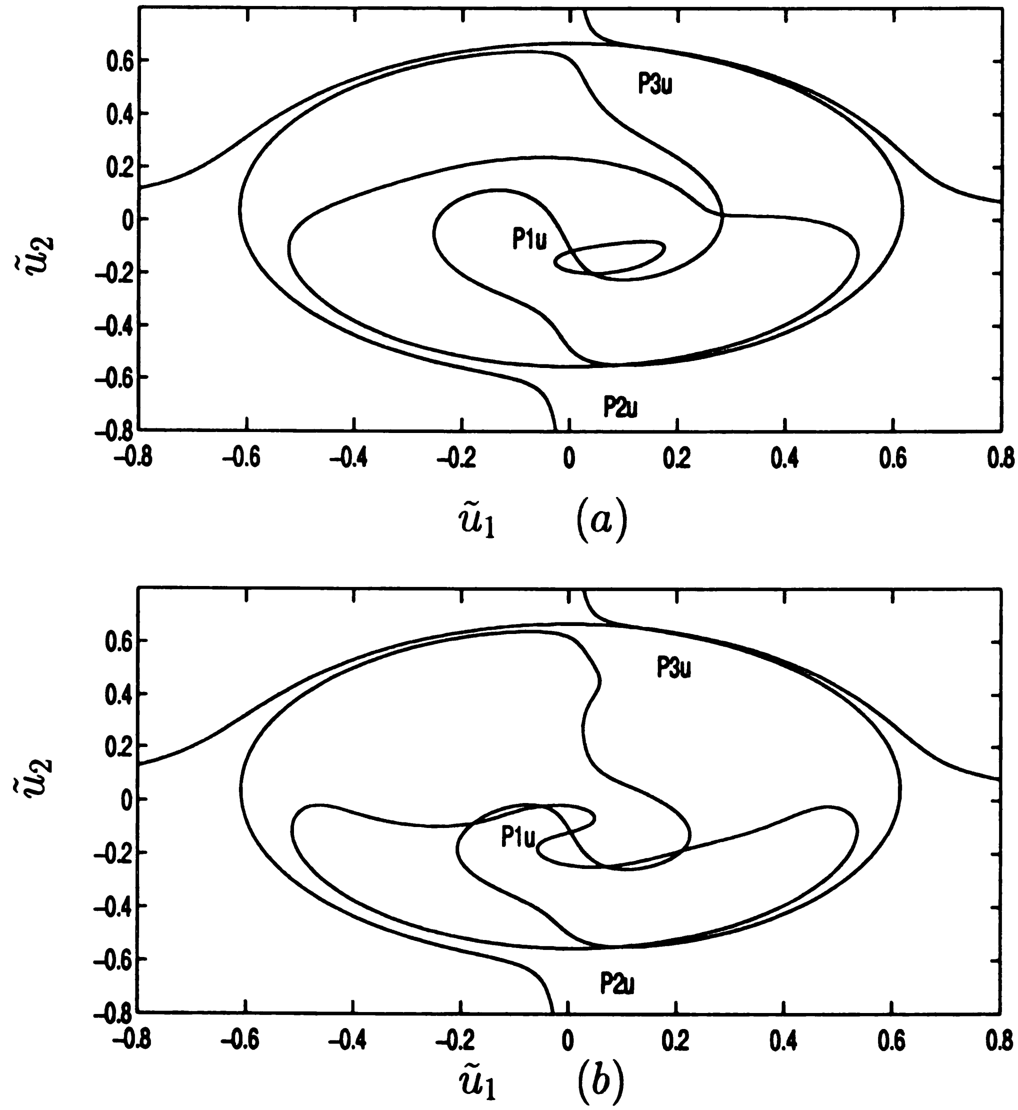

Figure 3.2. Steady-state solution conditions for a mistuned circular path with $\sigma = 0.1$, (a) M=1, (b) M=2, $\Gamma_\theta = 0.006$.

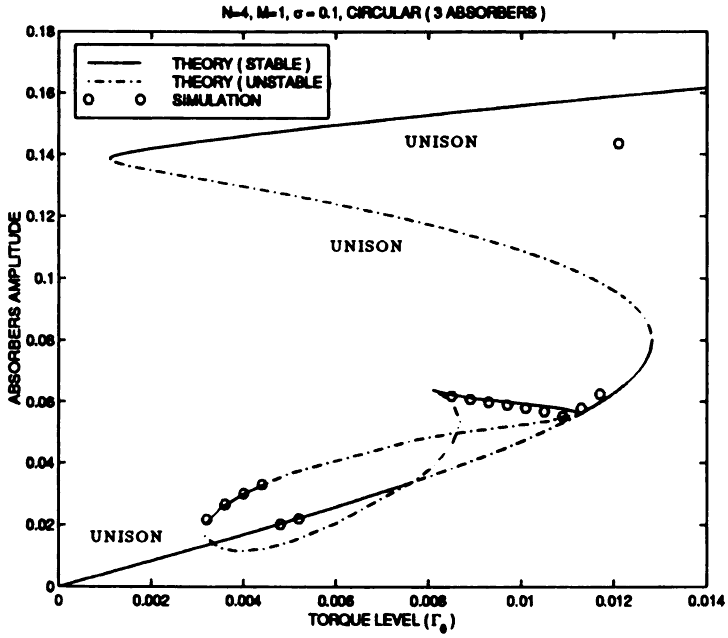

Figure 3.3. Response curves for three absorbers for the case M=1, N=4. Circular paths with $\sigma = 0.1$.

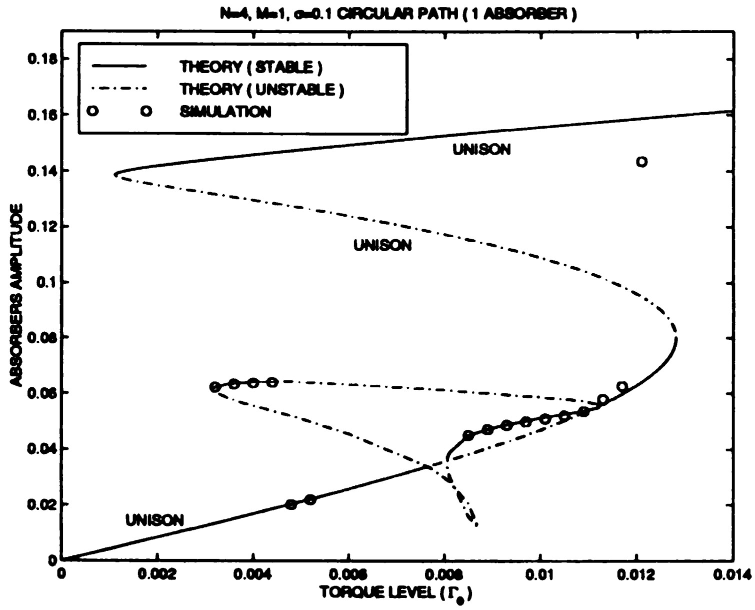

Figure 3.4. Response curves for one absorber for the case M=1, N=4. Circular paths with $\sigma = 0.1$.

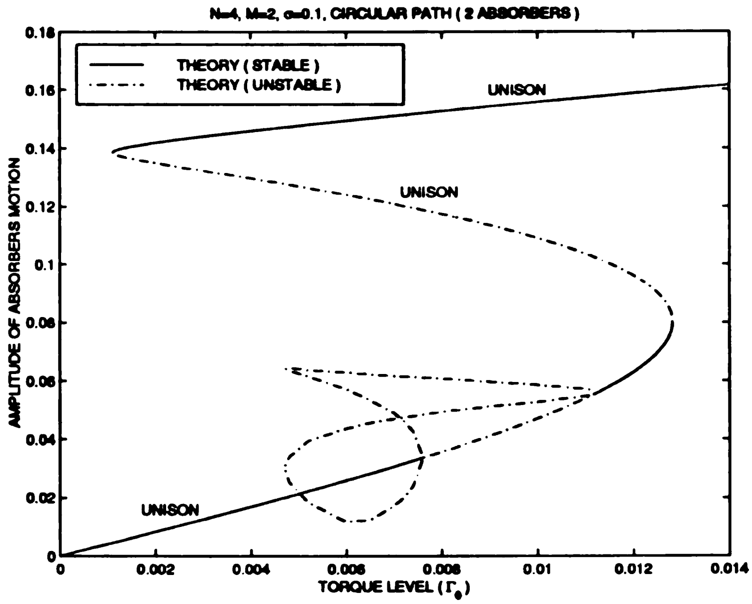

Figure 3.5. Response curves for two absorbers for the case M=2, N=4. Circular paths with $\sigma = 0.1$.

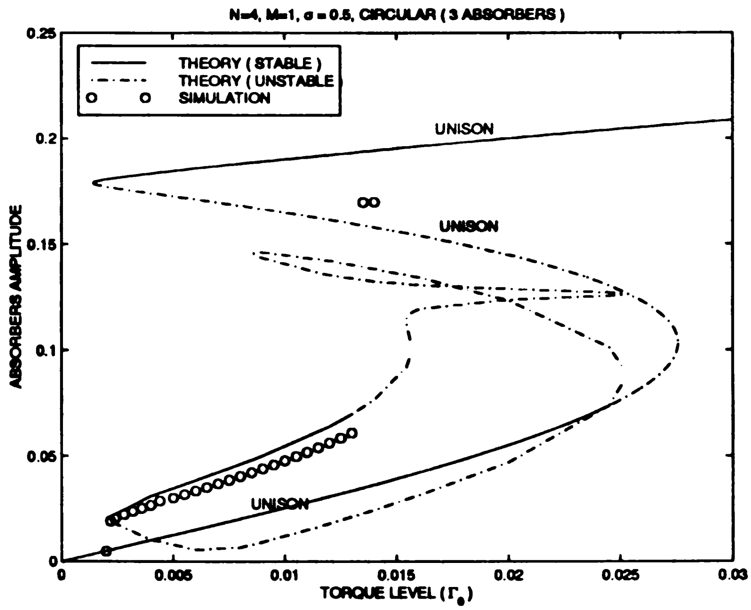

Figure 3.6. Response curves for three absorbers for the case M=1, N=4. Circular paths with $\sigma = 0.5$.

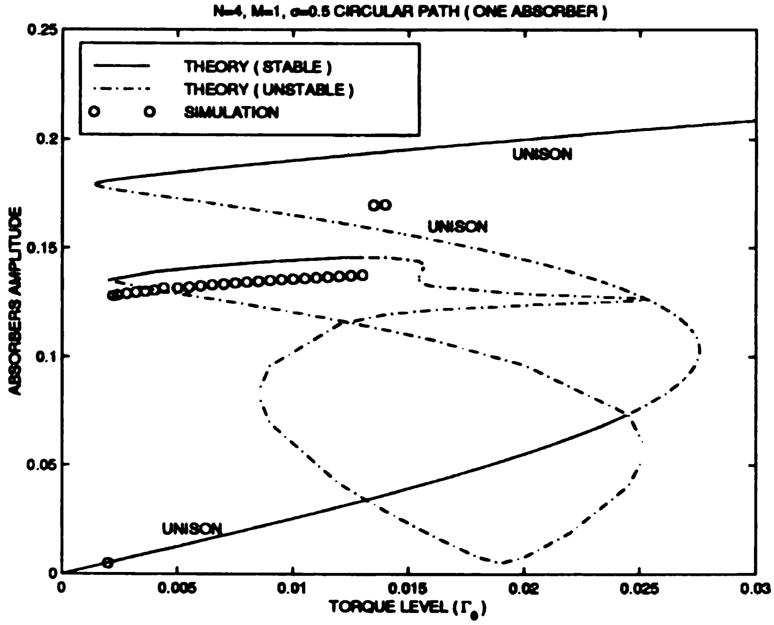

Figure 3.7. Response curves for one absorber for the case M=1, N=4. Circular paths with $\sigma = 0.5$.

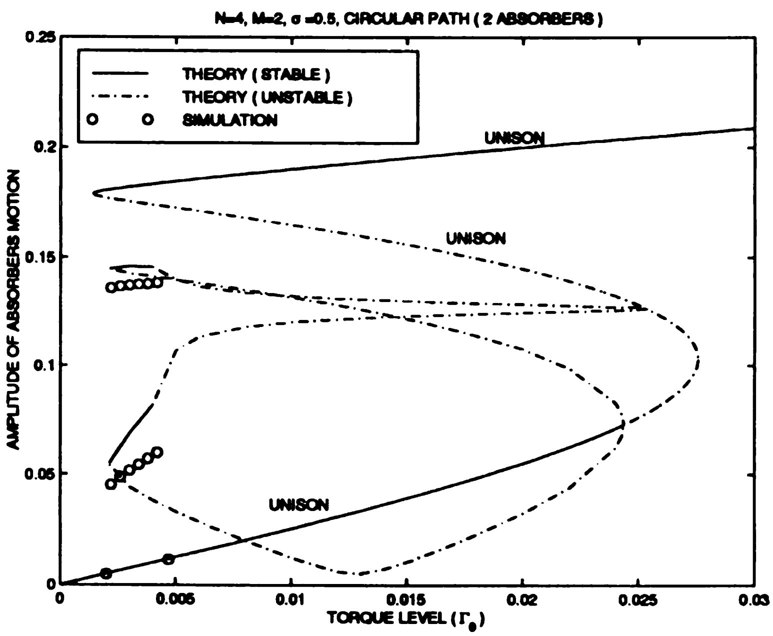

Figure 3.8. Response curves for two absorbers for the case M=2, N=4. Circular paths with $\sigma = 0.5$.

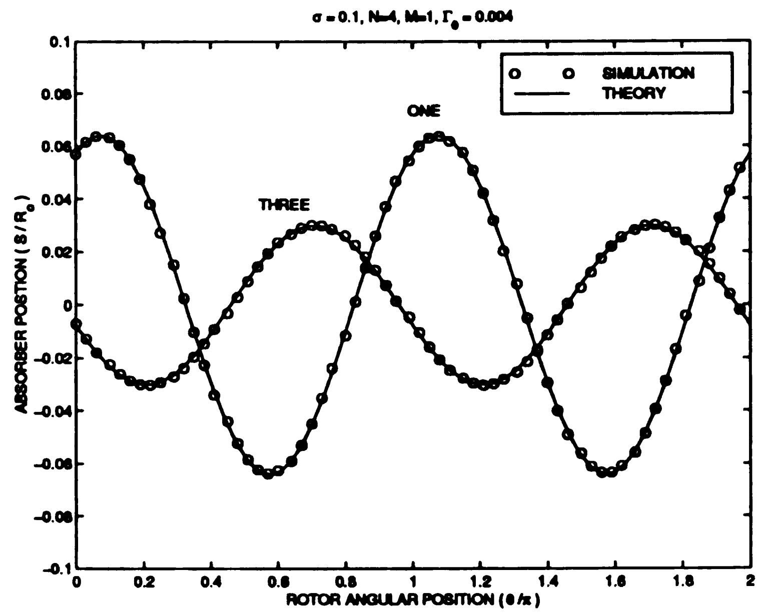

Figure 3.9. Typical localized response. $\sigma = 0.1$ circular path. N=4, M=1, $\Gamma_\theta = 0.004$.

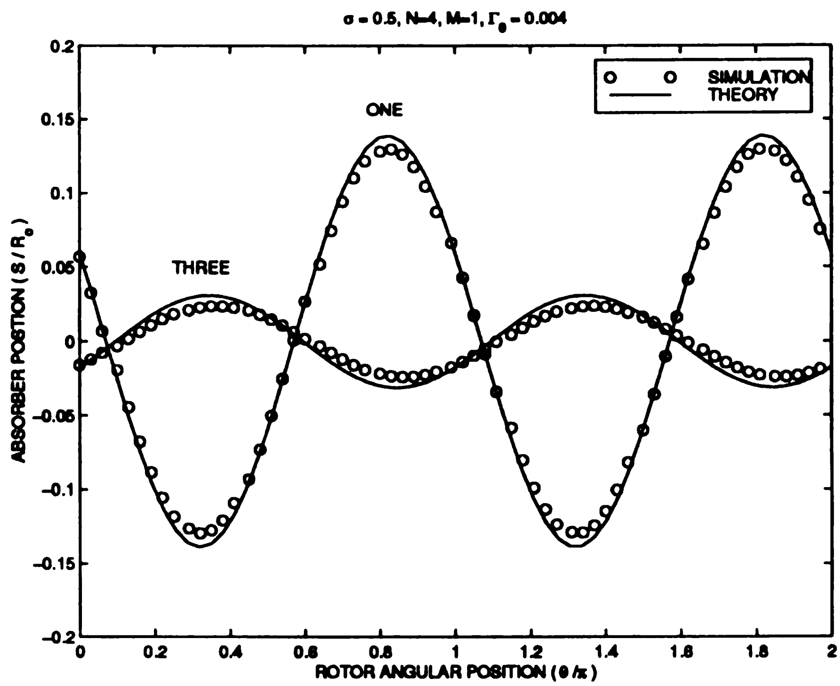

Figure 3.10. Typical localized response. $\sigma = 0.5$ circular path. N=4, M=1, $\Gamma_\theta = 0.004$.

to overcome some undesirable non-linear effects, and to increase the working range of the absorbers, solutions other than unison exist, as shown in Figures 3.2(a) and 3.2(b).

Figures 3.3–3.8 each show the unison response branches, along with some of the non-unison solutions. These figures indicate the accuracy of the asymptotic, approximate solution procedure, both in terms of existence and stability. Figures 3.3 and 3.4 show the response curves for the case $\sigma = 0.1$, $M = 1$, with Figure 3.3 indicating the response of the group of three absorbers and Figure 3.4 showing the response of the single absorber. An example of such a localized response for a particular torque level is depicted in Figure 3.9. For the same path parameters, Figure 3.5 shows the response of the group consisting of two absorbers moving in unison, *i.e.*, $M = 2$ for the case $\sigma = 0.1$. Note here that all such non-unison solutions are unstable.

Similarly, Figures 3.6, 3.7, 3.8 are the analogous plots for a case with larger mistuning, $\sigma = 0.5$. These figures clearly show the existence of non-unison solutions and the way they bifurcate from the unison solution. Figure 3.10 shows a simulation result at a particular level of torque excitation.

It is important to note that these non-unison responses co-exist with the stable unison response, but result in one or more absorbers undergoing a much larger amplitude of oscillation than predicted for the unison response. Also, in practice one introduces some level of mistuning in order to extend the operating range of the absorbers for a given amount of absorber mass; this can be observed by comparing the horizontal scales in Figures 3.3-3.5 with those of Figures 3.6-3.8, and noting that the lower unison response branch is the one of interest. However, the larger level of mistuning actually increases the possibility of encountering a non-unison response at a given torque level.

3.2.2 Cycloidal Paths

Steady state solutions other than unison were not found for perfectly and positively mistuned cycloidal paths. They exist only for negatively mistuned cycloidal paths. Since negatively mistuned paths are not of practical importance (see chapter 2 for more details), no results are presented here.

3.3 Conclusions

Based on the above results, the following conclusions can be drawn:

- For perfectly tuned circular CPVA paths, the only steady state solutions that were found were the ones that correspond to unison motions. When mistuning is introduced, other steady state solutions that depend on the level of mistuning appear. Those solutions must be taken into account when designing CPVA systems.

- For perfectly tuned or positively mistuned cycloidal CPVA paths, no solutions other than those that correspond to unison motions exist. This is one of many advantages that cycloidal paths have over circular paths [10, 17].

- The steady state responses where a subset of absorbers is not in unison with the remaining absorbers can often correspond to a non-linear localized response. The strength of this localized response and the range over which it is stable depend on the level of mistuning. This type of steady state solutions will be reconsidered in chapter 5.

CHAPTER 4

Localization of Free Vibration Modes in Systems of Nearly-Identical Vibration Absorbers

In this chapter, the linear free vibration of systems in which groups of nearly identical vibration absorbers are employed is considered. It is demonstrated that the phenomenon of mode localization occurs in these types of systems. In these systems the absorbers are not directly coupled to one another via flexibility elements, but rather the coupling is through the inertia of the primary mass. This coupling is of the order of the ratio of the absorber inertia to the primary mass inertia, and is typically small in applications. An eigenvalue/eigenvector perturbation technique is used to find approximations of the modes of free vibration, and it is shown to be accurate when the ratio of coupling to mistuning is small. Both translational and torsional absorber systems are considered, and the results obtained raise some interesting questions regarding the steady-state response of the overall system, and the performance limits of the absorber system, when it is subjected to periodic excitation at a frequency close to that of the absorbers'. This chapter is organized as follows. Section 4.1 describes the two types of absorber systems and formulates the equations of motion for each in such a manner that the perturbation technique can be readily applied. Section 4.2 describes the analysis and presents sample results, and the chapter closes with some conclusions in Section 4.3.

4.1 Formulation

4.1.1 Translational Vibration Absorbers

Consider a structure of mass M on which are mounted N vibration absorbers of masses m_i and spring stiffnesses k_i, $(i = 1.., N)$, as shown in Figure 4.1. We consider the case in which the natural frequency of the primary mass-spring system is much smaller than that of the absorbers, and use the limiting case in which the primary mass has no stiffness to ground, so that the overall system has a rigid body mode. In the analysis, this mode will be uncoupled via a simple change of coordinates. A similar system (only with stiffness to ground) has been considered by Weaver [40], who considered the response to random excitation of a system with a large number of substructures having a distribution of natural frequencies.

The equations of motion for free vibration of this system are

$$M\ddot{y} + \sum_{i=1}^{N} m(\ddot{z}_i + \ddot{y}) = 0, \tag{4.1}$$

$$m(\ddot{z}_i + \ddot{y}) + k_i z_i = 0. \tag{4.2}$$

It is assumed that the absorbers have equal masses (*i.e.*, $m_i = m$), and the stiffnesses will be used to introduce mistuning among the absorbers. The dynamics of the big mass can be uncoupled from the absorbers' by substituting $\ddot{y}$ from equation (4.2) into

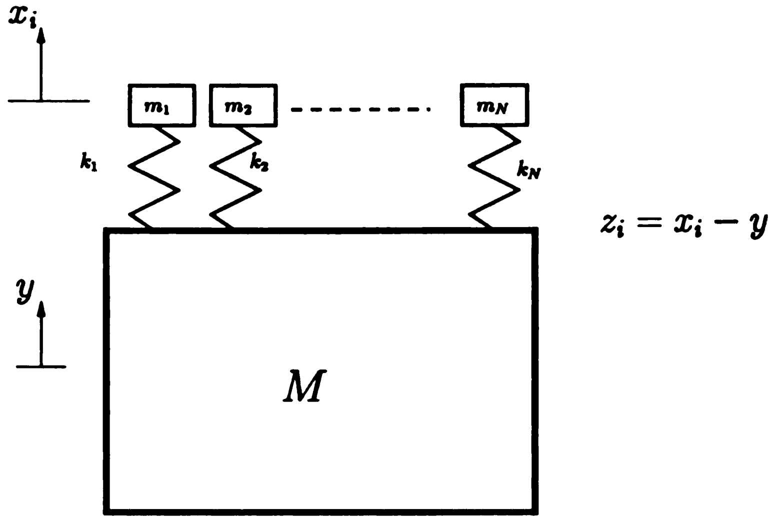

Figure 4.1. Translational vibration absorbers

equation (4.1), and rearranging. The following equations which describe the responses of the absorbers are obtained

$$\ddot{z}_i + (1 + \frac{1}{N}\frac{m_o}{M})\omega_i^2 z_i + \frac{1}{N}\frac{m_o}{M}\sum_{j=1,j\neq i}^{N}\omega_j^2 z_j = 0, \tag{4.3}$$

where $m_o = Nm$ is the total mass of all absorbers, and $\omega_i^2 = k_i/m$ are their individual, uncoupled frequencies.

In typical applications the absorber mass is significantly smaller than the primary mass. Therefore, the ratio of the absorber masses to the structure mass, denoted as ϵ, *i.e.*, $\epsilon = \frac{m_o}{M}$ is introduce as a small parameter. Since the absorbers are coupled to each other only through the primary mass, ϵ represents the degree of coupling between the individual absorbers. Equation (4.3) can now be expressed in matrix form as follows

$$\mathbf{I}\,\ddot{\tilde{z}} + \mathbf{A}\,\tilde{z} = \tilde{0}, \tag{4.4}$$

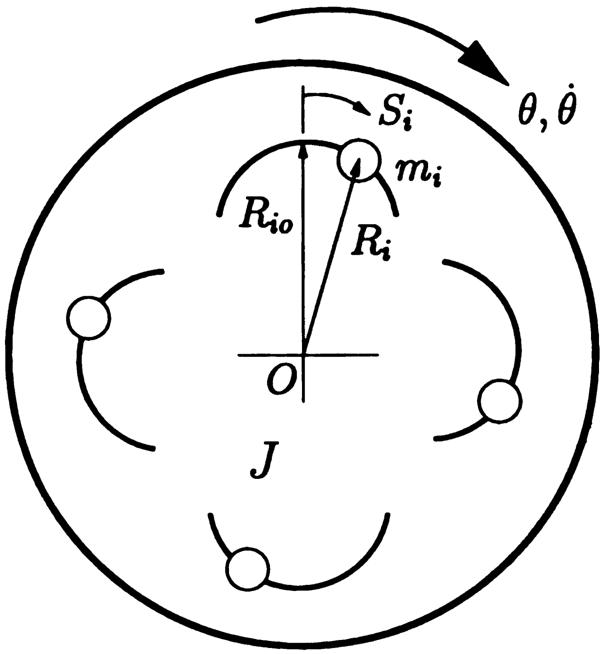

Figure 4.2. Torsional vibration absorbers

where

$$\begin{aligned} \mathbf{A} &= \mathbf{A_o} + \delta\mathbf{A} \\ \mathbf{A_o} &= Diag[\omega_i^2]. \end{aligned} \tag{4.5}$$

$\delta\mathbf{A}$ is an NXN matrix with each element equals to $\frac{\epsilon}{N}\omega_{nom}^2$, ω_{nom} is the nominal frequency of the absorbers. Since the diagonal matrix $\mathbf{A_o}$ has readily obtained eigenvalues and eigenvectors, equation (4.4) is in a form suitable for the application of an eigenvalue perturbation method. Before doing so, it is first shown that the dynamics of a system of torsional vibration absorbers can also be expressed in this form.

4.1.2 Centrifugal Pendulum Vibration Absorbers

A system of N torsional vibration absorbers which are mounted on a rotor of inertia J, as the one that was introduced in chapter 2 is considered. The free vibration equations of motion for this system, for arbitrary absorber amplitudes, are as follows:

$$\ddot{s}_i + g_i(s_i)\ddot{\theta} - \frac{1}{2}\frac{dx_i}{ds_i}(s_i)\dot{\theta}^2 = 0 \tag{4.6}$$

$$J\ddot{\theta} + \sum_{i=1}^{N} m_i R_{io}^2 [\frac{dx_i}{ds_i}(s_i)\dot{s}_i\dot{\theta} + x_i(s_i)\ddot{\theta} + g_i(s_i)\ddot{s}_i + \frac{dg_i}{ds_i}(s_i)\dot{s}_i^2] = 0, \tag{4.7}$$

where the functions $x_i(s_i)$ and $g_i(x_i)$ are as defined in chapter 2. For reasons that will be clear later, the i^{th} path order, $\tilde{n}_i$, which as indicated before represents the variability of the tuning of each absorber path from the nominal tuning of order n, is defined slightly in a different manner than its definition in chapter 2. It is defined here as follows:

$$\tilde{n}_i = n(1 + \sigma_i) \quad \sigma_i << 1.$$

Again assuming that the absorbers have equal masses and the value of R_i at the vertex of the path is the same for all the absorbers (*i.e.*, $m_i = m$, and $R_{io} = R_o$), using the definitions of the functions $g_i(s_i)$ and $x_i(s_i)$, and linearizing equations (4.6) and (4.7) about $s_i = 0$, and $\dot{\theta} = \Omega$, where Ω is the nominal speed of the rotor, the following linear equations for the system dynamics are obtained

$$J\ddot{\theta} + \sum_{i=1}^{N} mR_o^2(\ddot{\theta} + \ddot{s}_i) = 0 \tag{4.8}$$

$$\ddot{s}_i + \ddot{\theta} + \Omega^2\tilde{n}_i^2 s_i = 0. \tag{4.9}$$

Comparing equations (4.8) and (4.9) with equations (4.1) and (4.2), they are clearly seen to be equivalent. This implies that equation (4.4) also applies to torsional vibration absorbers systems. In this case, the small parameter ϵ represents the ratio of the total moment of inertia of the absorbers to the rotor moment of inertia ($\epsilon = \frac{NmR_o^2}{J}$), and ω_i is replaced here by $\Omega\tilde{n}_i$.

4.2 Analysis and Discussion

4.2.1 General Features of the System

The system of equations (4.1, 4.2) has some interesting properties when the absorbers are identical. When $k_i = k \ \forall i$, the absorbers have identical natural frequencies. In this case the overall $N+1$ degrees-of-freedom system has two modes in which the absorber masses move in a synchronous manner, and these correspond to the modes of an equivalent two-degrees-of-freedom system (one is the rigid body mode, the other is oscillatory). The remaining $N-1$ modes have identical frequencies and mode shapes that correspond to the absorber masses moving in such a manner that they exert zero net force on the primary mass, rendering it stationary. The selection of the modes in this degenerate case is highly non-unique. Therefore, the level of imperfections cannot be used as a small parameter in a perturbation scheme, since one does not have a specified set of modes that can be used as the starting point in the perturbation scheme. This unperturbed system has absolute sensitivity to the mistuning in the sense that different arrangements of mistuning lead to completely different sets of modes.

On the other hand, the case of zero coupling and nonzero mistuning is unique, since the modes are represented by the ideally localized responses in which only one absorber is active and the others are stationary. These are naturally suited for use as the seed modes in a perturbation scheme [25].

Singular perturbation schemes have recently been used to capture localized modes for all relative ranges of mistuning and coupling [39, 41]. However, in the present case this is not feasible, due to the completely degenerate nature of the system in the case of zero mistuning.

4.2.2 Perturbation Method Formulation

The normal modes of vibration are represented by the eigenvectors of the matrix $\mathbf{A}$ in equation (4.4). These can be determined here using a standard perturbation method of the eigenvalue problem [42]. The following expressions are used for the eigenvalues (λ_i) and the eigenvectors ($\tilde{v}_i$), up to second order in approximation

$$\lambda_i = \lambda_{oi} + \delta\lambda_i + \delta^2\lambda_i,$$

$$\tilde{v}_i = \tilde{v}_{oi} + \delta\tilde{v}_i + \delta^2\tilde{v}_i,$$

where $\lambda_{oi}, \tilde{v}_{oi}$ are the eigenvalues and eigenvectors of $\mathbf{A_o}$ respectively. The terms in the perturbation expansion are solved for by matching terms and are given by

$$\delta\tilde{v}_i = \sum_{k=1}^{N} \nu_{ik}\tilde{v}_{ok}, \quad \delta^2\tilde{v}_i = \sum_{k=1}^{N} \eta_{ik}\tilde{v}_{ok}, \quad i = 1, ..., N$$

$$\delta\lambda_i = \frac{\tilde{y}_{oi}^T[\delta\mathbf{A}]\tilde{v}_{oi}}{\tilde{y}_{oi}^T\tilde{v}_{oi}}, \quad \delta^2\lambda_i = \frac{\tilde{y}_{oi}^T[\delta\mathbf{A}]\delta\tilde{v}_i - \delta\lambda_i\tilde{y}_{oi}^T\delta\tilde{v}_i}{\tilde{y}_{oi}^T\tilde{v}_{oi}}, \quad i = 1, ..., N$$

where, for $j \neq i$, the coefficients are

$$\nu_{ij} = \frac{1}{\tilde{y}_{oj}^T\tilde{v}_{oj}} \frac{\tilde{y}_{oj}^T[\delta\mathbf{A}]\tilde{v}_{oi}}{\lambda_{oi} - \lambda_{oj}}$$

$$\eta_{ij} = \frac{1}{\tilde{y}_{oj}^T\tilde{v}_{oj}} \frac{\delta\lambda_i\tilde{y}_{oj}^T\delta\tilde{v}_i - \tilde{y}_{oj}^T[\delta\mathbf{A}]\delta\tilde{v}_i}{\lambda_{oj} - \lambda_{oi}},$$

and for $j = i$,

$$\nu_{ii} = 0, \quad \eta_{ii} = -\frac{\delta\tilde{v}_i^T\delta\tilde{v}_i}{2\tilde{v}_{oi}^T\tilde{v}_{oi}}.$$

Here the symbol $\tilde{y}_{oi}$ represents the left eigenvectors of $\mathbf{A_o}$. Note that these expressions are, as expected, singular if the frequencies are repeated. That is, this perturbation scheme accounts for the effects of coupling, but the results become invalid if the

Table 4.1. Data for example 1.

Absorber	Mistuning (a)	Mistuning (b)
1	2%	1%
2	-2.5%	-1.2%
3	3.5%	1.7%
4	-4.5%	-2.2%
5	-1.0%	-0.5%
6	0.5%	0.2%

Table 4.2. Data for example 2.

Absorber	1	2	3	4	5	6	7	8	9	10
% Mistuning	1.2	0.0	1.6	-0.4	0.4	0.8	-1.2	-1.8	-0.8	-1.6

mistuning among the absorbers is small [25].

These perturbation results can be used to find the frequencies and modes of vibration. This is easy in the present case, since the eigenvectors of the matrix $\mathbf{A_o}$ can be taken as the canonical unit vectors (for the case of distinct eigenvalues). Two numerical examples are given here.

4.2.3 Examples

The purpose of these examples is to demonstrate the localization phenomenon and to show the accuracy of the perturbation method.

SIX ABSORBERS WITH MODERATE COUPLING

In this example, we consider a system of six absorbers with the data given in Table 4.1, and with a coupling coefficient of $\frac{1}{20}$. Two cases of mistuning are considered, as indicated in Table 4.1.

Figures 4.3 and 4.4 show the modes of free vibration obtained by the second order perturbation method and by the exact solution of the full eigenvalue problem. As expected, the perturbation results start to deviate from the exact solution in the case of small mistuning.

TEN ABSORBERS WITH SMALL COUPLING

Here we consider a system of ten absorbers with the data given in Table 4.2. The coupling coefficient is $\frac{1}{75}$, a value taken from an existing light aircraft engine. Figure 4.5 shows the free vibration modes for this system of absorbers. The modes are seen to be highly localized, and, as expected, the perturbation method works very well in this case.

4.3 Conclusions

Consideration of results obtained from the examples clearly shows that localization indeed occurs for this class of systems, and that the perturbation method is a reliable tool for obtaining the modes of vibration for a range of small coupling relative to mistuning. These results also indicate that some interesting and unexpected behavior may be found in the forced response of system of tuned vibration absorbers, in particular since these systems are excited at a frequency that is very close to the frequencies of the absorbers. This topic is the subject of the next chapter.

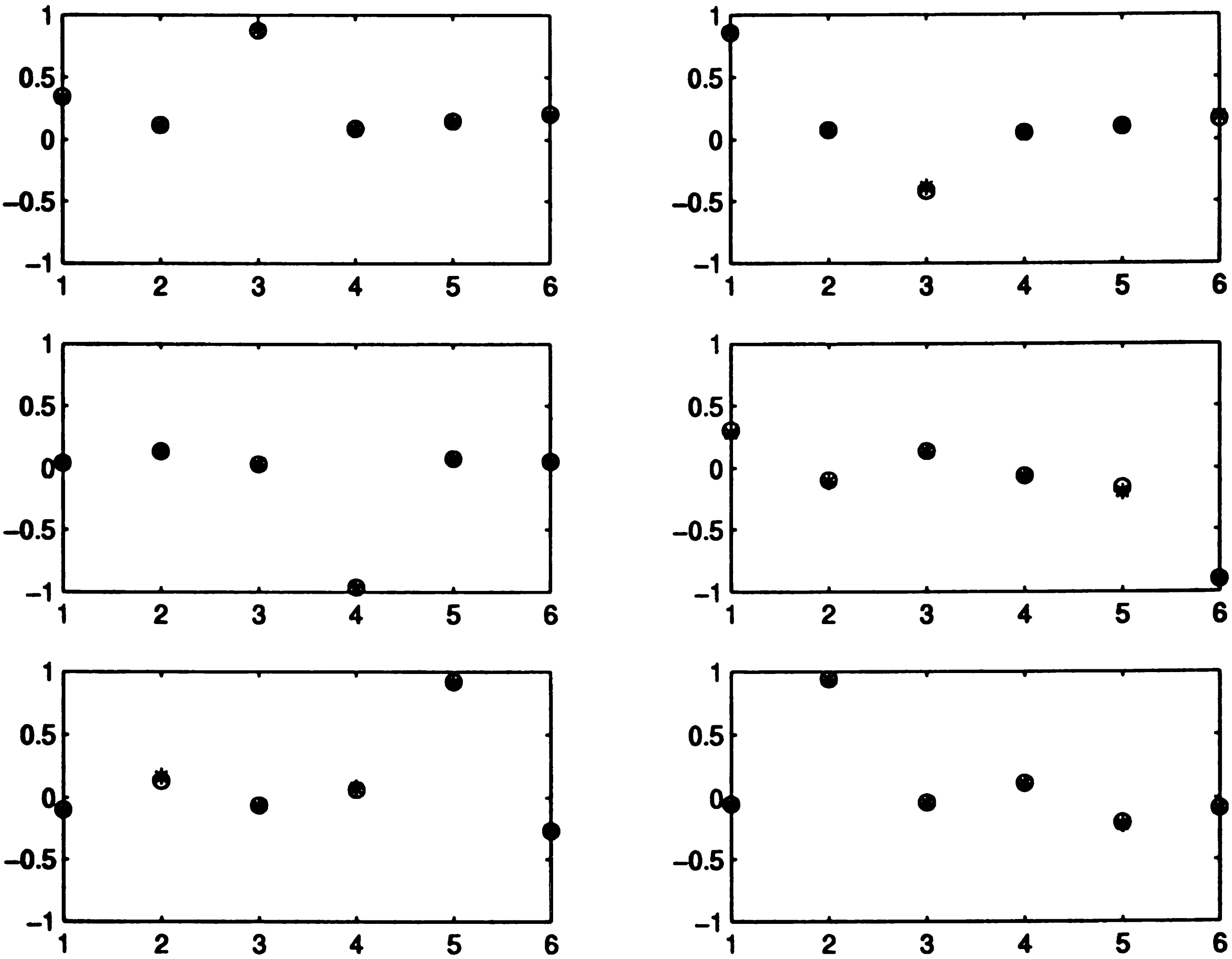

Figure 4.3. Modes of vibration for example 1(a). (*) Exact,(o) second order perturbation

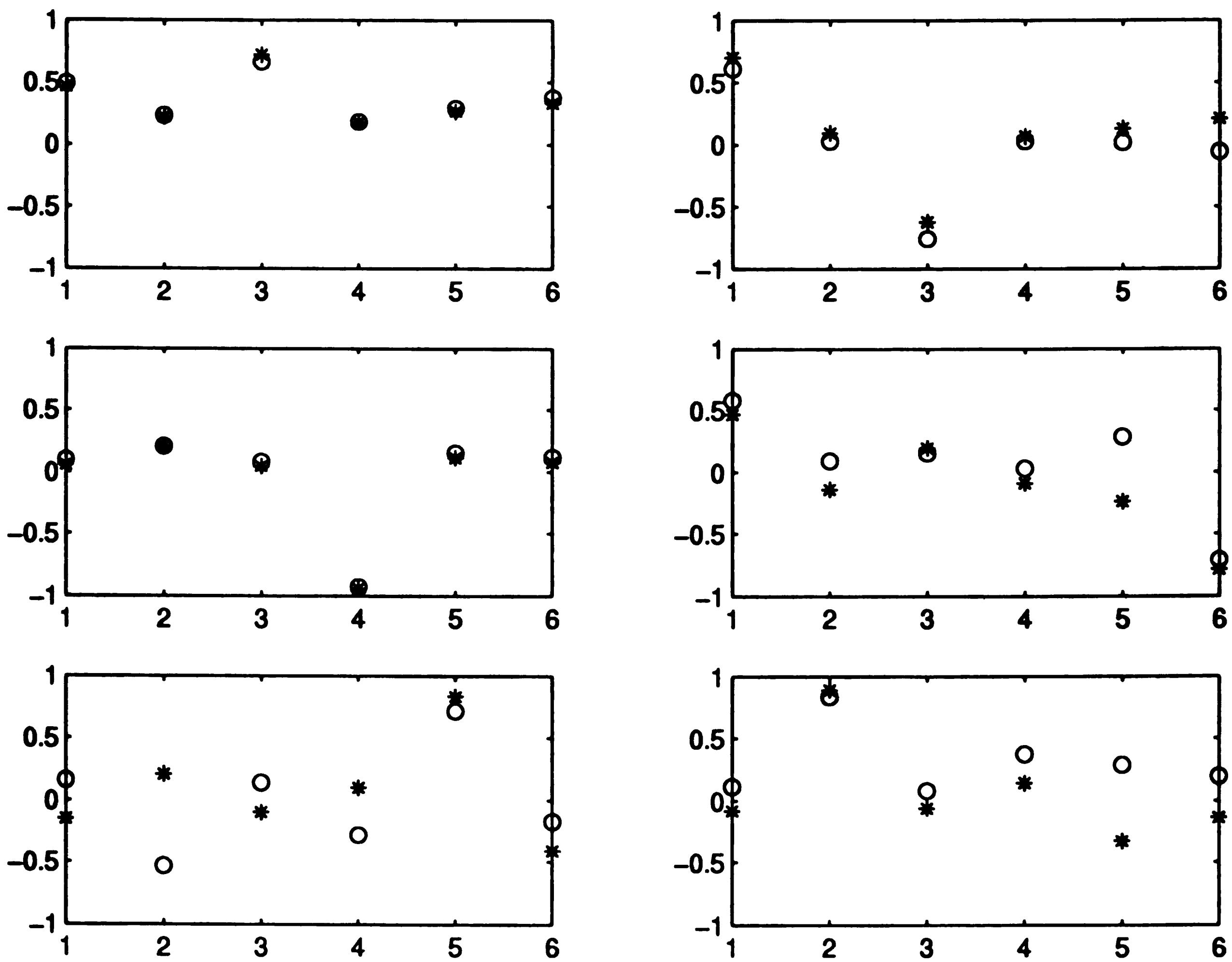

Figure 4.4. Modes of vibration for example 1(b). (∗) Exact, (∘) second order perturbation.

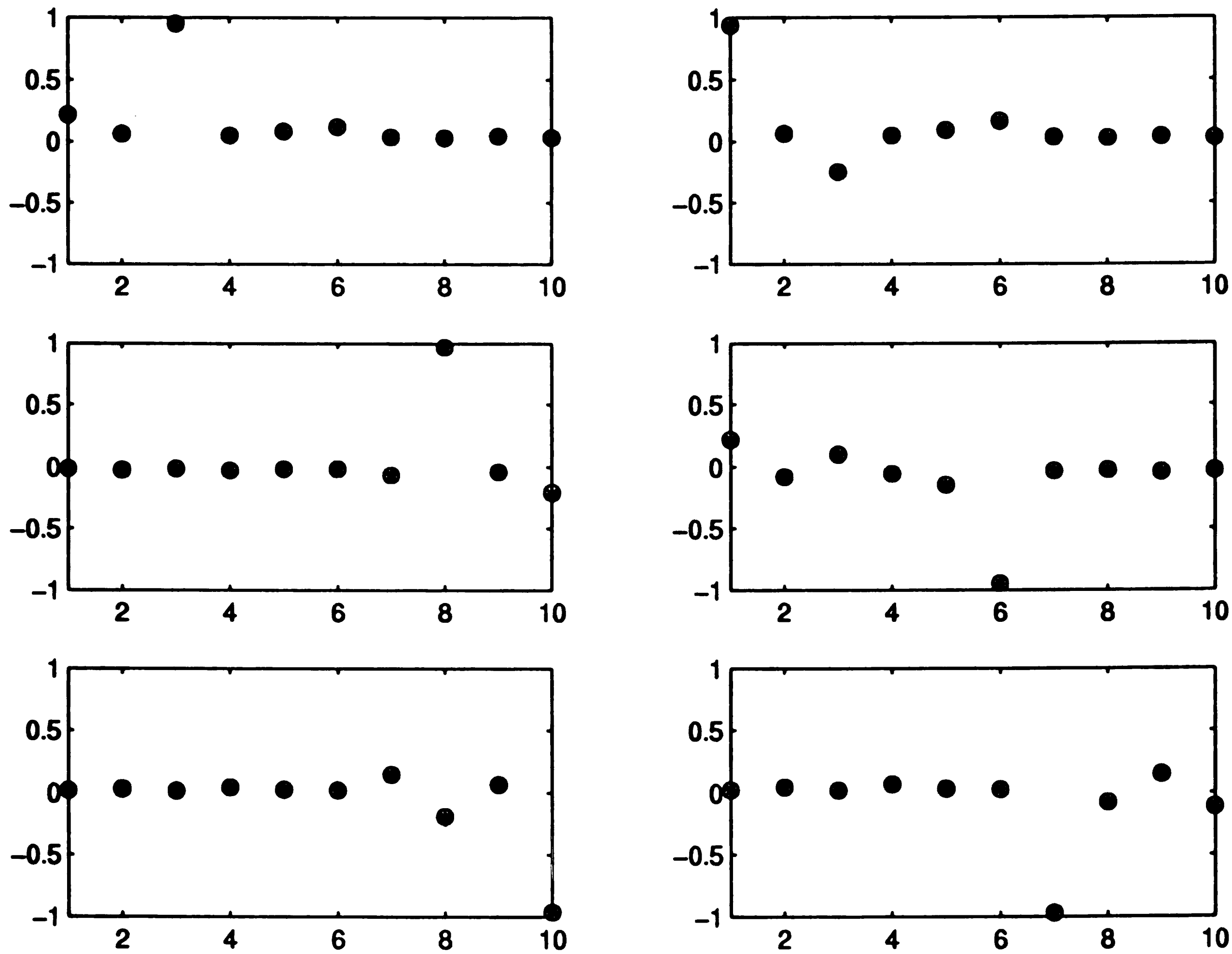

Figure 4.5. Some modes of vibration for example 2 . (∗) Exact, (∘) second order perturbation

CHAPTER 5

Forced Localized Response of Vibration Absorbers

In the previous chapter, localization of the absorbers' modes of free vibration was considered. It was found that when the ratio of coupling to imperfection is small, free vibration modes do localize. This result motivates the investigation of the localization phenomenon in the more important case, namely, when the system is under operation and subjected to periodic excitation. The study done in this chapter focusses on torsional vibration absorbers. The translational vibration absorbers case can be analyzed in a similar manner.

5.1 Linear Forced Response

5.1.1 Mathematical Formulation

Similar to the system studied in chapter 2, a system of N torsional vibration absorbers is considered. After scaling the system variables and parameters in the same way, and linearizing the equations that describe the absorbers dynamics, the following linear equations are obtained:

$$z_i'' + n^2 z_i = \epsilon[-2n^2\sigma_i z_i - \tilde{\mu}_a z_i' - \frac{1}{N}\sum_{j=1}^{N} n^2 z_j - \tilde{\Gamma}_\theta \sin(n\theta)] + HOT, \quad (5.1)$$

where all variables and parameters are defined in chapter 2. Rearranging and writing these equations in matrix form, one obtains

$$I_N \tilde{z}'' + n^2 Diag_N\left(1 + 2\epsilon\sigma_i\right)\tilde{z} + \epsilon\frac{n^2}{N}Ones(N)\tilde{z} + \epsilon\tilde{\mu}_a I_N \tilde{z}' = \epsilon\tilde{\Gamma}_\theta(1)_N \sin(n\theta) \quad (5.2)$$

where I_N denotes the NXN identity matrix, $Diag_N(x)$ denotes an NXN diagonal matrix with x in each diagonal entry, $Ones(N)$ denotes an NXN matrix with every element equal to one, and $(1)_N$ denotes an $NX1$ vector with every element equal to one. To formulate the problem so that the steady state responses, $\tilde{z}_{ss}$, can be found, we assume that $\tilde{z} = \tilde{z}_{ss}e^{jn\theta}$, where $j = \sqrt{-1}$, and $\tilde{z}_{ss} \in C^N$. When this is substituted in equations 5.1, the following equations are obtained:

$$(\mathbf{A} + \mathbf{B})\,\tilde{z}_{ss} = \tilde{f}, \quad (5.3)$$

where

$$\mathbf{A} = Diag\left(2\sigma_i + j\frac{\tilde{\mu}_a}{n}\right), \ \mathbf{B} = \frac{1}{N}Ones(N), \ \tilde{f} = \frac{1}{n^2}(1)_N\tilde{\Gamma}_\theta.$$

To find the steady state solutions, this NXN coupled linear system of equations must be solved. When this system is examined, it can be seen that it is not difficult to uncouple it. This can be done by employing the following procedure. For $m \in [1, N]$, $m \neq i$, subtract the m^{th} equation from the i^{th} equation for every value of m to get an expression for each z_{ssm} in terms of z_{ssi}. Substitute these expressions back in the equation for the i^{th} absorber to reach to the following uncoupled set of equations:

$$(Re_i + j\ Im_i) z_{ssi} = f, \tag{5.4}$$

where

$$Re_i = \left[\frac{1}{N} + 2\sigma_i + \frac{1}{N} \sum_{j=1, j\neq i}^{N} \frac{4\sigma_i\sigma_j + \left(\frac{\tilde{\mu}_a}{n}\right)^2}{4\sigma_j^2 + \left(\frac{\tilde{\mu}_a}{n}\right)^2} \right],$$

$$Im_i = \frac{\tilde{\mu}_a}{n} \left(1 + \frac{2}{N} \sum_{j=1, j\neq i}^{N} \frac{\sigma_j - \sigma_i}{4\sigma_j^2 + \left(\frac{\tilde{\mu}_a}{n}\right)^2} \right), \quad f = \frac{1}{n^2} \tilde{\Gamma}_\theta$$

The scaled steady state vibration amplitude of the i^{th} absorber will then be

$$|z_{ssi}| = \frac{f}{\sqrt{(Re_i)^2 + (Im_i)^2}} \tag{5.5}$$

When damping is small compared to mistuning, this amplitude becomes

$$|z_{ssi}| = \frac{f}{\left(\frac{1}{N} + 2\sigma_i + \frac{1}{N} \sum_{j=1, j\neq i}^{N} \frac{\sigma_i}{\sigma_j} \right).} \tag{5.6}$$

Examining this equation, it can be clearly seen that the amplitudes of vibration for all the absorbers will be the same as long as the levels of mistuning are the same. However, due to the fact that perfectly identical paths are not possible to manufacture and there are always some imperfections, one should not omit the possibility of the existence of some localized response, due the presence of the ratio $(\frac{\sigma_i}{\sigma_j})$ in equation (5.5). This equation says that when the mistuning levels of all absorbers are close to zero and a sub-group of absorbers have mistuning levels that are lower than the remaining absorbers, then those with the low mistuning levels will localize, *i.e.*, their amplitudes of vibration will be significantly higher than those of the remaining absorbers. The strength of this localized response depends on how close the levels of mistuning of the sub-group that is localizing are to zero and how far they are from those of the remaining absorbers.

Table 5.1. Data for example 5.1

Absorber	a. $\sigma(\%)$	b. $\sigma(\%)$	c. $\sigma(\%)$	d. $\sigma(\%)$
1	0.01 (0.16)	0.010 (0.16)	0.010 (0.16)	0.010 (0.16)
2	0.07 (1.16)	0.008 (0.13)	0.008 (0.13)	0.008 (0.13)
3	0.05 (0.83)	0.050 (0.83)	0.009 (0.15)	0.009 (0.15)
4	0.06 (0.99)	0.060 (0.99)	0.060 (0.99)	0.011 (0.18)

In the presence of small damping (recall that damping should be small for good absorber performance, see chapter 2 for more details), this result will not be significantly affected. However, when damping is large compared to the mistuning levels, localization will not occur.

It should be noted here that localization is expected to occur only when the levels of mistuning of all absorbers are close to zero and there are relatively significant variations among them. This suggests that a solution to avoid localized responses is to introduce some positive, nearly identical intentional mistuning among the absorbers.

5.1.2 Numerical Examples and Discussion

Example 5.1: Small damping compared to imperfections

In this example, a system of four absorbers with the following numerical data is considered: inertia ratio $\epsilon = 0.1662$, n=2 (this data is taken from the 2.5 liter, in-line, four stroke, four cylinder engine considered by Denman [11]), and $\tilde{\mu}_a = 0.008N$. Four cases are considered with the mistuning levels shown in Table 5.1. The first case corresponds to a situation where one absorber has a smaller mistuning level than the remaining three. The second case corresponds to a situation where two absorbers have smaller mistuning levels than the other two. The third case corresponds to a situation where one absorber has a larger mistuning level than the other three. The fourth case corresponds to a situation where all the mistunings are small and close

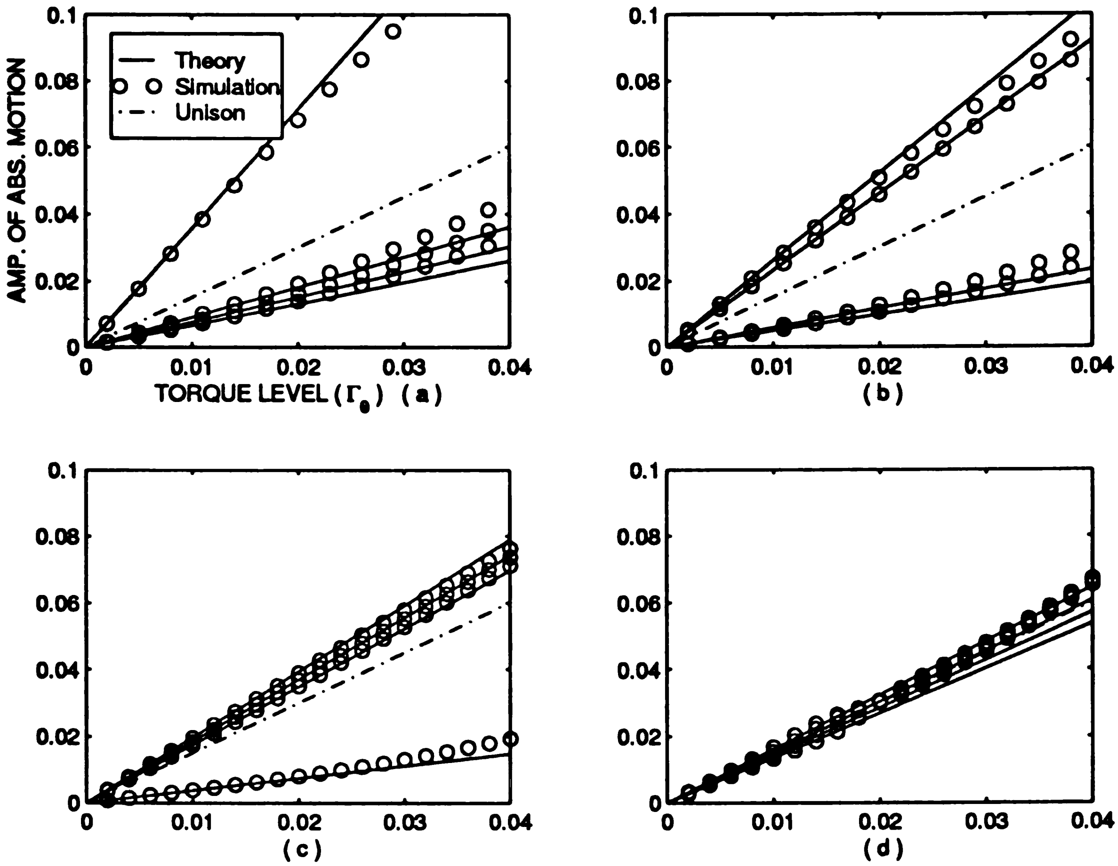

Figure 5.1. Absorbers amplitudes verses fluctuating torque level for example 5.1.

to each other. The amplitudes of the steady state responses of the absorbers versus the applied torque level for these four cases are shown in Figure 5.1. It should be mentioned here that the simulation results are obtained by numerically solving the full non-linear equations represented in chapter 2 for the case of epicycloidal path, which is the closest to being linear over a wide range of amplitudes. It is clear from Figure 5.1 that localization indeed occur for this system. The severity of the localization depends very much on the mistuning differences between the absorbers. Absorbers with smaller mistunings do localize as long as there are other absorbers

Table 5.2. Data for example 5.2

Absorber	a. $\sigma(\%)$	b. $\sigma(\%)$
1	0.002 (0.03)	0.001 (0.02)
2	0.014 (0.23)	0.007 (0.12)
3	0.010 (0.17)	0.005 (0.08)
4	0.012 (0.20)	0.006 (0.10)

with larger levels of mistuning. It is also clear from the figure that the strength of the localized response depends on the number of absorbers that are localizing. The most severe case is when only one absorber has a smaller level of mistuning than the remaining absorbers, *i.e.*, case (1) Figure 5.1(a).

Example 5.2: Large damping compared to imperfections

This example is limited to the most severe case where only one absorber may localize, i.e., only one absorber has a smaller level of mistuning than the remaining absorbers. Here, the damping level is kept the same as that in example 5.1. The two cases shown in Table 5.2 are considered. The first is the case where the mistunings among the absorbers are one fifth those in example 5.1(a). The second is the case where the mistuning levels are one tenth those in example 5.1(a). The amplitudes of the absorbers' steady state responses versus the applied torque level for these two cases are shown in Figure 5.2. It is clear that localization gets weaker as the levels of mistuning get smaller.

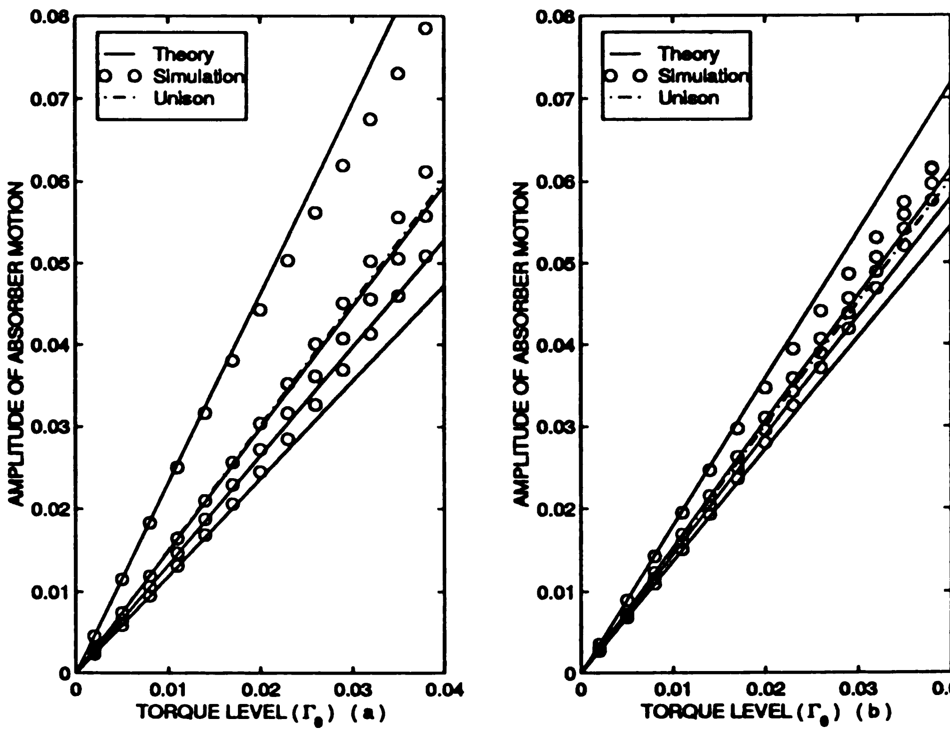

Figure 5.2. Absorbers amplitudes verses fluctuating torque level for example 5.2.

Example 5.3: Small damping compared to imperfections- with intentional mistuning

In this example, three nominal intentional mistuning levels of 0.1, 0.2, and 0.3 are applied to all four absorber paths of example 5.1. The imperfections among the absorbers' paths are similar to those of example 5.1(a), and shown in Table 5.3. The amplitudes of the absorbers' steady state responses versus the applied torque level for these three cases are shown in Figure 5.3. It is clear from this figure that the system becomes more robust when a positive intentional mistuning that is large compared to the imperfections in the absorbers' paths is introduced. This robustness depends on the magnitude of the introduced intentional mistuning.

Table 5.3. Data for example 5.3

Absorber	a. σ	b. σ	c. σ
1	0.11	0.21	0.31
2	0.17	1.27	0.37
3	0.15	0.25	0.35
4	0.16	0.26	0.36

Effect of damping level on localization

To clearly see the effect of the damping level on localization, example 5.1(a) and example 5.2 above are reconsidered with variable damping levels. The ratios of the maximum to the minimum absorber amplitudes, $\frac{S_{max}}{S_{min}}$, versus the scaled damping level, $\tilde{\mu}_a$ are plotted for these examples and shown in Figure 5.4. This figure clearly demonstrates the effect the level of damping has on the localized response. In all cases, increasing the damping level decreases the strength of the localized response. However, example 5.1(a) is the most severe case because its absolute amplitudes of mistunings are larger than the other two (it is 5 times larger than those of examples 5.2(a) and 10 times larger than those of examples 5.2(b)).

As a direct result of this, one may think of having relatively higher damping level in order to avoid localization. However, one should keep in mind that the damping level directly influences the absorbers' performance. The lower the damping level, the more effective the absorbers (see chapter 2). A better solution to avoid localization is to introduce a small intentional mistuning in the absorbers' paths which makes the system to be more robust, as was shown in Figure 5.3. However, again one has to keep in mind that mistuning also affects the performance, as discussed in chapter 2.

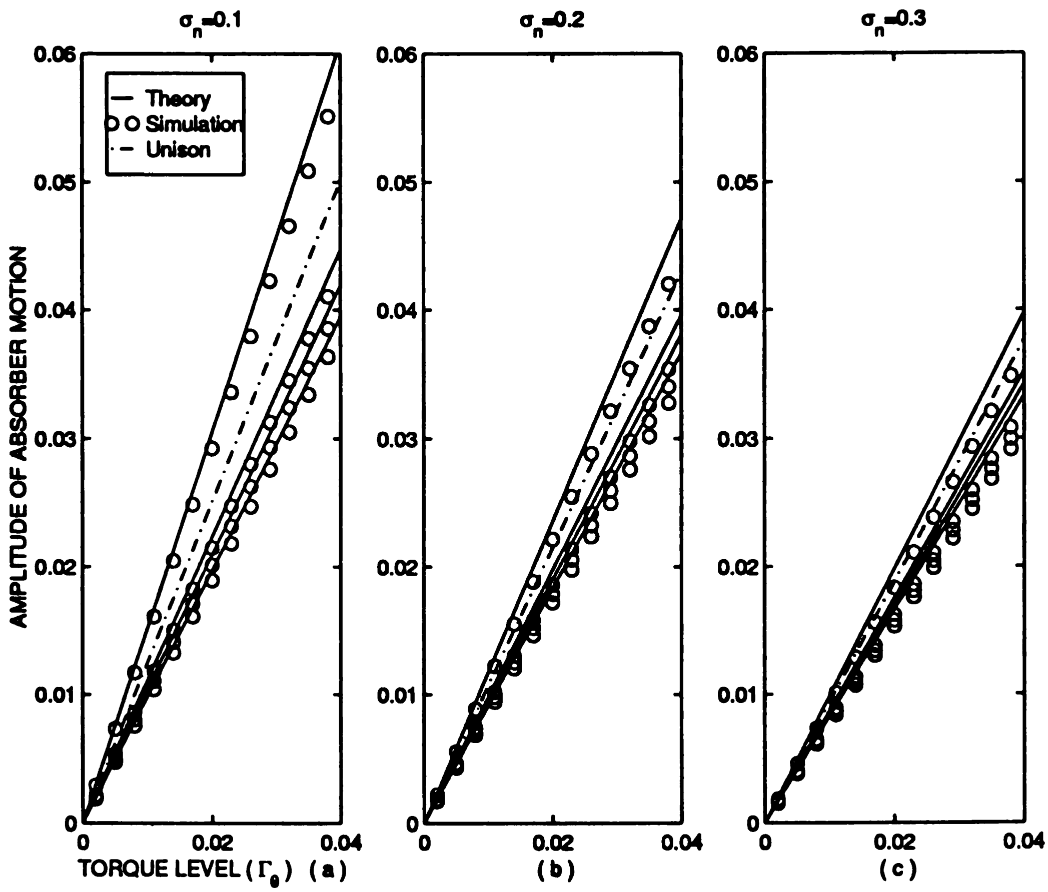

Figure 5.3. Absorbers amplitudes verses fluctuating torque level for example 5.3.

Effect of differences in imperfections on localization

Figure 5.5 shows the effect the differences in imperfections among the absorbers have on localization for $N = 4$ absorbers with the same numerical data given above. Two cases of absolute mistunings are assigned to three absorbers, namely, 0.07 and 0.01. In each case, the level of mistuning of the fourth absorber is varied from zero to the corresponding value of its group. It is clear that as the difference in mistuning between the fourth absorber and the other three becomes larger, localization becomes stronger. It is also clear that localization strength depends on the absolute magnitudes of the

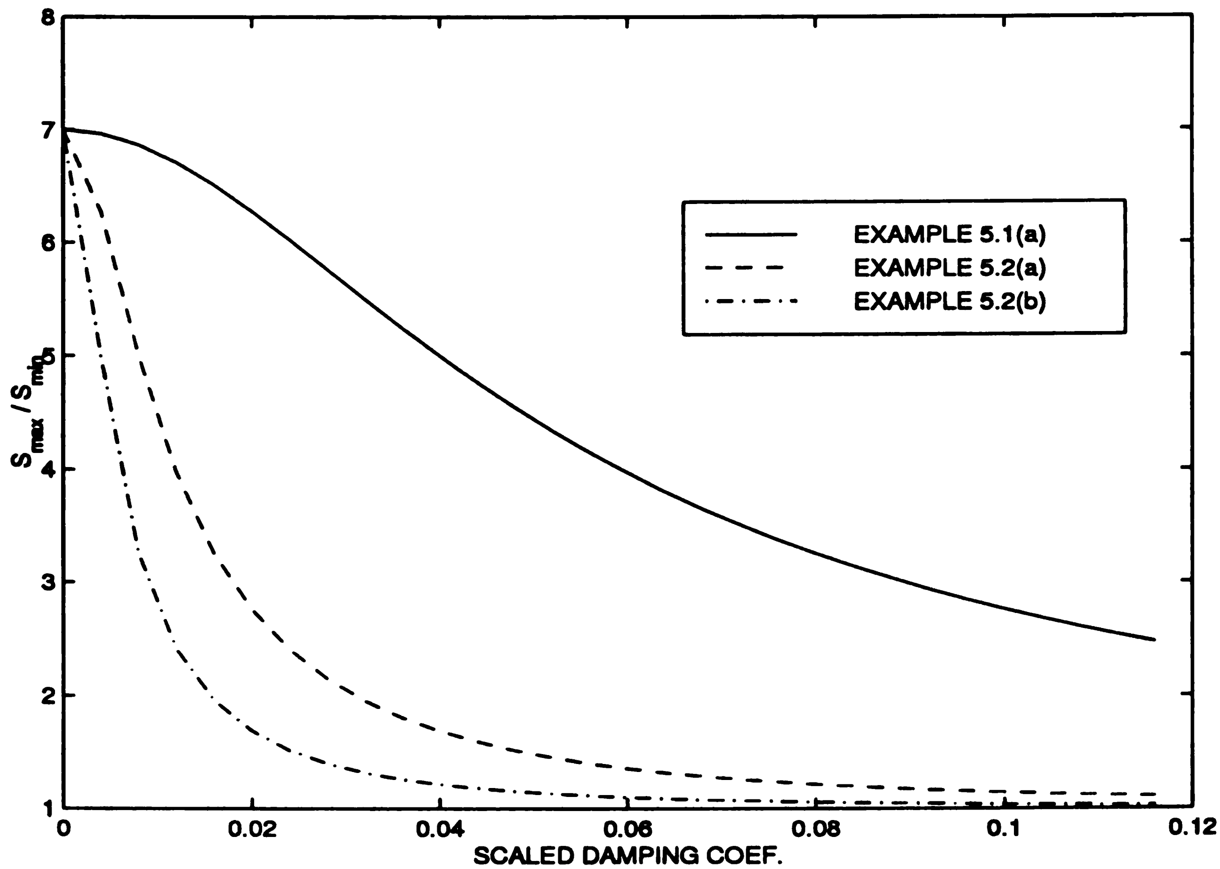

Figure 5.4. Effect of damping level on localization

mistuning. Localization is stronger for higher absolute magnitudes of mistunings.

Mainly, there are two reasons why localized responses should be avoided. The first is that localization deceases the system's performance as shown in Figure 5.6. The second is the fact that the localizing absorber(s) will hit its amplitude limits at a smaller level of applied torque than if there were no localization. This means that localization decreases the system's operating range.

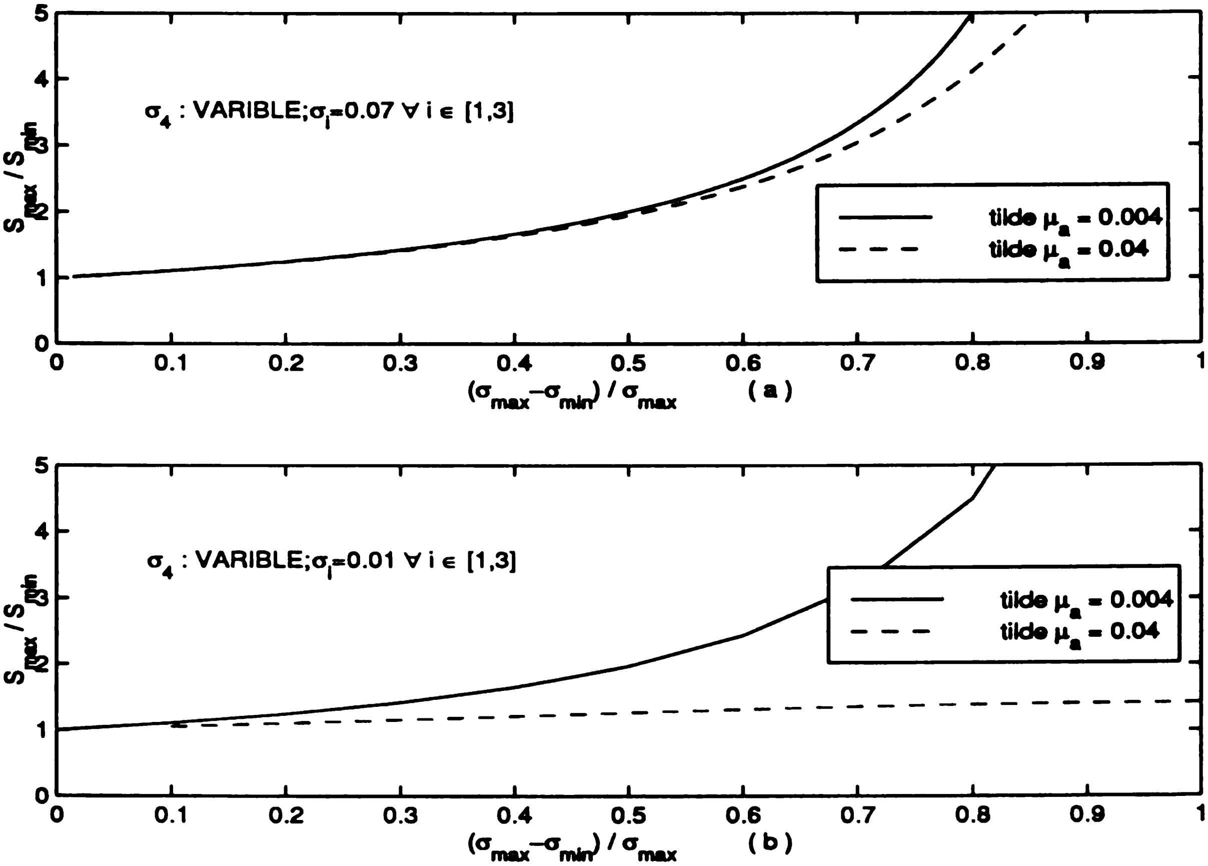

Figure 5.5. Effect of mistuning differences on localization

5.2 Nonlinear Forced Response

In this section, non-linear localization phenomenon in systems of absorbers with identical paths is investigated. The mathematical tool used to perform this task is the same one used in chapter 3 to investigate the existence and the stability of steady state responses other than the unison response in systems of multiple identical CPVAs. Therefore, the mathematical model will not be presented here.

Based on the findings of chapter 3, path types where responses other than the unison response can occur are the positively mistuned paths ranging from circular

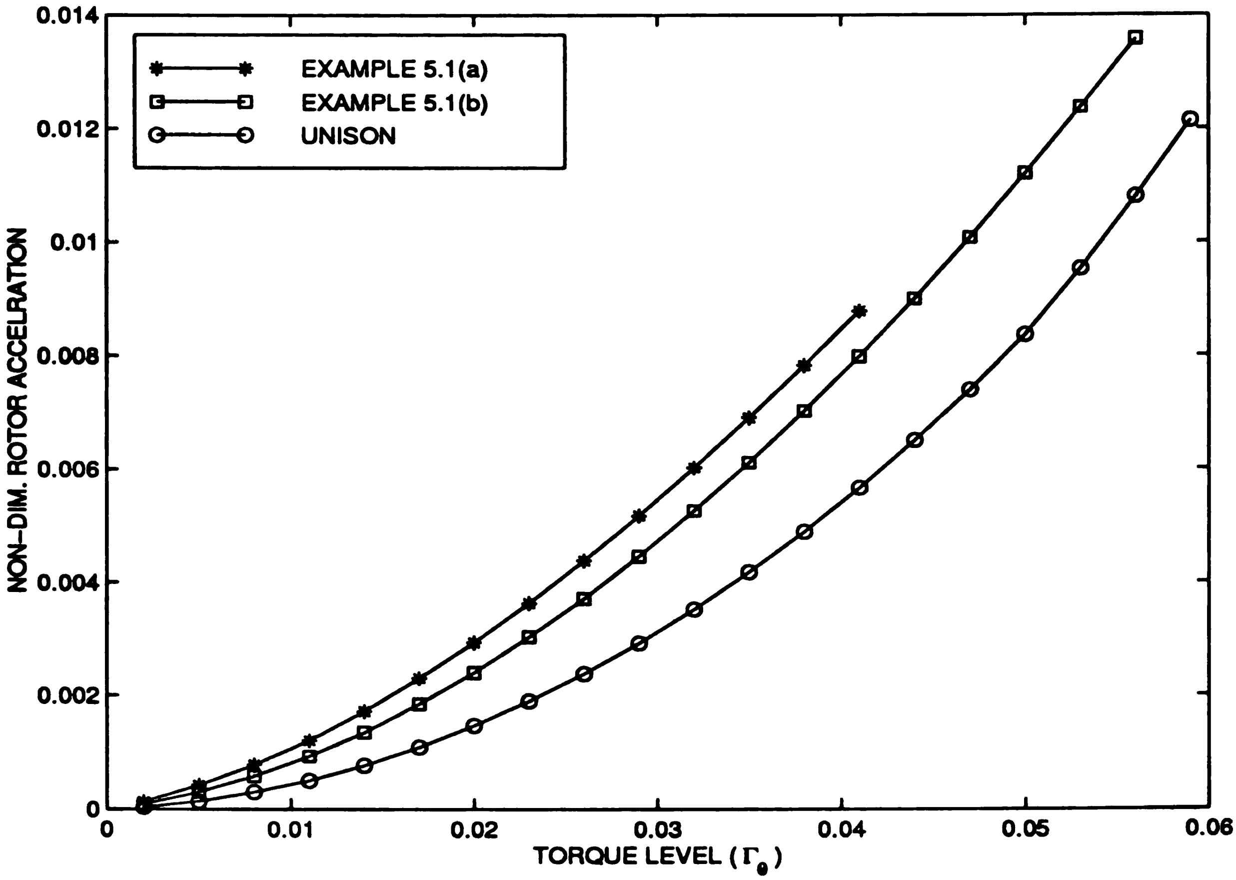

Figure 5.6. Non-dimensional rotor acceleration verses fluctuating torque level for example 5.1. (From numerical simulations)

to, but not including, epicycloidal paths, *i.e.*, paths with $0 \leq \lambda < \sqrt{\frac{n^2}{n^2+1}}$. Here, the search will be more specific, and we will only seek localized solutions. The six absorber system with the inertia ratio of $\frac{1}{75}$, a value taken from an existing light aircraft engine, that was considered in chapter 4, will again be studied here as an example. The absorbers of this system ride on circular paths. The order of the applied torque, n, is 3. The procedure presented in chapter 4 is used and the values of M that are of interest here are 1 and 2. This means that we are looking for two types of localized responses. The first is where one absorber has a higher amplitude of

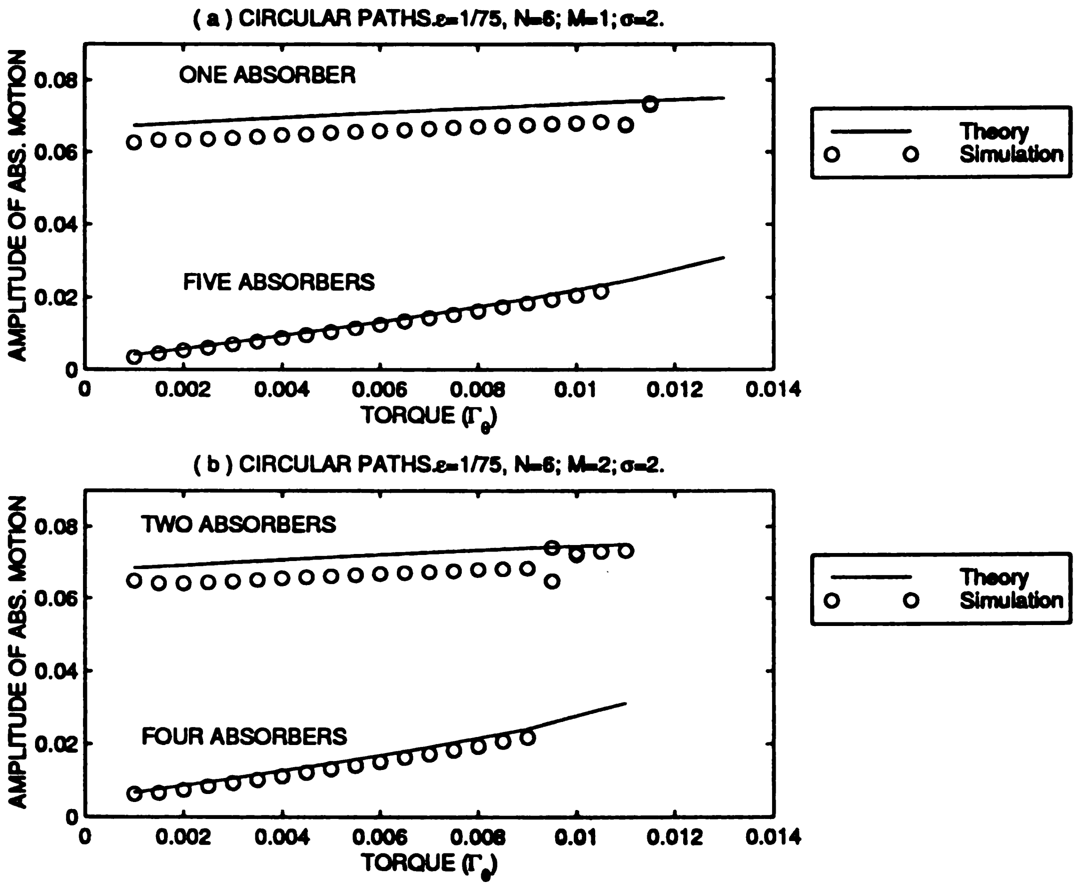

Figure 5.7. Localized response curves. $N = 6$ circular path absorbers with $\epsilon = 1/75$, and $\sigma = 2.0$. (a) The case M=1. (b) The case M=2.

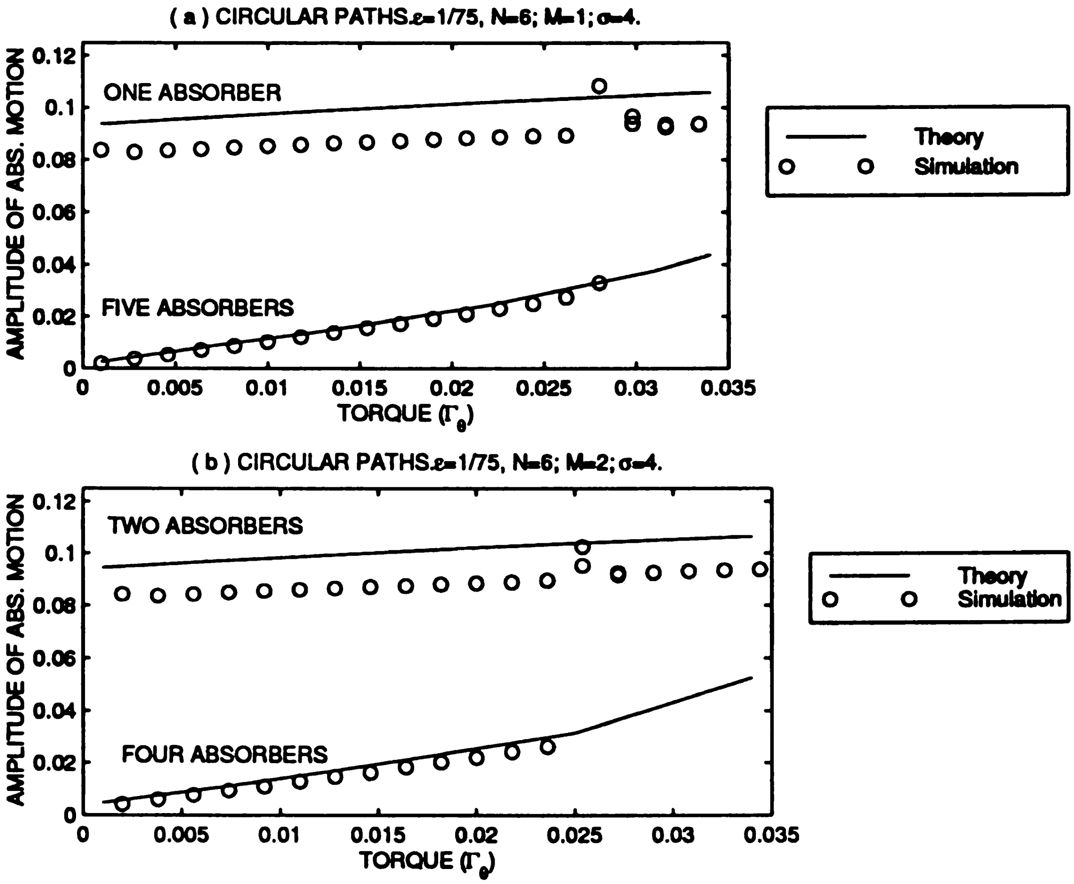

Figure 5.8. Localized response curves. $N = 6$ circular path absorbers with $\epsilon = 1/75$, and $\sigma = 4.0$. (a) The case M=1. (b) The case M=2.

vibration than the remaining five which move in relative unison. The other is where two absorbers move in relative unison and have a higher amplitude of motion than the remaining four. Two levels of mistuning are considered, namely, $\sigma = 2\,(2.67\%)$, and $\sigma = 4\,(5.33\%)$. Figure 5.7 show the results for the cases M=1 and M=2 for the paths with $\sigma = 2$ and Figure 5.8 shows the corresponding cases for the paths with $\sigma = 4$. Examining these figures, it can be clearly seen that nonlinear forced localized responses do exist and are stable over certain ranges of the applied torque. It is also clear that the strength of these localized responses and the ranges over which they occur are in direct relationship with the level of mistuning, i.e., they increase as the level of mistuning is increased. It should be mentioned here that these localized responses coexist with the stable unison response over a wide operating range (see chapter 3 for more details).

5.3 Conclusions

The following conclusions can be drawn from the findings of this chapter:

- In the presence of small imperfections between the perfectly tuned absorber paths, linear localization does exist in the forced response of CPVA systems. The relative strengths of the localized responses depend on both the ratio of the level of damping to the level of imperfections and the variations of imperfections among the paths. Systems with lower damping to imperfection ratio are expected to have stronger localized responses. Also, systems with higher differences in imperfections are expected to have stronger localized responses.

- An effective solution to avoid linear localization in CPVA systems is to introduce a small, but large when compared to imperfections, intentional mistuning in the absorber paths. This renders CPVA systems robust against localization.

- For positively mistuned circular paths, non-linear localized responses exist. The strength of these responses and the applied torque ranges over which they exist and are stable depend on the level of mistuning. As the level of mistuning is increased, the localized responses become stronger and occur over more ranges of the applied torque.

- For positively mistuned paths ranging from circular to but not including epicycloidal, *i.e.*, paths with $0 \leq \lambda < \sqrt{\frac{n^2}{n^2+1}}$, there is no way to avoid the possibility of encountering nonlinear localization. However, with paths ranging from but not including epicycloidal to cycloidal, *i.e.*, paths with $\sqrt{\frac{n^2}{n^2+1}} < \lambda \leq 1$, localized responses do not exist.

CHAPTER 6

Summary, Conclusion, and Future Work

6.1 Summary

In this dissertation some important extensions of previous research efforts in the field of mechanical vibration reduction have been investigated. These extensions focussed on some important aspects of systems of **multiple** vibration absorbers. While the main focus was on CPVA systems, the main results are applicable to certain translational absorber systems as well. To achieve the objectives of this work, three main tasks were performed. The first task was to investigate the existence and stability of the desired response in which multiple vibration absorbers move in a synchronous manner, and the effects that linear mistuning and nonlinearities in the absorbers have on the absorbers' performance. The second task was to explore the existence and stabilities of other types (specifically, non-unison) of responses. The third task was to investigate systems of multiple vibration absorbers for the possibility of the existence of the phenomenon of localization. Linear free vibration modes, linear forced vibration responses, and non-linear forced responses of vibration absorbers were considered for localization. What follows summarizes the findings of this dissertation.

Performance and Stability of Unison Response of Multiple CPVAs Riding on General Paths

It was found that there are two types of instabilities one should take into consideration when designing CPVA systems. The first is one where the absorbers loose stability of their synchronous motion, and the second corresponds to jumps in the absorbers' response curves. Both of these instabilities were found to exist in all path types ranging from the commonly used circular paths up to, but not including, epicycloidal paths, *i.e.*, paths with $0 \leq \lambda < \sqrt{\frac{n^2}{n^2+1}}$. For proper absorber performance, both of these instabilities should be avoided. It was determined that an effective method for increasing the operating range, by delaying these instabilities, is to introduce some intentional positive mistuning on the absorbers' paths. However, the introduction of this mistuning reduces the overall performance of CPVA systems in terms of vibration reduction. This means that there are trade-offs between absorber performance and wide operating ranges. The above instabilities were not found to exist for paths ranging from, but not including, epicycloidal up to cycloidal paths, *i.e.*, paths with $\sqrt{\frac{n^2}{n^2+1}} < \lambda \leq 1$. This suggests that cycloidal paths are more robust and most suitable for practical implementations. Although epicycloidal paths were not considered in this work, they are not the best choice. This is true because it has been shown by Chao *et al.* [20] that the first instability type mentioned above, where the absorbers loose their synchronous motion, does exist for this absorber path, and this has been observed in numerical simulations.

Existence and Stability of Responses Other Than Unison in Systems Of CPVAs Riding on General Paths

Here it was found that certain types of stable, non-unison responses exist for positively mistuned path types with $0 \leq \lambda < \sqrt{\frac{n^2}{n^2+1}}$. These responses result from the bifurcations to non-unison that take place at the points where unison responses first become unstable. It should be mentioned here that these solutions can coexist with the stable unison response over a wide range of operating conditions leading to an undesirable situation in terms of absorber robustness. With paths ranging from, but not including, epicycloidal up to cycloidal, *i.e.*, paths with $\sqrt{\frac{n^2}{n^2+1}} < \lambda \leq 1$, it was found that such responses do not exist. This is another and important advantage that cycloidal paths have over other paths.

Localization in Vibration Absorber Systems

Modes of Linear Free Vibration

It was found that as long as there exist some imperfections between the weakly coupled vibration absorbers, then the free vibration modes will indeed localize. The strength of this localization depends on the ratio of the coupling between the absorbers to the relative imperfections among their paths. When this ratio is small, the localization is strong and it becomes weaker as this ratio is increased. The parameter that measures the strength of the coupling between the absorbers is the ratio of absorbers' inertia to the main inertia, which is always small. As a result, localization of free vibration modes is almost always expected to exist in these systems of absorbers.

Forced Response Localization

Linear forced response localization

It was found that linear forced localized responses exist in systems of CPVAs that ride on perfectly tuned paths with some small imperfections. The strengths of these localized responses depend on the variations of the imperfections among the absorbers' tunings and on the ratio of these imperfections to the absorbers' damping level. As the variations in the imperfections and the ratio of these imperfections to the damping level gets larger, the localized response becomes stronger. When slight positive intentional mistuning is introduced in the absorbers' paths, the strength of the linear localized responses will be highly weakened. Thus, slight over-tuning is a good solution for avoiding this type of localized responses in these systems of absorbers. However, again this comes at the price of reduced absorber performance.

Nonlinear forced response localization

Nonlinear localized responses in systems of identical CPVAs were investigated for existence and stability. This is a special case of the work summarized above where non-unison solutions were investigated. The same conditions of existence apply here, *i.e.*, they exist only for systems of absorbers that ride on positively mistuned paths ranging from circular up to, but not including, epicycloidal, *i.e.*, paths with $0 \leq \lambda < \sqrt{\frac{n^2}{n^2+1}}$. The effects of intentional mistuning on these localized responses were also studied. It was found that as the level of mistuning is increased, the localized responses become stronger and occur over larger ranges of applied torques.

Note on linear verses nonlinear forced localization

For all path types considered in this work, *i.e.*, paths ranging from circular up to, but not including, epicycloidal and from, but including, epicycloidal up to cycloidal, the linear and the nonlinear localized responses are distinct in nature. This is because, as mentioned above, nonlinear localization exists only for systems of identical absorber paths when a bifurcation to non-unison exists, *i.e.*, paths ranging from circular up to, but not including, epicycloidal, with some positive level of mistuning. For these systems, linear localization is not expected to occur because of the absence of relative mistunings among the paths. Even in the presence of some small relative imperfections among the paths, linear localization is not expected to occur as well. This is due to the presence of the intentional over-tuning.

The only path type where linear and nonlinear localization can be linked is the perfectly tuned epicycloid. This is because it has been shown by Chao *et al.* [20] that for this path type, a bifurcation to non-unison does exist, to a stable, nonlinear localized response. The present work shows that in the presence of some small imperfections in zero mistuned paths, linear localization exists irrespective of the path type. As mentioned in chapter 2, due to the scaling used, the mathematical model of this work fails to capture the nonlinear effects for the case of epicycloidal paths. So, in order to link the linear and the nonlinear localization for this path type, a different scaling should be employed.

6.2 Conclusion

Based on the findings of this work, it can be concluded that the most suitable path type for CPVA systems is a slightly over-tuned cycloidal path. This is because, in contrast with other common paths, *i.e.*, circular and epicycloidal, absorbers riding on cycloids do not undergo any kind of instability. Furthermore, they are robust against linear and nonlinear localization in their steady-state response. These facts make this path type the best choice for practical implementation.

6.3 Future Work

The following are some directions suggested for future work:

- The effect that absorber path mistunings have on the absorbers' stabilities and performances for the case of epicycloidal paths should be investigated using a different scaling than what has been used herein. One can start from the work done by Chao *et al.* [20] to achieve this goal.

- Although the the method presented here allowed for drawing very useful and important conclusions for the paths ranging from, but not including, epicycloidal up to cycloidal, the accuracy was not as good for these paths as it was for the case of circular and nearly circular paths. This is due to strength of the nonlinearity and the scaling. A method that allows one to capture non-linear effects other than those that come from the path will, off course, be more accurate. It is believed that this could be done by employing a technique that allows one to formulate the problem without scaling the absorbers' amplitudes. An example of such a technique is to formulate the problem as done in Chao *et al.* [20] and analyze it using action angle coordinates.

- A more general study of CPVA systems should account for the multi-harmonic nature of the applied torque, which is a much better model for IC engines and other rotating machinery. This is because the torque acting on the crankshaft is periodic, but not harmonic, in the crankshaft rotation angle, although it can be well approximated by its first several harmonics.

- It would be of interest to investigate the possible connection between linear and nonlinear localization. It would require that one find a method that can describe the entire range of localized behaviors and use it to obtain general results.

- The effect of rotor flexibility on CPVA systems is another subject for research. Although some preliminary work showed that this effect is of higher order, *i.e.*, it is not relatively important, it deserves further consideration.

- A very important direction of future work in this field is the experimental verification of the findings of the present work and all previous related theoretical works. This is of great importance because in all theoretical developments the system dynamics is idealized in several aspects to obtain analytical estimates of system behavior. A very important example of such idealization is the damping, which is taken to be small and of viscous type. Work on this topic is underway.

BIBLIOGRAPHY

BIBLIOGRAPHY

[1] C. F. Taylor, 1985 *The Internal Combustion Engine in Theory and Practice.* The M. I. T. Press, Cambridge, Massachusetts.

[2] O'Connor, 1947 *Society of Automotive Engineering Quarterly Transactions* **1:87**. The viscous torsional vibration damper.

[3] W. Ker Wilson, 1968 *Practical Solutions of Torsional Vibration Problems*, Chapter XXX. Volume IV. Champman and Hall Ltd, London.

[4] Pierce, 1945 *Transactions of Society of Automotive Engineering* **53:480**. Rubber mounted dampers, examples of application.

[5] J. Q. Sun, M. R. Jolly, and M. A. Norris, 1995 *Transactions of the ASME, Special 50th Anniversary Design Issue* **117**. Passive, adaptive and active tuned tuned vibration absorbers-a survay.

[6] C. T. Lee, 1994 *On the Nonlinear Dynamics of Centrifugal Pendulum Vibration Absorbers*, PhD thesis, University of Michigan.

[7] V. Garg, 1996 *Effects of Mistuning on the Performance of Centrifugal Pendulum Vibration Absorbers*, MS thesis, Michigan State University.

[8] C. P. Chao, 1997 *The Performance of Multiple Pendulum Vibration Absorbers Applied to Rotating Systems*, PhD thesis, Michigan State University.

[9] B. C. Carter, 1929 *British Patent No. 337, 446.*

[10] J. F. Madden, 1980 *United States Patent No. 4218187.* Constant frequency bifilar vibration absorber.

[11] H. H. Denman, 1992 *Journal of Sound and Vibration* **159**, 251-277. Tautochronic bifilar pendulum torsion absorbers for reciprocating engines.

[12] V. J. Borowski, H. H. Denman, D. L. Cronin, S. Shaw, J. P. Hanisco, L. T. Brooks, D. A. Milulec, W. B. Crum, and M. P. Anderson, 1991 *The Engineering Society for Advanced Mobility Land, Sea, Air, and Space.* SAE Technical Paper Series **911876**. Reducing vibration of reciprocating engines with crankshaft pendulum vibration absorbers.

[13] C. T. Lee and S. W. Shaw, 1995 *ASME Design Engineering Technical Conference* Volume DE-Vol. 84-1, Volume 3-Part A, 487-492. Torsional vibration reduction in internal combustion engines using centrifugal pendulums.

[14] J. P. Den Hartog, 1938 *Stephen Timoshenko 60th Anniversary Volume*, pages 17-26. Tuned pendulums as torsional vibration eliminators. The Macmillan Company, New York.

[15] D. E. Newland, 1964 *ASME Journal of Engineering for Industry* **86**, 257-263. Nonlinear aspects of the perfomance of centrifugal pendulum vibration absorbers.

[16] C. T. Lee and S. W. Shaw, 1994 *Nonlinear and Stochastic Dynamics, ASME*, Volume AMD-Vol. 192/DE-Vol. 78, 91-98. A comparative study of nonlinear centrifugal pendulum vibration absorbers.

[17] S. W. Shaw, V. Garg, and C. P. Chao, 1997 *SAE Noise and Vibration Conference and Exposition.* Attenuation of engine torsional vibrations using tuned pendulum absorbers.

[18] C. T. Lee, S. W. Shaw, and V. T. Coppola, 1997 *ASME Journal of Vibration and Acoustics* **119**, 590-595. A subharmonic vibration absorber for rotating machinery.

[19] C. P. Chao and S. W. Shaw, 1998 *Journal of Sound and Vibration* **215**(5), 1065-1099. The effects of imperfections on the performance of the subharmonic vibration absorber system.

[20] C. P. Chao, C. T. Lee, and S. W. Shaw, 1996 *ASME journal of Applied Mechanics* **64**, 149-156. Stability of the unison response for a rotating system with multiple tautochronic pendulum vibration absorbers.

[21] C. P. Chao, C. T. Lee, and S. W. Shaw, 1997 *Journal of Sound and Vibration* **204**(5), 769-794. Non-unison dynamics of multiple centrifugal pendulum vibration absorbers.

[22] C. P. Chao and S. W. Shaw. The dynamic response of multiple pairs of subharmonic torsional vibration absorbers. To appear.

[23] P. W. Anderson, 1958 *Physical Review* **109**, 1492-1505. Absence of diffusion in certain random lattices.

[24] C. H. Hodges, 1982 *Journal of Sound and Vibration* **82**, 411-424. Confinement of vibration by structural irregularity.

[25] C. Pierre and E. H. Dowell, 1987 *Journal of Sound and Vibration* **114**, 549-564. Localization of vibrations by structural irregularity.

[26] C. Pierre, D. M. Tang and E. H. Dowell, 1987 *AIAA Journal* **25**, 1249-1257. Localized vibrations of disordered multispan beams: theory and experiment.

[27] S. T. Wei and C. Pierre, 1988 *Journal of Vibration, Acoustics, Stress, and Reliability in Design* **110**, 429-438. Localization phenomena in mistuned assemblies with cyclic symmetry Part I: Free vibrations.

[28] S. T. Wei and C. Pierre, 1988 *Journal of Vibration, Acoustics, Stress, and Reliability in Design* **110**, 439-449. Localization phenomena in mistuned assemblies with cyclic symmetry Part II: Forced vibrations.

[29] A. F. Vakakis and T. K. Centikaya, 1993 *SIAM Journal on Applied Mathematics* **53**, 265-282. Mode localization in a class of multi-degree of freedom systems with cyclic symmetry.

[30] M. E. King and P. A. Layne, 1998 *Nonlinear Dynamics* **15**, 225-244. Dynamics of nonlinear cyclic systems with structural irregularity.

[31] C. P. Chao and S. W. Shaw, paper DETC97/VIB-3956, *Proceedings 1997 ASME Design Engineering Technical Conferences.* Nonlinear localization in systems of tautochronic vibration absorbers.

[32] J. P. Den Hartog, 1985 *Mechanical Vibrations.* Dover Publications, Inc. New York.

[33] M. Golubitsky, I. Stewart, and D. G. Schaeffer, 1988 *Singularities and groups in bifurcation theory.* Vol. II, Springer-Verlag, New York.

[34] D. E. Newland, 1964 *ASME Journal of Engineering for Industry* **86**, 257-263. Nonlinear aspects of the performance of centrifugal pedulum vibration absorbers.

[35] M. Sharif Bakhtiar and S. W. Shaw, 1988 *Journal of Sound and Vibration* **126**, 221-235. The dynamic response of centrifugal pendulum vibration absorber with motion-limiting stops.

[36] A. G. Ulsoy and C. Pierre and S. Choi, 1998 *ASME Journal of Vibration and Acoustics* **120**, 138-148. Vibration localization in rotating shafts, Part 1: Theory.

[37] A. G. Ulsoy and C. Pierre and S. Choi, 1998 *ASME Journal of Vibration and Acoustics* **120**, 149-155. Vibration localization in rotating shafts, Part 2: Experiment.

[38] C. T. Lee and S. W. Shaw, 1997 *Journal of Sound and Vibration* **203**, 731-743. Nonlinear dynamic response of paired centrifugal pendulum vibration absorbers.

[39] G. S. Happawana, A. K. Bajaj, and O. D. I. Nwokah, 1991 *Journal of Sound and Vibration* **147**, 361-365. A singular perturbation perspective on mode localization.

[40] R. L. WEAVER,1996 *Theoretical and Applied Mechanics, University of Illinois at Urbana-Champaign* TAM Report No.**823**. Mean and mean-square responses of a prototypical master/fuzzy structure.

[41] G. S. Happawana, O. D. I. Nwokah, A. K. Bajaj, and M. Azene 1998 *Journal of Sound and Vibration* **211**, 761-789. Free and forced response of mistuned linear cyclic systems: a singular perturbation approach.

[42] J. H. Wilkinson, 1965 *The Algebraic Eigenvalue Problem.* Oxford University Press.